CONF-9312109--Abstr.

UCRL-ID-114972-1

SERS Internship
Fall 1993 Abstracts and Research Papers

Barry Goldman

April 1994

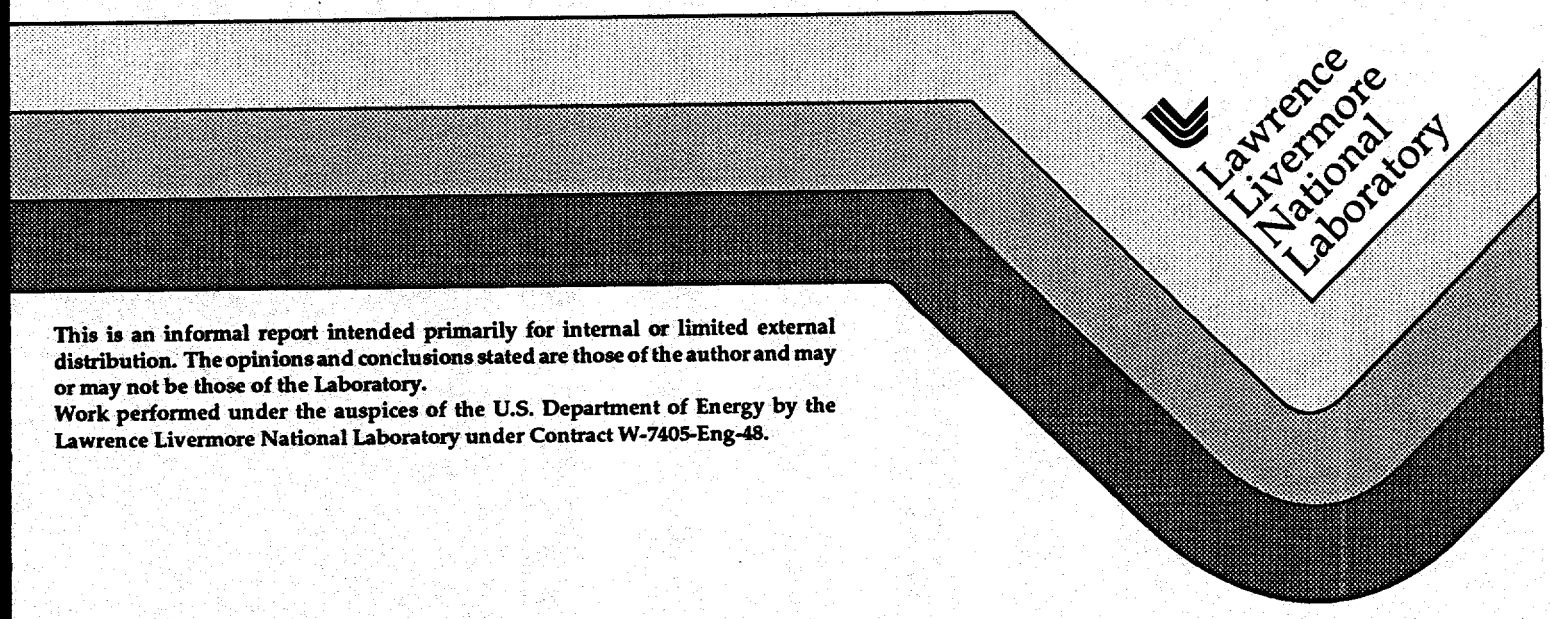

DISCLAIMER

SCIENCE & ENGINEERING

SERS

RESEARCH SEMESTER

Lawrence Livermore National Laboratory

Fall 1993

ABSTRACTS FOR STUDENT SYMPOSIUM

December 10, 1993

Sponsored by:

The U.S. Department of Energy
Office of Energy Research

SCIENCE & ENGINEERING

SERS

RESEARCH SEMESTER

Fall 1993 Student Symposium Abstracts

Table of Contents

Characterization and Optimization of an Experimental Laser Glass for a Kerr Lens Self-Mode-Locked Laser Cavity

Andrew J. Bayramian
Montana State University
Laser Program

ABSTRACT

Initial investigations into the properties of a new experimental laser glass indicated that it would be a prime candidate for Kerr lens mode-locking. A high thermal Figure of Merit and broad bandwidth made the new glass seem to be designed for high power short pulse work. As a result, cavity designs and optic parameters were calculated to test this hypothesis, as well as characterization of the lasing properties of the glass. Laser emission was observed for the first time in the new glass. In addition, laser slope efficiencies of this glass were measured at various output couplings. When the new laser glass was compared to commercially available laser glasses LG-750 and APG-1, something appeared to be inhibiting smooth laser action. Further investigations indicated the thermal lens in the new glass was much larger than in the other glasses making the laser resonator unstable. This thermal lens was modeled and quantified in a separate experiment, and a laser cavity was designed to compensate for the thermal lens.

New Height Field Editor

Jennifer Cano
Wayne State University
Computation Organization

ABSTRACT

The focus of this project is to modify and write new code for a program named WireMan. WireMan draws in 3-D using items from a menu (cones, spheres, etc.). One of the items which can be selected is called the height field. The height field, as it currently appears in WireMan, is a 3-D graph of a set equation. Originally, the height field was supposed to be able to display any curve the user may need. However, because of lack of time and programmers, the height field was never completed and has remained at this constant curve since its creation. To change it a user needs to modify program code, thus, a height field editor is necessary. Through the editor, the user will be able to modify the height field by either equation or matrix. The latter will allow the user to determine a curve for the height field according to matrix or grid entries (of the form n x n, where up to 10 x 10 entries can be made). The grid will then be stretched and evaluated over the height field plane (which consists of 512-512 generated entries) and the curve will then be generated.

The difficulties and the results of the project are outlined according to their occurrences throughout the paper.

Lead in Food and Food Containers

Anna O. Chu
University of California at Berkeley
Chemistry and Material Science

ABSTRACT

Food and food containers suspected of containing high levels of lead were investigated. A 4% glacial acetic acid leaching test was performed on Mexican potteries, Chinese porcelain ware, and the lip area of coffee mugs to determine the amount of leachable lead. Candy stored in Mexican clay pots and beans cooked in Mexican cooking pots were investigated for lead content. A dry ash was performed on the candy and beans so as to be able to test for lead on the atomic absorption spectrophotometer. Lead in these foods and food containers was measured by flame atomic absorption spectroscopy.

Removal of Hexavalent Chromium from Groundwater Using Ion Exchange Resins

Duncan Cottrell
Georgia State University
Environmental Protection Department

ABSTRACT

Groundwater being treated for removal of organic contaminants must also be cleaned of hexavalent chromium by using ion exchange resins. The chemistry of ion exchange is explained. Experimental apparatus setup and analyses are described. The performance of different commercial resins is compared.

The Fabrication of Fiber Optic Sensors for pH Measurement

Jennifer N. Fisher
University of Central Florida
Environmental Sciences Division

ABSTRACT

The Department of Energy is currently supporting the development of a fiber optic pH sensor. This sensor is being developed to monitor contaminates, which were created during the weapons development era. These contaminants are being stored in large vats while decomposition occurs. These vats have proven to be very pH sensitive, and need to be monitored. An optical sensor is inherently safer than traditional electric pH sensors.

The sensor is being developed using the dye fluorescein. This dye fluoresces differently when exposed to different pH environments. The dye is chemically bonded to the end of the optical sensor. Ultraviolet light is used to activate a reaction, between fluorescein and other chemicals, to create the sensor. Then a device, a fluorimeter, is used to measure the pH of a given solution. This apparatus sends light of a given wavelength down the fiber. The dye at the top fluoresces, and light of a new wavelength travels back up the fiber. This light is converted to a voltage signal by a detector, and this signal can be used to determine the unknown pH.

A wide range of parameters are being tested to determine how to create the best sensor, i.e., the one with the largest signal range over the pH scale and with the fastest response. Some of the parameters being tested include whether an acid bath is required to cleanse the fiber tip before the dye is polymerized onto the end. This is a time consuming step, and should be eliminated if possible. Also, which type of filter should be used to eliminate unnecessary, and damaging, visible light during the polymerization process? What is the best light exposure time during this process? Should a neutral density filter be used to limit the intensity of light flowing through the fiber while the dye is being chemically bonded to the sensor, and thus possible increasing the exposure time? Should a capillary tube be used when applying the dye solution to the fiber tip? The chemicals used react adversely with water, and exposure to air during the process could affect the outcome. But, by using the tube, the polymer becomes thick, and the response time becomes slow. Thus far, with so many parameters to consider, and some probably still unknown, the sensors have proven to be unreproducible. Understanding what affects this polymerization process, and how, is the key objective of this project. Without reproducible results, no sensor, no matter how good it may be, is useless.

Replacing CFC's in the Metal Cleaning Process

Sophia C. Hsu
Indiana University at Bloomington
Alternative Testing Program
Environmental Protection Department

ABSTRACT

Because the Montreal Protocol requires industries to stop production of Freon 113 by 1995, LLNL has opted to replace the hazardous solvent with environmentally friendly alternatives. My project is to test/evaluate alternative solvents in order to replace Freon 113 in the metal cleaning process, specifically on copper printed circuit boards. All of the alternative cleaners we have chosen for our project have the ability to adequately remove flux/contaminants off printed circuit boards via ultrasonic cleaning. However, we also want to know how these alternative cleaners will react on the printed circuit boards if aged a simulated 15-20 years. In my paper, I will begin by giving a brief background of the Alternative Testing Program. I will then proceed to explain the testing process of the alternative solvents on the printed circuit boards. I will conclude by analyzing the data taken from the testing process and select the best alternative (if one exists).

Predator/Prey Simulation

Brant A. Lindhorst
Northeastern Illinois University
Computation Organization

ABSTRACT

My project involved creating a simple predator/prey model. It is actually an extension of the game of LIFE. The game of LIFE is a computer simulation/game that was developed by John Conway to test a theory of J. Von Neumann. The game involves simple objects and rules governing those objects. The rules determine if an object lives, dies, or is born. The game starts with an initial pattern, user defined or random. Each iteration applies the rules to the objects, and the objects are displayed on the screen. Will the pattern remain constant, die off, or possible evolve? We want to extend this system. The objects become species, and the rules become changeable. The user can define many different species, each of which has its own rules. In doing this, LIFE becomes a simple subset of our proposed simulation. The ultimate purpose in doing this is to see how various systems change over time and to demonstrate that making small changes in a system can drastically change outcomes.

Detection of Micronuclei in Germ Cells of Male Mice using Multi-color Fluorescence *in situ* Hybridization

Marek Ma
University of Michigan
Biology & Biotechnology Research Program

ABSTRACT

The ability to detect genetic abnormalities in germ cells helps further our understanding of the effects of toxicants on congenital defects during birth and development. We are currently developing a method to detect one such genetic abnormality, the micronucleus in the male germ line. A micronucleus, a chromatin piece separated from the main nucleus, is an indicator of a chromosomally abnormal gamete.

The mouse serves as a model in our search for the micronuclei in male germ cells. The stages of sperm development are well defined and easily distinguishable morphologically. Stem cells develop into ejaculated sperm in a very predictable fashion. Our goals are to detect micronuclei in spermatids, the haploid precursors of sperm, and to investigate the effects of exposure of mice to germinal mutagens.

To make microscope slide preparations of spermatid micronuclei, seminiferous tubules were teased apart, treated with collagenase and trypsin, centrifuged in testis isolation medium, dropped on glass slides, and air dried. The slides were then baked before fixing in an ethanol series. Micronuclei were evident when DNA was stained with DAPI. Also, to determine their chromosomal origin, DNA probes for the pan-centromeric regions and X chromosome were labeled with digoxigenin and biotin by nick translation and the signals were detected using a combination of rhodamine and FITC. Two types of micronuclei can be discerned by these multi-probe procedures; one carries a chromosomal fragment missing a centromere. This micronucleus could arise as a consequence of a DNA breakage event during spermatogenesis. The other type of micronuclei contains a whole chromosome due to an error in chromosomal segregation.

The developed methods are now being applied to a current study. The effect of the aneugen chloral hydrate on the development of the germ cells of male mice is being investigated with the micronuclei and fluorescence *in situ* hybridization methods. By sampling mice shortly after exposure, we investigate the sensitivity of the meiotic phase of spermatogenesis, whereas sampling mice at a longer time interval will reveal effects on spermatogonial cells in mitosis. Such information may have important consequences for human males exposed to this anesthetic agent.

Methods of Determining DNA Conformation

Eric L. Mayes
Arkansas State University
Biology and Biotechnology Research Program

ABSTRACT

While the basic structure of DNA has been known since 1953, there is still a great void in terms of knowing how DNA interacts with its surroundings. Because the structure of biological molecules determines their function, the conformation of DNA is of prime importance in understanding its role in living organisms.

We present two methods of determining some components of DNA's conformation. One uses atomic force microscopy to determine the dimensions of DNA's base pairs, and the other seeks to computationally determine the structure of DNA in different chemical environments.

Stimulated Brillouin Scattering as a Function of Bandwidth

Alison B. Peck
University of Nebraska at Kearney
Laser Department

ABSTRACT

Stimulated Brillouin scattering (SBS) is a non-linear optical effect which has been of interest to laser scientists for many years. SBS can be extremely useful as a phase conjugator, but is can also cause damage in large lasers by scattering light transversely to the beam. In this experiment, transient SBS has been generated in two materials with a 104-GHz, 13-ns pulse from the OSL Nd:YLF laser, and then compared to SBS generated in the same materials with a narrowband pulse of equal length. Also investigated are the effects of variation of focal volume at narrow and broad bandwidth. Results show that the transient threshold is higher for the broadband pulse than for the narrowband, and also indicate a difference in shape between the input and the output pulse.

Sample Sequencing

Christa K. Prange
St. Mary's College
Biology and Biotechnology Research Program

ABSTRACT

The goal of the Human Genome Project is to locate and sequence all the genes in the human body. At Lawrence Livermore National Laboratory, attention is focused on Chromosome 19, which has been estimated to contain approximately 2000 genes. So far, only 250 have been mapped to specific areas on the chromosome. For this reason, a simple method is needed to predict the most likely locations of the coding regions in the DNA. Sample sequencing uses a newly developed vector in addition to standard cloning techniques to make the process of DNA preparation more efficient. Once sequence is obtained, it is analyzed using databases to predict the regions most likely to contain genes. So far, 12 fragments from three different clones have been completely sequenced in both forward and reverse directions, with fragments from ten more clones in progress. Constant improvement of methods to increase efficiency and accuracy combined with utilization of the most current databases available make sample sequencing a useful tool for reaching the goals of the Human Genome Project.

Evaluation and Assessment of Education Programs

Mona L. Ramsey
Fort Valley State College
Education Program

ABSTRACT

To ensure quality products, the Department of Energy is emphasizing the evaluation and assessment of education programs. In response, Lawrence Livermore National Laboratory is preparing its program managers to conduct formative evaluations of each education program. In preparation for designing evaluation tools, the program managers have been exposed to an assessment guide that will broaden their knowledge of writing goals and objectives. Data collected will support the design of evaluation tools created by each of the program managers.

Neural Network Analysis of Nuclear Glass Composition vs. Durability

Cindy K. Seibel
University of California at Davis
Earth Sciences Department

ABSTRACT

The relationship between the chemical composition of oxide glasses and their physical properties is poorly understood, but is becoming more important as vitrification (turning into glass) of high level nuclear waste becomes the favored method for long term storage. The vitrified waste will be stored deep in geologic repositories where it must remain intact for approximately 10,000 years. A strong resistance to ground water exposure, i.e., a slow rate of glass dissolution, is of great importance. This project deals specifically with glass samples developed and tested for the nuclear fuel reprocessing facility near West Valley, New York which needs to dispose of high level radioactive waste stored in stainless steel tanks. A back propagation artificial neural network is used to analyze the glass dissolution data for the effects of composition and the resulting durability of borosilicate glasses in an aqueous environment. The neural network is being trained to reliably determine the durability of a borosilicate glass from it's chemical composition which can then be used to systematically optimize the properties of the complex nuclear glasses and slow the dissolution rate of radionuclides into the environment.

Cathode Development and Fabrication for a Rechargeable Lithium Ion Battery

Dyuti Sengupta
University of Washington
Chemistry & Material Science Department

ABSTRACT

Lithium ion batteries have been the subject of much research in recent years. The cathode of this battery continues to pose many processing questions, in terms of its viability as a component in a long life rechargeable battery. Here, we have examined some of these questions, and designed and performed experiments involving several additives in varying amounts with lithium cobalite powder, the primary material in the battery cathode. The main properties examined in the material were material conductivity, adhesive qualities, and fractional intercalation.

Indonesian Snails: Key to Ocean Circulation

Timothy W. Sullivan
Michigan State University
Physics, Center for Accelerator Mass Spectrometry

ABSTRACT

Previous radiocarbon measurements using mollusk shells indicate that reservoir ages vary considerably throughout the Indonesian conduit. By studying ^{14}C concentrations in mollusk shells, we investigate the source of this variation. Mollusks of known calendar age were sampled along their growth axes and analyzed at the Center for Accelerator Mass Spectrometry. Results indicate that radiocarbon concentrations along growth axes fluctuate seasonally. We attribute this fluctuation to the upwelling of deep, "old" water during seasonal monsoon weather patterns. Furthermore, we believe the source of variation in the reservoir ages may be caused, in part, by sampling mollusk shells at only one location and not averaging over their growth axes.

Optimization and Performance Evaluation of a Fibre Channel Three Stage Switching System

Marcus I. Weber
Santa Clara University
Advanced Telecommunications Program, Electronics Engineering

ABSTRACT

Fibre Channel, as defined in the ANSI standard X3T9.3, is an emerging technology in high speed data communications and has become the choice of many organizations for their future data networking needs. The system to be tested is the distributed three stage switching system designed by Ancor Communications. Optimization and testing of the Ancor three stage switching system is necessary to characterize the performance of the prototype system before one is implemented. This paper presents a discussion of optimization techniques and achieved performance numbers under different conditions as well as a comparison to single stage switching systems.

Computer Design of Efficient Photoreceivers

Mark A. Wistey
Montana State University
Electronics Engineering

ABSTRACT

This paper describes the design of new high speed vertically coupled, impedance matched photoreceivers through the application of simulated annealing. We customized a beam propagation method simulator in order to test the filtering characteristics of a number of designs. Additionally, we applied traditional analytical techniques to several of the same designs and found some disagreement with the results of the BPM methods; the paper discusses the most likely sources of such discrepancies, as well as caveats for limiting the errors which they could introduce.

Lawrence Livermore National Laboratory Science and Engineering Research Semester (SERS) students are participants in a national program sponsored by the Department of Energy/Office of Energy Research. The SERS program provides students the opportunity to participate in research at one of seven Department of Energy facilities during the academic year. Argonne National Laboratory in Illinois, Brookhaven National Laboratory in New York, Lawrence Berkeley National Laboratory in California, Lawrence Livermore National Laboratory in California, Los Alamos National Laboratory in New Mexico, and Pacific Northwest Laboratory in Washington place students in research appointments in this program. The Department of Energy initiated the SERS program to encourage undergraduates to pursue advanced degrees and careers in science or engineering.

Characterization and Optimization of a New High-Average Power Laser Glass

Andy Bayramian

Montana State University

Lawrence Livermore National Laboratory
Livermore, California 94550

December 12, 1993

Prepared in partial fulfillment of the requirements of the Science and Engineering Research Semester under the direction of Chris Marshall, Research Mentor, in the Lawrence Livermore National Laboratory.

*This research was supported in part by an appointment to the U.S. Department of Energy Science and Engineering Research Semester (hereinafter called SERS) program administered by LLNL under Contract W-7405-Eng-48 with Lawrence Livermore National Laboratory.

Abstract

A new High-Average Power laser glass with favorable thermal-mechanical properties was recently developed by Schott Glass Technologies. We refer to this glass as APG-2, although it does not have an official designation. Fracture studies were conducted which verified the thermomechanical utility of the glass. Consequently, the glass was a promising candidate for a variety of application such as a Kerr-Lens mode-locked short-pulse laser. As a result, cavity designs and optical parameters were calculated to test this hypothesis, and characterization of the lasing properties began. The glass was lased for the first time, and laser slope efficiencies were measured at various output couplings. Laser efficiencies were observed to drop radically when the pump light duty cycle was increased from 10% to unity. When the new laser glass was compared to commercially available laser glasses LG-750 and APG-1, something appeared to be inhibiting smooth laser action. Further investigations indicated that the thermal lens in the new glass was much larger than in the other glasses making the laser resonator unstable. This thermal lens was then modeled and quantified in a separate experiment.

A new experimental high-average power laser glass was recently developed by Schott Glass Technologies. We refer to this glass as APG-2, although it does not have an official designation. This new glass had reported thermal-mechanical characteristics which were far superior to previous laser glasses. The large thermal constants mean a greater mechanical strength under pumping conditions, and the broad bandwidth makes the glass well suited to a variety of fusion laser applications such as beam smoothing, favorable laser-plasma interaction, and possibly mode-locked short pulse generation.

The mode-locking of solid-state lasers to produce ultrashort pulses is desirable for applications such as high speed communications and ultrafast spectroscopy. Generating such short pulses requires several material properties to come together simultaneously. The newest method currently being explored by the scientific community uses the Kerr effect, a nonlinear optical phenomena based on an intensity dependent refractive index. During the summer of 1993, laser scientists applied KLM to a Nd:glass laser for the first time, producing pulses of 129 femptoseconds in LG-760, a commercial laser glass[1]. From a material standpoint this was by no means easy given the relatively small bandwidth and poor thermal characteristics inherent to all laser glasses. Two criterion must be met by the gain medium before it is ever used as a KLM laser. First, if one wants pulses to be short in time, then one must have broad pulses in the frequency regime as dictated by the Heisenberg Uncertainty Principal; i.e., the gain medium must lase along a relatively large bandwidth. Second, the gain medium must be able to withstand the thermal effects of the pump beam. Therefore, to further shorten pulses we can either fine tune the method of KLM or try to fine tune the material.

This paper focuses on the promising new High-Average Power laser glass (APG-2) developed by Schott Glass Technologies. In Fig. 1, we see that the bandwidth of APG-2 is similar to other common laser glasses[2]. In light of the fact that LG-760 has the narrowest bandwidth of the bunch, the other glasses appear to be appropriate substitutes for applications requiring broad bandwidth. Next, in Table I are listed some of the thermal

characteristics of APG-2 and two commercial laser glasses, LG-750 and APG-1[3]. The Figure of Merit (FOM_{th}) is a composite term which quantifies the ability of the glass to withstand thermal gradients without fracture[3]; $FOM_{th} = \kappa K_{1c}/\alpha E$, where κ is the thermal conductivity, K_{1c} is the fracture toughness, α is the expansion coefficient, and E is Young's modulus. Here again, APG-2 has an advantage in nearly every material constant, and when quantified in terms of the FOM_{th} is 2.3 times larger than it's closest competitor.

Initially, to prove the theoretical FOM_{th} values, we studied the fracture threshold of these glasses. As we can see in Fig. 2, the results closely follow the theory. LG-750 and APG-1 failed at much lower power densities than APG-2. It is interesting to note that at the level of power where APG-2 is indicated to fail, only a single fracture was observed in the 18 samples studied. Rather than fracture at this power level, the glass begins to glow red around the pump beam indicating that APG-2 often melts before it fractures.

With these promising characteristics in hand, we set out to study the laser emission properties of APG-2. First, we constructed an oscillator based on APG-2 as the gain media. Using two 5 cm radius of curvature mirrors to form an oscillator, and a 20 cm focal length lens to concentrate the pump light to match the cavity mode as depicted in Fig. 3, we lased APG-2 for the first time. Although relatively successful, the cavity emission was unstable. Next, we optimized and quantified the efficiency of the oscillator. After initial difficulties with the confocal cavity due to the large spot size in the gain medium and thus low energy density, we switched to a concentric cavity configuration. We measured the slope efficiency of a 5.12 mm thick piece of APG-2 at a duty cycle of 10% using several different output couplings. As can be seen in Fig. 4, our initial slope efficiency measurements were relatively low (~7%), which we hoped would disappear at higher output coupling (which minimizes internal losses). However, as can be seen in Figs. 5 and 6, the slope efficiency only increased about a factor of two. At its highest value the slope efficiency was only 16.4%, which is still much less than the theoretical limit[4] of 49% which is defined as $\eta_{qd} = \lambda_p/\lambda_l$, where λ_p is the pump wavelength = 514 nm, and λ_l is the

lasing wavelength = 1054 nm. To assure ourselves that our measurements were sound, we graphed the intrinsic slope efficiency[4], which is defined as:

$$\eta = \eta_o \left(\frac{T}{T + L}\right), \tag{1}$$

where η is the intrinsic slope efficiency, η_o is the theoretical slope efficiency if the material had no losses, T is the total output coupling, and L is the losses in the material. As seen in Fig. 7, all three slope efficiencies lie along a line, which indicates sound measurements, but also indicates some problem with APG-2's lasing ability. In this case, $\eta_o = 18.5\%$ and $L = 2.4\%$.

To relate this information to previous measurements, comparisons of the lasing efficiency were also made with APG-1 (APG-2's predecessor), and LG-750, the laser glass used in the NOVA laser. Keeping all parameters in the cavity configuration fixed at a duty cycle of 10%, we exchanged one glass for the other and took measurements. The results were surprising and are depicted in Fig. 8 as slope efficiencies. Both APG-1 and LG-750 appear to be lasing near their theoretical limits while APG-2 crawls along at less than 1/3 of that value. The output power of APG-1 and LG-750 was double to triple the power output of APG-2, and the laser output also remained much more stable - varying less than 1% while APG-2's output signals often varied as much as 10%.

In addition, we endeavored to pump APG-2 continuously since this would be required to use the glass in a KLM cavity. However, the overall efficiency, defined as η = power output / power absorbed decreased. Using a 16% output coupler at a 10% duty cycle, our efficiency was 8%, yet when pumped continuously, the efficiency dropped to 2%.

These results indicate that either internal scattering and/or absorption losses or thermal effects are adversely affecting laser action. We chose to concentrate on the thermal effects by investigating the thermal lensing that existed under pump conditions. Therefore, the lens was modeled theoretically, using known material constants. The theoretical effective focal length[5,6,7] is expressed as:

$$f_{th} = \frac{K\pi r_o^2}{P_a}\left(\frac{1}{2}\frac{dn}{dT} + \alpha C_{r,\phi} n_o^3 + \frac{\alpha r_o (n_o - 1)}{L}\right)^{-1}, \quad (2)$$

where r_o is the 1/e radius of the pump beam, K is the thermal conductivity, P_a is the total power absorbed by the pump beam, dn/dT is the change in the index of refraction with temperature, α is the coefficient of expansion, $C_{r,\phi}$ is the stress optic coefficient, n_o is the index of refraction at room temperature, and L is the length of the gain medium, and f_{th} is the focal length of the effective thermal lens. The first term in parenthesis represents the contribution to the lens due to the change in index. The second term represents the lensing due to the stress caused by the change in the index. The third term represents the physical bulging of the ends due to thermal expansion. This model assumes that the rod is pumped in a cylindrically symmetric manner evenly along the length of the rod, and that the outer surface of the rod is at a fixed temperature, T. The key assumption is that the radius of the beam approximates the radius of the rod. For materials which are highly conductive, this assumption would be invalid and the two distance scales would have to be separated in the equation. However, since glass is very poorly conductive, the time, $\Delta\tau$, that it takes for the heat to radiate is slow beyond ro. Assuming only one glass sample is used, L remains fixed, which only leaves the power absorbed and the input radius as variables. Consequently, Equation 1 is a good approximation of the physical situation at hand. The predicted thermally induced focal lengths of APG-2, APG-1, LG-750, and LG-760 were compared using L = 0.510 cm, ro = 0.00375 cm, and various the material constants - published by Schott Glass Technologies[8,9] and measured in APG-2[10]. The inverse focal length, $1/f_{th}$, versus power absorbed is shown in Fig. 9, where the magnitude of the slope of the line indicates the strength of the thermal lens. We see that APG-2 is predicted to have the largest lens effect, and that all the other glasses have significantly smaller lensing problems.

Finally , we endeavored to match the theory to the experiment by measuring the focal

power of the thermal lens. Using the configuration in Fig. 10, the effect of varying the input power on the diameter of the beam coming out of the glass was documented. The experimental setup consisted of a 10 cm focal length lens and a 0.412 cm sample of APG-2 were used at a distance of 10.0 cm from center to center, and a distance of 5.0 cm from glass center to camera. A disk with variable neutral density coating allowed us to vary the intensity of the beam incident on the camera to keep the picture from saturating. Using a digital CCD camera system (Big Sky BeamView Analyzer), the Gaussian radius as a function of the power absorbed was documented. This experiment was performed with the glass 1.8 cm to the left of focus, at focus, and 1.2 cm to the right of focus. Fig. 11 displays what happens to the output beam for the above conditions. When the glass is to the left of focus, the thermal lens causes the beam to focus sooner and thus to expand along a greater distance - effectively enlarging the beam. When the glass is to the right of focus, the beam focuses again and thus expands along a smaller distance - effectively shrinking the beam. When the glass is at the center of focus, the effect changes with the focal power of the lens. At low power, the lens is small and the beam focuses again - effectively shrinking the beam. At high power the lens is so strong that it focuses the beam sooner - effectively enlarging the beam. The raw data are depicted in Fig. 12, where we see the tendencies indicated in Fig. 11.

In an attempt to counteract the lensing effect observed in APG-2, the glass was cooled. By sandwiching a 1 mm x 5.14 mm x 10.0 mm piece of APG-2 between two sheets of Indium and then between two water cooled stainless steel blocks, we could hold the outer surface of the glass at approximately 20 degrees Celsius. In Fig. 13, we see that the effect of cooling on the change in beam diameter is negligible. Please note however, that the change from a bulk slab of APG-2 (10 mm x 5.14 mm x 10 mm) to the thin slab does seem to have an effect that could be used in some cavity configurations to compensate for part of the thermal lensing caused by pumping conditions in APG-2.

Finally, in order to compare the measured beam diameters directly to the theoretical focal

lengths, we need to related the focal length to beam diameter. Using ABCD matrices[11] to represent the optical elements in the beam measurement setup, the beam diameters can be related to effective focal lengths in the glass. Referring to Fig. 14, the following matrix calculation was used to obtain our results:

$$\begin{pmatrix} \theta_o \\ d_o \end{pmatrix} = M_1M_2M_3M_4M_5M_6M_7M_8 \begin{pmatrix} \theta_i \\ d_i \end{pmatrix} , \quad (3)$$

where a_o is the incident angle of the light onto the lens, d_o is the incident diameter of the beam on the lens, a_i is the incident angle of the beam onto the camera, d_i is the incident diameter of the beam on the camera, M_1 is the refraction into the lens, M_2 is the transmission through the lens, M_3 is the refraction out of the lens, M_4 is the transmission to the glass, M_5 is the refraction into the glass, M_6 is the transmission through the glass, M_7 is the refraction out of the glass and M_8 is the transmission to the camera. We solve these for the effective curvature of both surfaces of the glass. Our only assumption is that these radii are equal, but this is reasonable for lengths less than 0.600 cm, where the absorption along the glass is approximately linear . This yields a value for d_o in terms of the radii of the glass thermal lens:

$$\begin{aligned} d_i &= D_{45}a + \frac{aD_{45}D_{34}(n_3-1)}{n_3R_3} + \frac{bD_{45}(n_3-1)}{R_3} + \frac{aD_{34}}{n_3} + b \\ b &= \frac{d_oD_{23}(1-n_2)}{R_1} + \frac{d_oD_{12}(1-n_2)}{n_2R_1} + d_o \\ a &= \frac{d_o(1-n_2)}{R_1} + \frac{b(1-n_3)}{R_2} \end{aligned} , \quad (4)$$

where n_1 is the index of refraction of air, n_2 is the index of the lens, n_3 is the index of APG-2, R_1 is the radius of curvature of the lens, R_2 is the radius of curvature of the front surface of the APG-2, R_3 is the radius of curvature of the back surface of the APG-2 (we set $R_2 = R_3$), D_{12} is the thickness of the lens, D_{23} is the distance between the lens and the

glass, D_{34} is the thickness of the APG-2, and D_{45} is the distance to the image plane, as depicted in Fig. 14. By using this solution to convert the beam diameters to focal lengths, a direct comparison to theory is now possible. Fig. 15 displays the line of theory on top of the data points of experiment. The experimental data approximate a straight line which implies simple lensing. These points also approximate the line of theory which validates Equation 2 and the assumptions made to use that equation. The modeling had only one adjustable parameter, r_o = 0.0090 cm. Thus, the theory can be used in the future to closely approximate the thermally induced focal length in laser pumped APG-2.

In summary, the high thermal figure of merit was verified for the first time experimentally, by thermally loading the different glass samples. APG-2 was confirmed as the toughest laser glass available to date. APG-2 was lased for the first time, and the efficiency was found to be surprisingly low, presumeably due in part to thermal lensing. This thermal lens was modeled and quantified for the first time experimentally. The lens, which precluded continuous pumping implied that concentric and even confocal cavity designs will be inefficient and unstable. However, other cavity geometries, such as zig-zag slab lasers or disc lasers, which pump APG-2 in a manner which negates the effect of a thermal lens will lase more efficiently while taking advantage of APG-2's thermomechanical strength.

References

(1) U. Keller, T.H. Chiu, and J.F. Ferguson. "Self-starting femptosecond mode-locked Nd:glass laser that uses intracavity saturable absorbers." Opt. Lett. **18**, 1077-9, (1993).

(2) G. Wilke. Advanced Solid-State Lasers Group, Lawrence Livermore National Laboratory. (emission plots for APG-2)

(3) S. Payne and G. Wilke. "Improved high-average power Nd-doped phosphate glass II." Lawrence Livermore National Laboratory Internal Report. 4, July 20, 1993.

(4) L. Smith. Advanced Solid State Lasers Group, Lawrence Livermore National Laboratory. (efficiency equations)

(5) W. Koechner. "Thermal Lensing in a Nd:YAG Laser Rod." Appl. Opt. **9**, 2548-53, (1970).

(6) D.W. Hughes, J.R.M. Barr, D.C. Hanna. "A high power, high efficiency, laser-diode-pumped, continuous wave miniature Nd:glass laser." Opt. Comm. **84**, 401-8, (1991).

(7) J. S. Uppal and J.C. Monga "Contribution of stress-dependent variation of refractive index to thermal lensing in Nd:glass laser rods." Appl. Opt. **24**, 3690-2, (1985).

(8) Laser Glass Catalog. Schott Glass Technologies Inc. (1993).

(9) D. Sapak. "Photoelastic Equations." Schott Glass Technologies Inc.. (1993).

(10) L. DeLoach. Advanced Solid State Lasers Group, Lawrence Livermore National Laboratory. (value of dn/dT for APG-2)

(11) Klein, V. Miles, and T.E. Furtak. *Optics*. 151-64, (John Wiley & Sons, Inc., New York, 1896).

Figure Captions

Table I Thermal and Mechanical constants of APG-2, APG-1, and LG-750.

Fig.1 Relative emission versus wavelength comparing bandwidth at along peak lasing wavelengths.

Fig. 2 Energy density versus fracture threshold comparison of laser glasses.

Fig. 3 Laser optimization setup

Fig. 4 Power output versus power absorbed slope efficiency with a 1.55% output coupler.

Fig. 5 Power output versus power absorbed slope efficiency with a 5.9% output coupler.

Fig. 6 Power output versus power absorbed slope efficiency with a 16.07% output coupler.

Fig. 7 Inverse intrinsic slope efficiency versus inverse output coupling showing losses and experimental limit.

Fig. 8 Power output versus power absorbed slope efficiency comparison of APG-2, APG-1, and LG-750.

Fig. 9 Inverse focal length versus power absorbed comparing lensing strength of APG-2, APG-1, LG-750, and LG-760.

Fig. 10 Setup for measuring beam diameter

Fig. 11 The effect of moving the thermal lens through focus.

Fig. 12 Beam diameter versus power absorbed for APG-2 to the left, at center, and to the right of focus.

Fig. 13 Beam diameter versus power absorbed for APG-2 cooling comparison.

Fig. 14 Ray-tracing diagram for beam diameter measurement

Fig. 15 Inverse focal length versus power absorbed comparing theoretical and experimental thermal lens values.

Table I

Properties	LG-750	APG-1	APG-2
k (W/m^{o}C), 90^{o}C	0.51	0.85	0.86
K_{1c} (MPa&m$^{1/2}$)	0.40	0.60	0.80
a (10^{-7}/^{o}C), 20-300^{o}C	131	98.4	63.8
E (GPa)	50.0	71.0	64.4
$FOM_{th} = 10^{4}\&kK_{1c}/aE$	0.31	0.73	1.67

Fig. 1

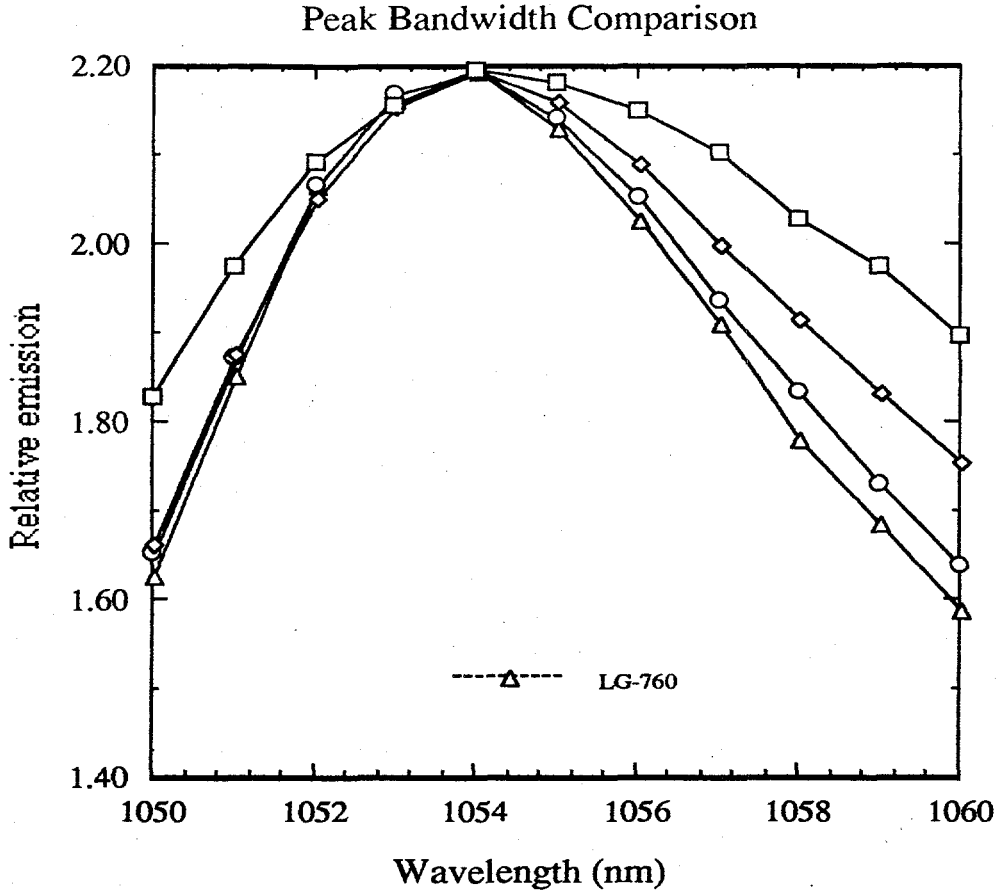

Fig. 2

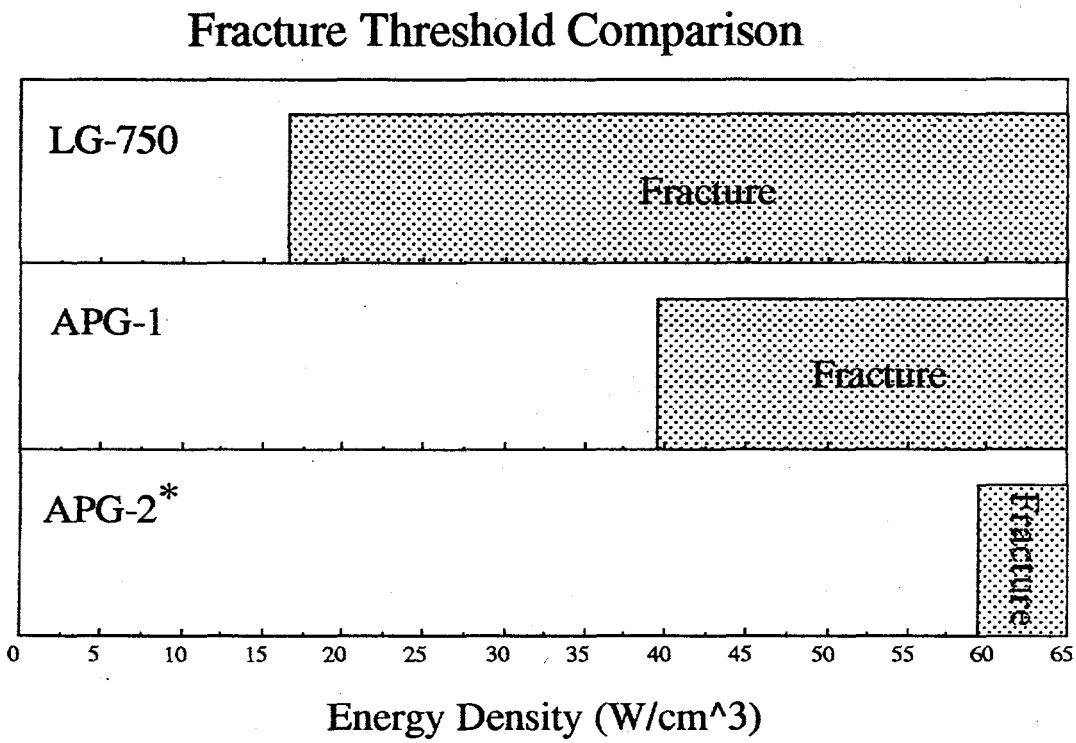

*APG-2 typically melts before it fractures.

Fig. 3

Laser Optimization Setup

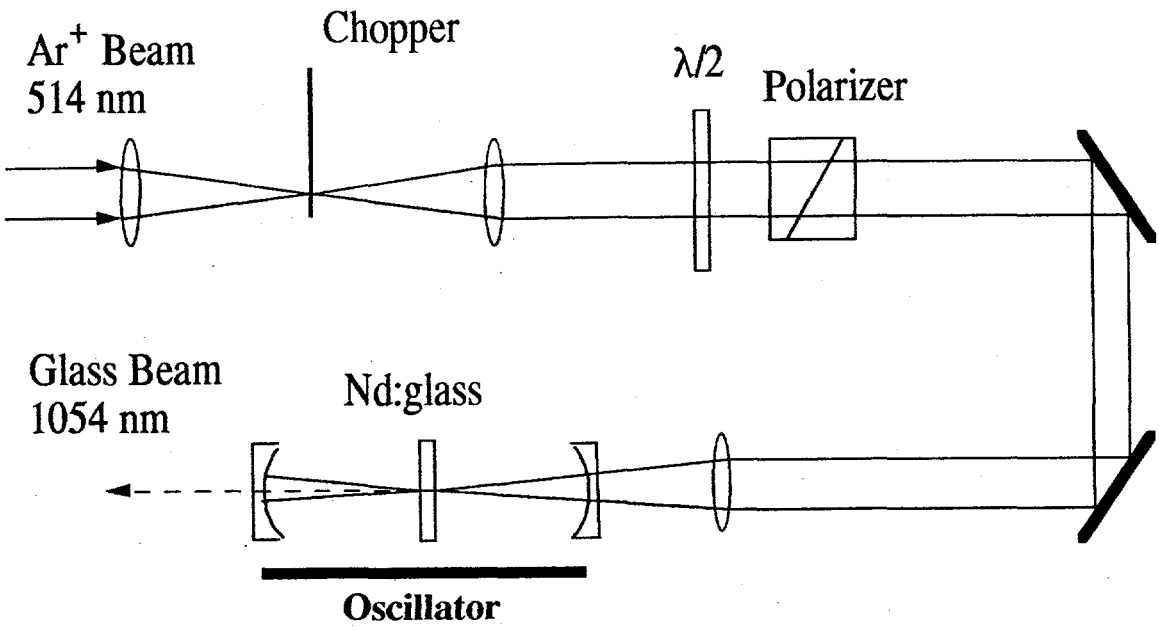

Fig. 4

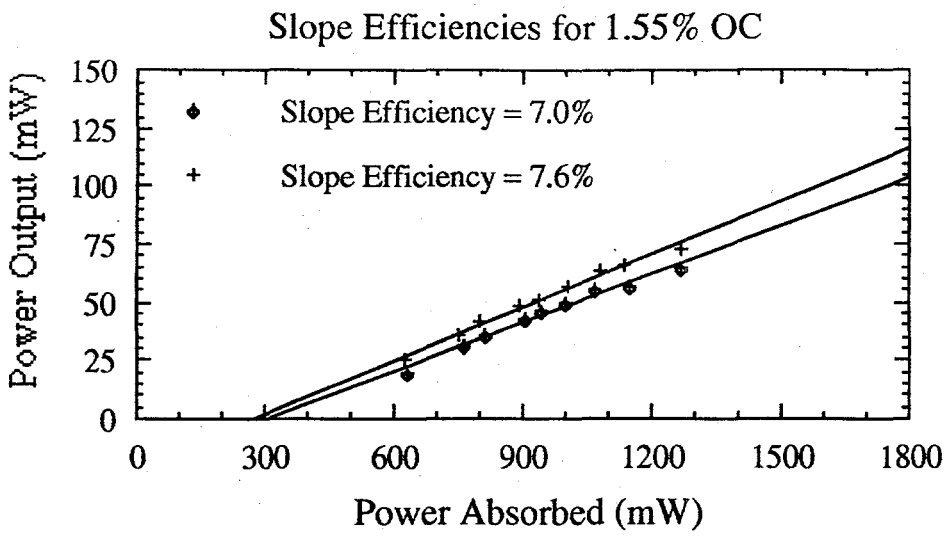

Fig. 5

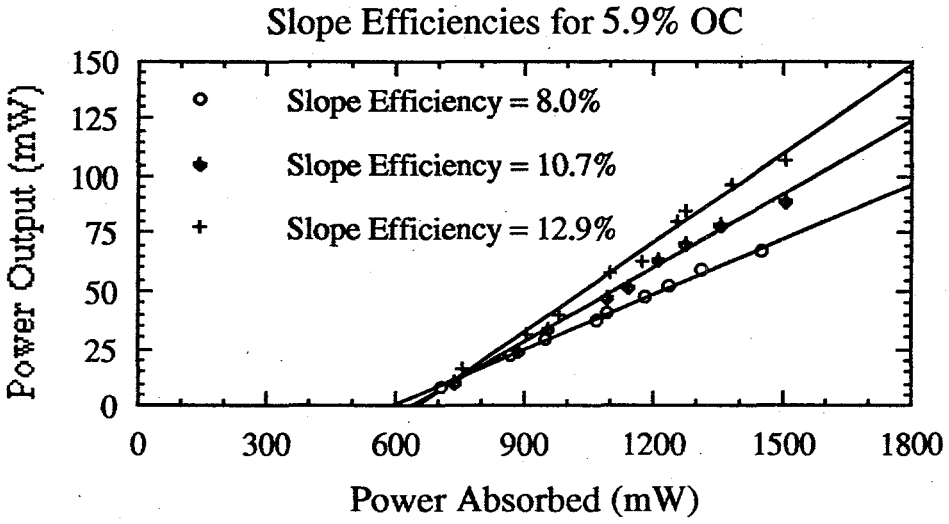

Fig. 6

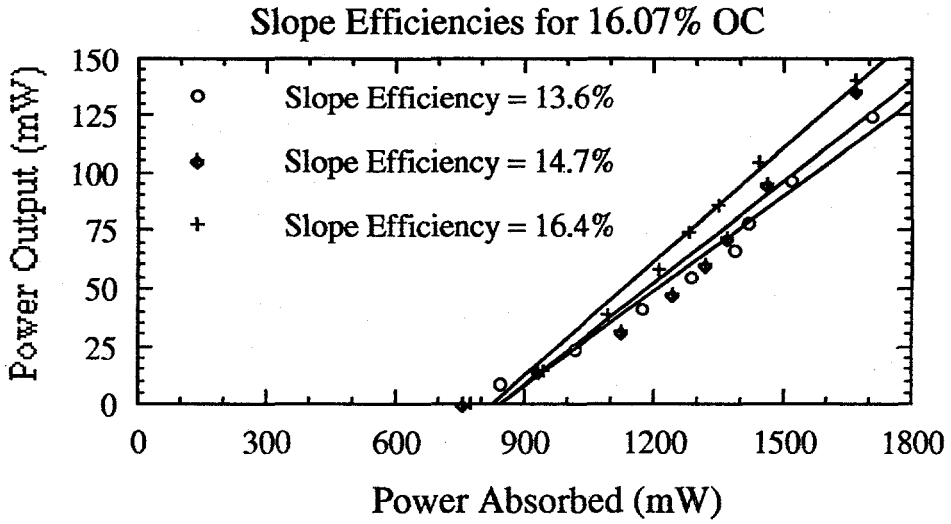

Fig. 7

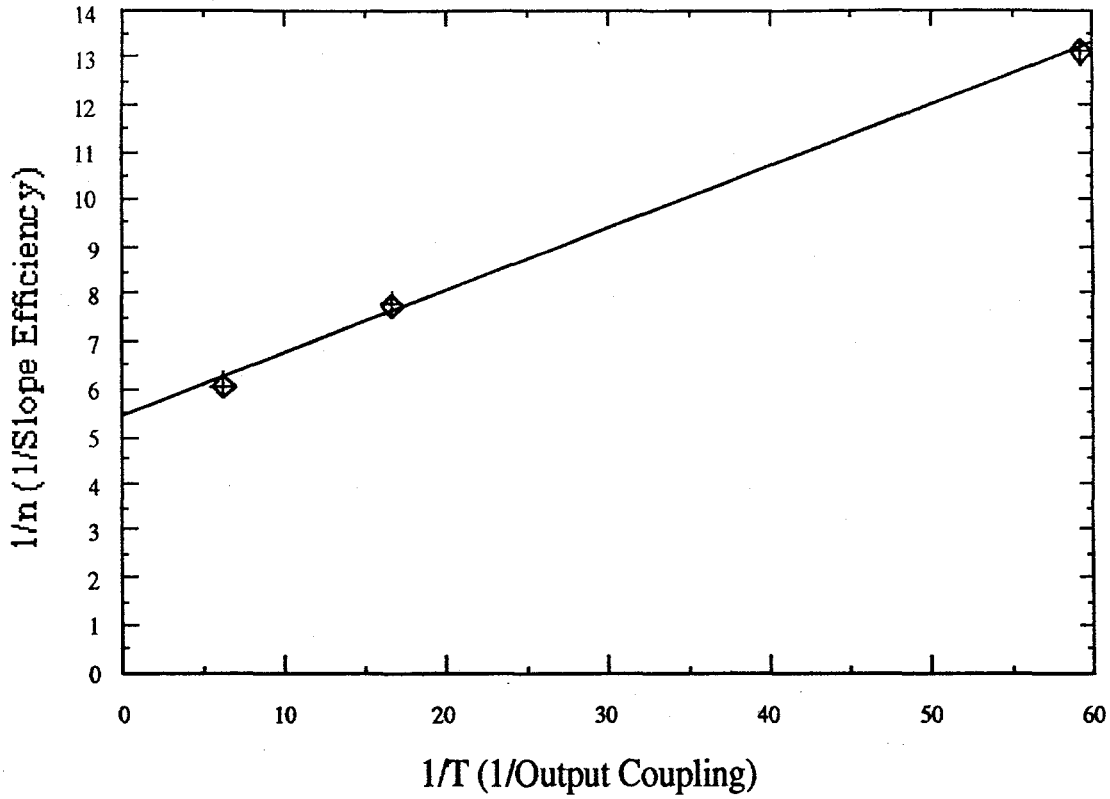
Intrinsic Slope Efficiency
1/η (1/Slope Efficiency)
1/T (1/Output Coupling)
0
1
2
3
4
5
6
7
8
9
10
11
12
13
14
0
10
20
30
40
50
60

Fig. 8

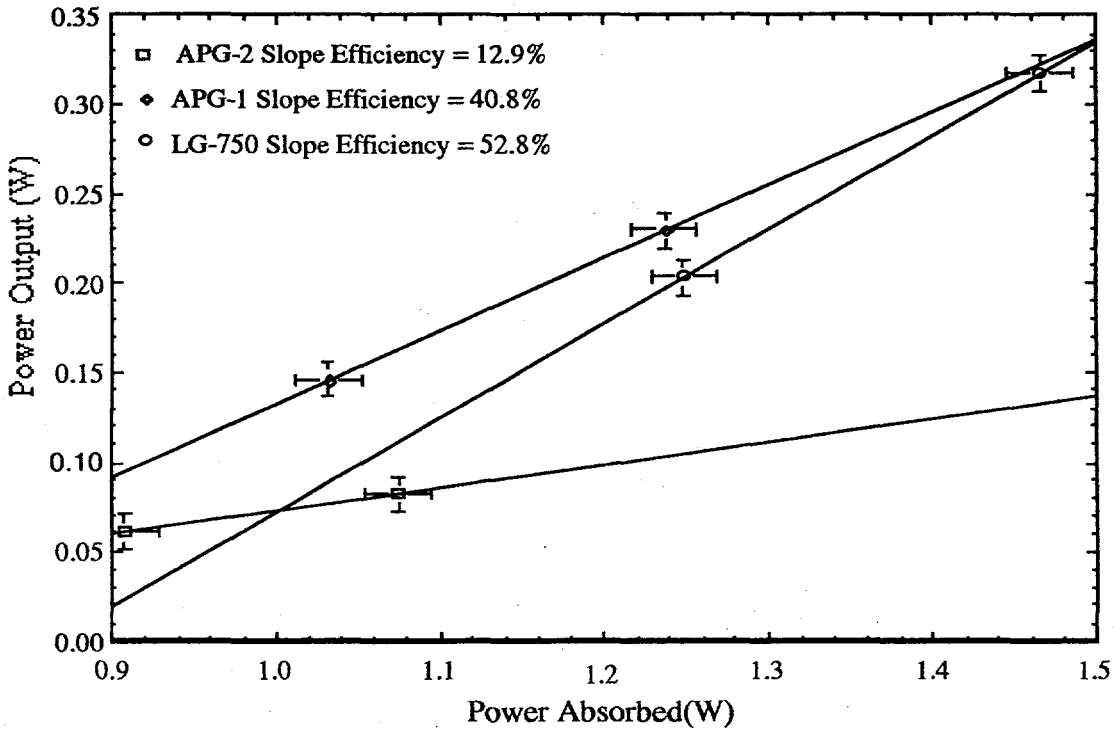
Slope Efficiency and Absorption Comparison
APG-2 Slope Efficiency = 12.9%
APG-1 Slope Efficiency = 40.8%
LG-750 Slope Efficiency = 52.8%
Power Output (W)
Power Absorbed(W)
0.00
0.05
0.10
0.15
0.20
0.25
0.30
0.35
0.9
1.0
1.1
1.2
1.3
1.4
1.5

Fig. 9 Theoretical Thermal Lens Comparison

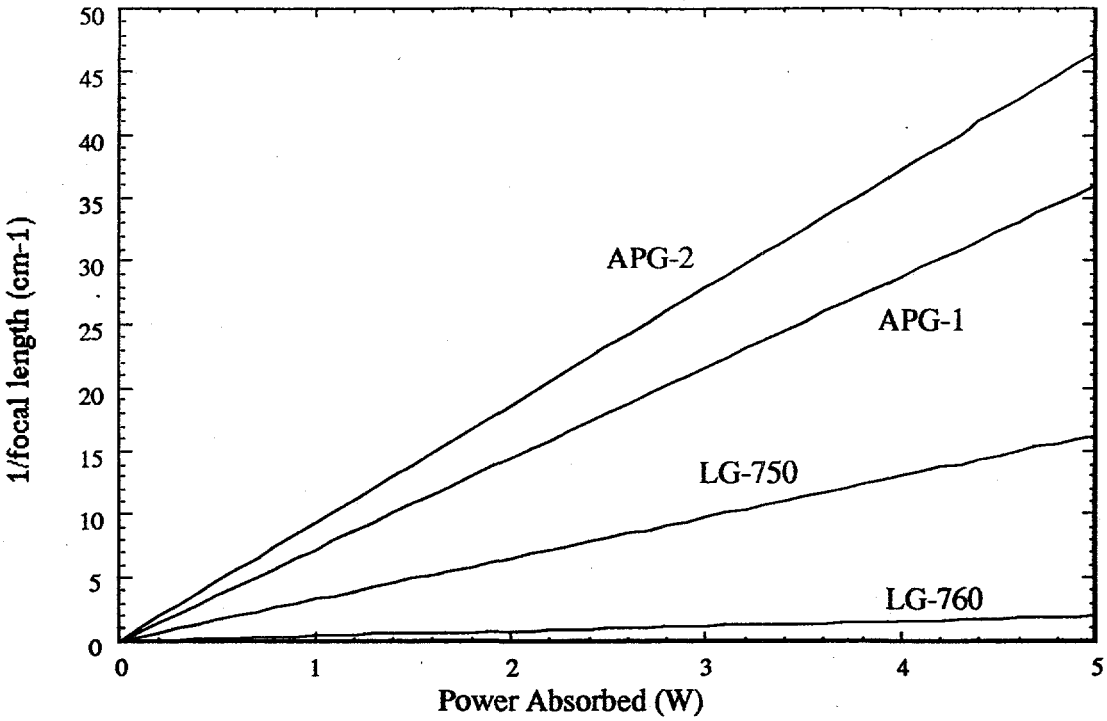

Fig. 10 Setup for measuring beam diameter

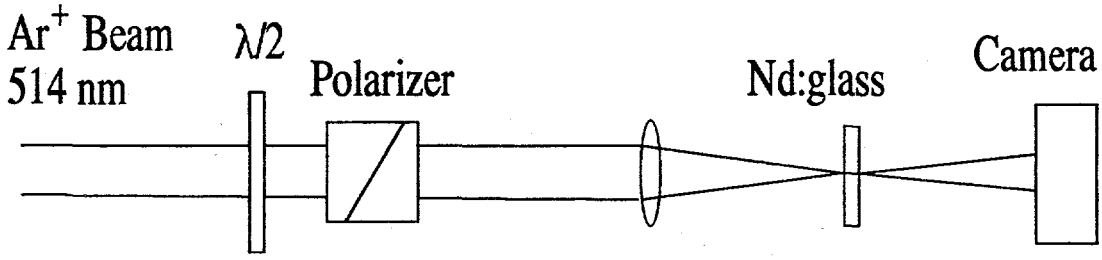

Fig. 11

Effect of Lens on Beam Diameter

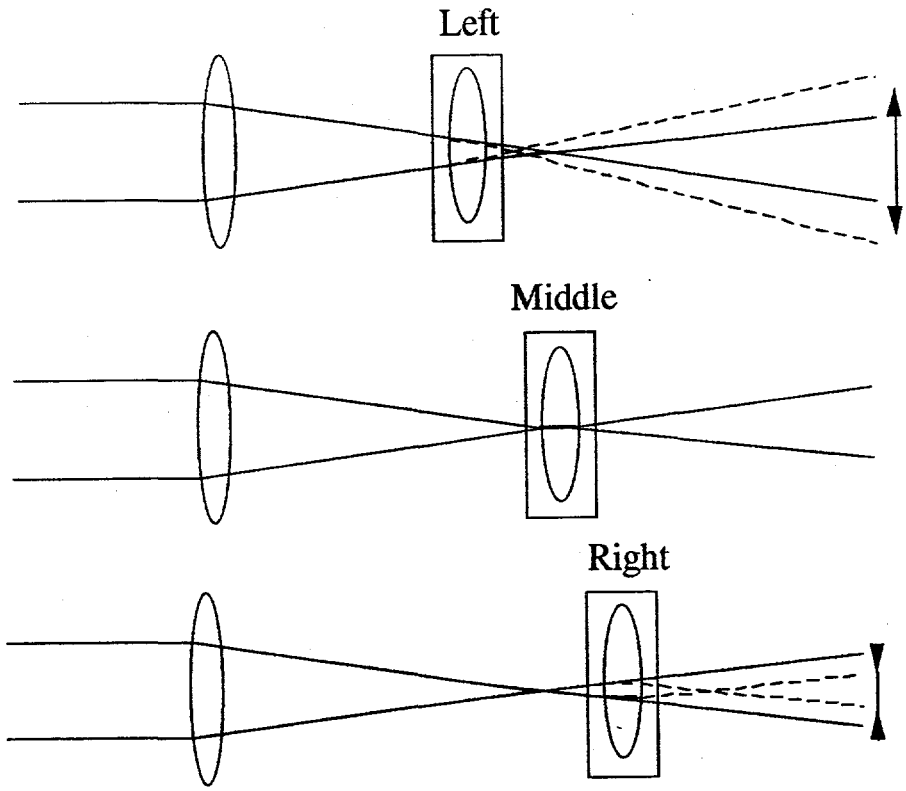

Fig. 12

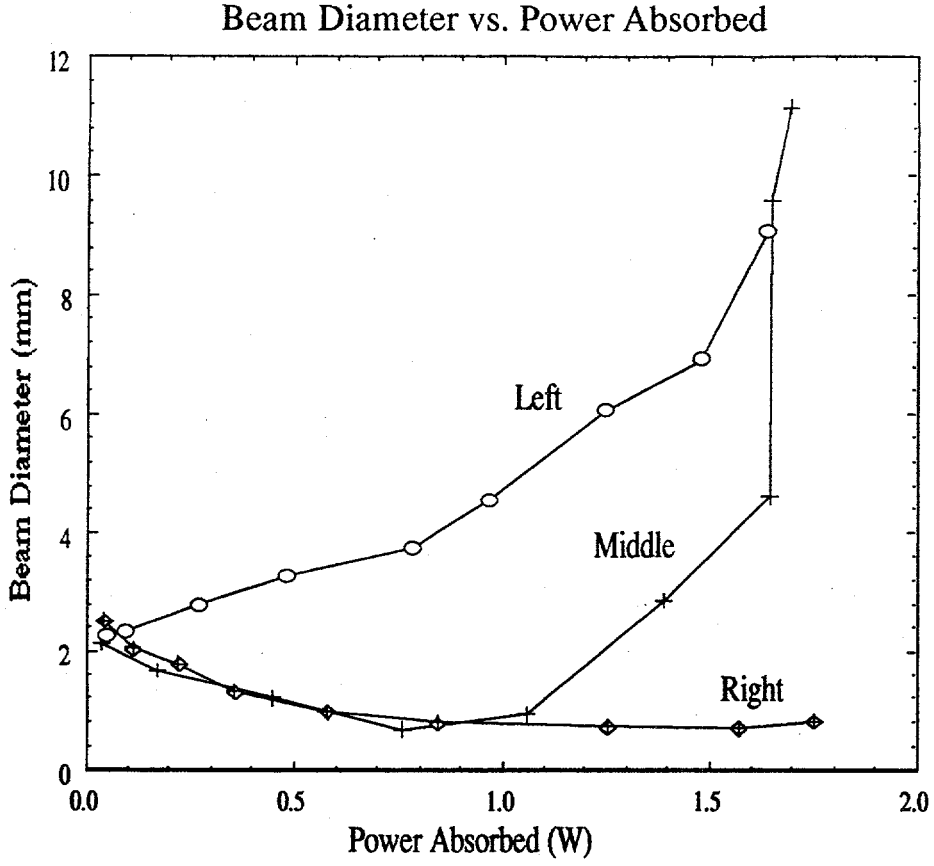
Beam Diameter vs. Power Absorbed
Beam Diameter (mm)
Power Absorbed (W)
Left
Middle
Right
0
2
4
6
8
10
12
0.0
0.5
1.0
1.5
2.0

Fig. 13

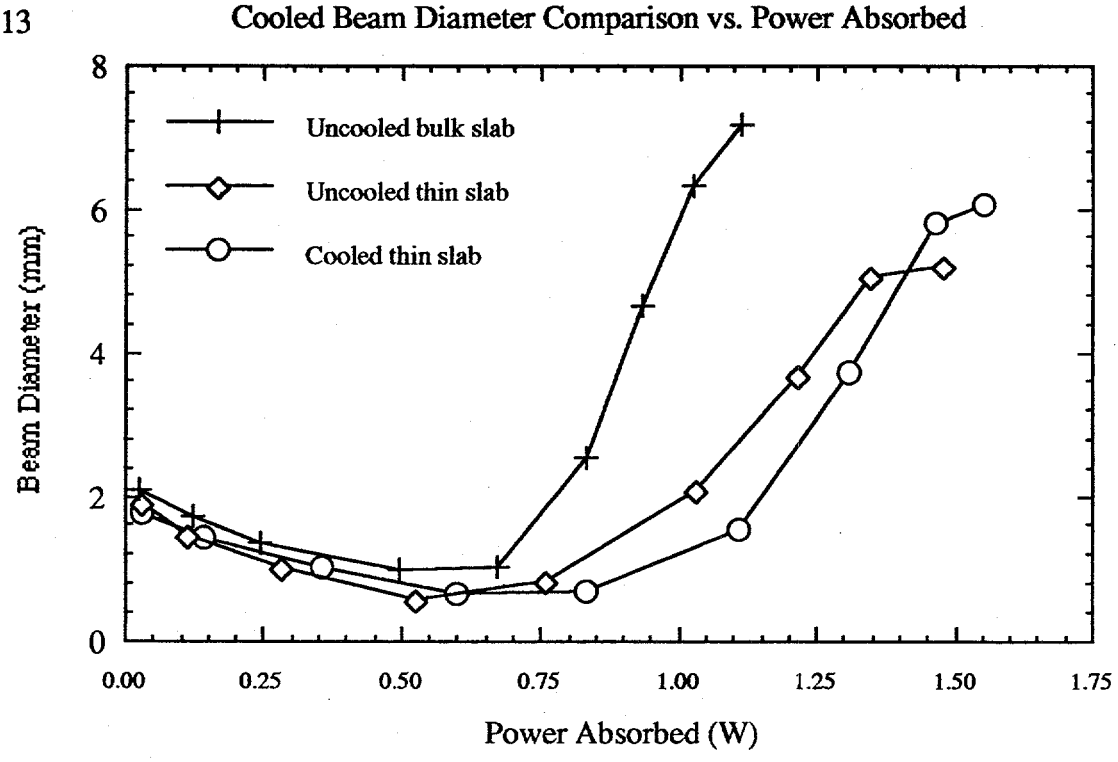
Cooled Beam Diameter Comparison vs. Power Absorbed
Beam Diameter (mm)
Power Absorbed (W)
Uncooled bulk slab
Uncooled thin slab
Cooled thin slab
0
2
4
6
8
0.00
0.25
0.50
0.75
1.00
1.25
1.50
1.75

Fig. 14

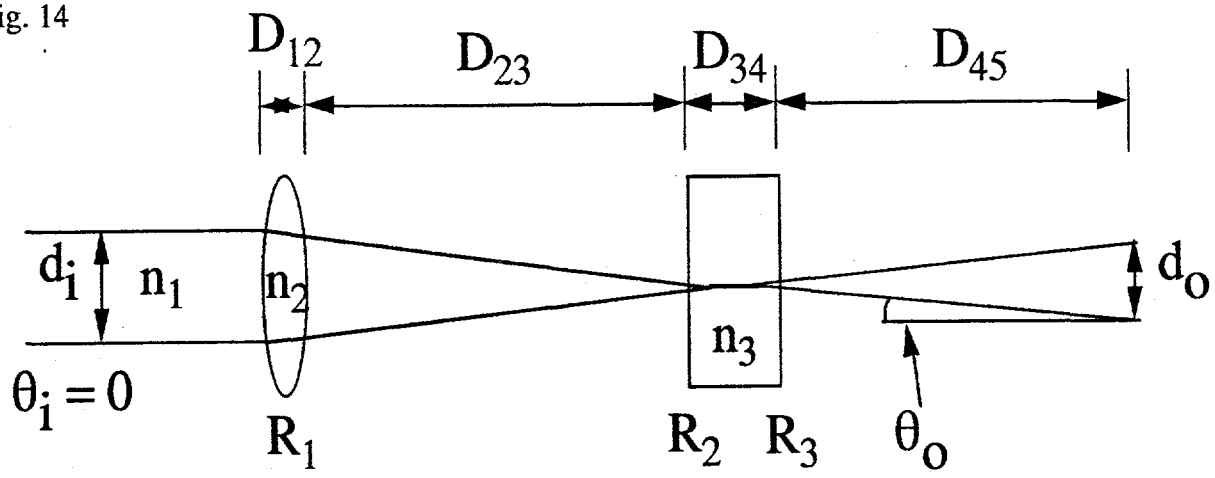
D12
D23
D34
D45
di
n1
n2
n3
do
θi = 0
R1
R2
R3
θo

Fig. 15

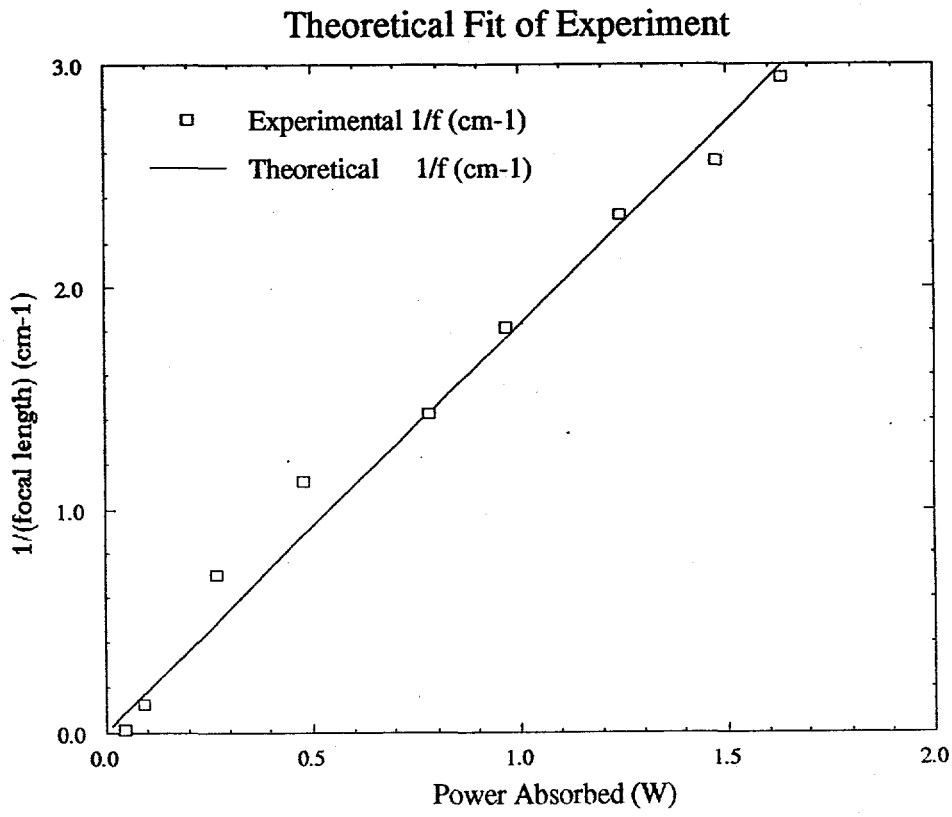
Theoretical Fit of Experiment
Experimental 1/f (cm-1)
Theoretical 1/f (cm-1)
1/(focal length) (cm-1)
Power Absorbed (W)
3.0
2.0
1.0
0.0
0.0
0.5
1.0
1.5
2.0

Making a Height Field Editor for WireMan*

Jennifer Cano

Wayne State University

Lawrence Livermore National Laboratory
Livermore, California 94550

Dec 15, 1993

Prepared in partial fulfillment for the requirements of the Science and Engineering Research Semester under the direction of Brian Lindow, Research Mentor, at the Lawrence Livermore National Laboratory.

*This research was supported in part by an appointment to the U.S. Department of Energy Science and Engineering Research Semester (hereinafter called SERS) program administered by LLNL under Contract W-7405-Eng-48 with Lawrence Livermore Nationall Laboratory.

Making a Height Field Editor for WireMan

Jennifer Cano

Wayne State University

Computations Division

ABSTRACT

The goal of this paper is to inform and educate the reader about a new editor for WireMan which will soon be made available to users. The editor is for the Height Field, a figure previously unalterable, which will give the user the ability to change the appearance of this figure. This paper outlines problems which occurred during the making of this editor as well.

Introduction to WireMan and its Height Field

Wireman is shareware made available through DOE to the general public. It has been used in classrooms across the United States to illustrate three dimensional geometry for high school and elementary school students. WireMan allows users to draw in three dimensions by selecting wire figures (such as cones, spheres, cylinders, height field, etc.) from its menu and then moving these figures to specific locations in space. Through this kind of three dimensional drawing, students learn how to build objects in relation to space .

After all the selected figures are placed where the user wants them, he or she can then take snapshots of the picture and move the objects around to create an illusion of motion. A movie is generated by storing the snapshots in what is called a "fly" file of the format "*filename* . fly". An object file can also be created of the format "*filename* .wm". This stores all the figures used and their locations in space at the time of saving it. The .fly file is then uploaded to the National Education Sciences (NES) Supercomputer to allow the raytracer to finish off the movie by adding the colors and textures, specified by the user, to the figures. It is also possible to generate, instead of a movie, the fortran program which controls the raytracing of the movie and ultimately the movie itself upon compilation.

Since most figures, except possibly the height field, in Wireman are self explanitory, I have decided also to include a short introduction to the height field, since it will be the focus of this paper.

The height field in wireman appears as a wire plane. The user can stretch and move this plane according to the picture which he or she wants to create. It is over this plane that the height field currently graphs the equation : $2\cos(x) * \tan(z)$ between the range -2π to 2π for x and z. What the height field does is draw a line from the point

(x,z) on the plane to the indicated point in space (at height y, as described by the equation). It is possible to get WireMan to draw other curves by generating the Fortran program instead of the movie and then changing the equation in the fortran program which controls the height field. Mathematics and geometry teachers have continually requested that changing the height field be made more accessable for younger students, who usually do not have the programming knowledge nessasary to make those changes. This project's goal is to create an editor which will simplify the process of changing the height field.

Project Background

This project was initiated as a request from elementary and high school teachers who have found the height field to be an important figure in WireMan but too difficult to alter. The height field editor suggested was to be constructed with easy to understand interfaces using dialogs and menus.

The height field is the result of values contained within a two dimensional array (513 by 513), so, creating an editor for the height field means designing a way to manipulate the generation of these 263,169 numbers. There were originally four different ways the height field editor could have been constructed : by selecting an equation, making an equation, using a matrix or grid , or using a paint which would correlate heights of the figure with colors.

The first method was to generate the height field by an equation pre-selected by the programmer (i.e., the programmer would decide what equations would be useful and then gives the user the option to select from listed equations). The first method is the easiest because upon examination of the Fortran code (fig. 1) of WireMan, the only

change which would have to be made would be a few (or perhaps many, depending on the number of equations the programmer made available to the user) "if" or "case" statements. Below is displayed the segment of code which controls the use of the equation. The two dimensional array could just as easily be altered by allowing a control variable to dictate which equation to use.

```
subroutine mheigh(ihei,hdata)
      real hdata(-256:256,-256:256)

      do 10 ix = -256,256
       do 20 iz = -256,256
         x = real(ix)/256.*2.*3.141592653
         z = real(iz)/256.*2.*3.141592653
         hdata(ix,iz) = 2* cos(x)* tan(z)
20       continue
10     continue
      return
      end
```

Fig.1 Fortran code which controls the appearance of the height field

---

The second method the height field could be generated by is the "create your own equation method". This method is considerably difficult than the first in that the programmer has to face the problems of operation precedence and equation evaluation. An even larger problem arose when I considered allowing the user to type in the needed equation. It became apparant that the user may try to apply a

function which was not available or else mispell those which were. However, this second method is better than the first because it allows the user the freedom to create the height field through the equation he or she wants without having to spend the time searching through a list or else not finding the needed equation alltogether.

The third proposed method to generate the height field was through use of a matrix of real numbers . Thiswould more likely accompany rather than substitute the equation builder. The individual using WireMan, then, could create a curve without having to know the specific equation which describes the curve (such in the case of elementary school children) but knowing the equation for the curve would be equally valuable. The matrix would be a 10x10 matrix allowing for smaller nxn matrices, however, up to a 100x100 would be able to be created by altering the data file.

The fourth method would be a visual editor, much like a paint program with colors indicating the height or depth of a point off the plane. Although I didn't touch upon this portion during my semester, it was explained to me. The colors would range from white to black and vary in either a series of red or blue hues. A certain color of blue, for example, would be set to the plane (or altitude 0) darker colors would indicate negative values and lighter colors higher values. The maximum and minimum heights would need to be defined either by the user or the programmer. This would be the one restriction of using this type of editor. Because it is not as tedious as a user input matrix (third method) it could be placed over a larger matrix (perhaps a 200x200 grid size) and would be a more accurate description.

Programming Methods

Writing the code for the new height field editor presented a few problems to me, these were: I had very little programming experience in C, which this project required, I had never programmed using Macintosh windows, and I had never worked on modifying another programmer's code. Thus, the first 4 to 6 weeks of the project was spent reading and learning C programming methods (the code of the program is written using the ThinkC editor) and windows. The first two problems resolved, I worked on the third by familiarizing myself with WireMan's code and the program's structure and documentation.

After I obtained the clearly defined problem of the height field editor, I started work on simpler problems which could be built upon to create the height field editor. Primarily, this editor was a number generator and reader. The generator would work off the WireMan program directly through the use of menus and dialogs and would create a file containing information about the height field. The reader would work with the Xwire program on the NES by exchanging the file's contents for the 513x513 array needed.

The first draft of the program was a simple number generator and reader from a single dimensional array. In the first draft the number generator simply figured the equation's value according to some variable 'x' into a single array and printed the array to a file. Then the results would be read in. During this program I learned more about manipulating data files in C. I encountered very few errors, and those which I did were easily corrected.

After this proved successful, I put the different funcitons of the program into procedures and built upon them.Eventually, I was able to accept user input to determine one of three equations to evaluate data over a range for x and z. The user

was then also allowed to choose the range. This simulated the "simple equation" or first approach to the height field editor where the equations would not be determined by the user.

After having modified the program to accept changes to the equation and the range, I worked on storing and generating values by a two dimensional array. Hoping later be able to get it to easily conform to the structure I saw in the Fortran program.

At this time I was fairly tired of programming and reprogramming thenumber reader and generator, so I began working on the interfaces for Wireman. I started by designing the dialog boxes which would be used as the new addtions were made. The design I had most difficulty with was the design of the ranges and equations dialog. Should both of these be written in one dialog box? I started by first making them their own dialogs and items on the height field menu. Later, it became obvious that the two needed to be combined because the other functions to set the height ranges would not use altering x and z ranges (the ranges would have no effect on neither the matrix nor color height fields). The choice to set the height field by equation remained, and the range selector became a subdialog to this.

I also programmed in sections of the Wireman code called dialog.c (the section of WireMan code dealing with dialog display) and inits.c (the initialization segment). The goal was to display and preform excercises on accepting input from the windows I was creating. I was successful in the integration of the dialogs throughout my portion of the program because calls to display and draw functionality from the dialogs already existed in many places. It became a case of duplicating them.

After adding the menus and dialog boxes (which at this point included a new height field menu, and a "set ranges", "set equation" and " matrix" dialog, the latter designed by Brian Lindow) into the code, it was nessasary to make possible the alterations to the height field through these interfaces. In other words, the output file of

the generated should be easily controlled by the dialogs. Each change made to the ranges or equations, would be saved in variables and written to a file only when the final "Ok" or "Cancel" button was hit for that dialog.

After working on it for a couple of weeks, the bugs were corrected and the changes reflected in the data file were done only for the equation being of the "pick from a list" sort and varying ranges (including writing own ranges in). From there, I moved on to design and code the portion of the program which would deal with the matrix. As before, I began with a very simple example.

I started with a small one-dimensional array which was to be put in a larger one-dimensional array and then the blank entries were to be filled in accordingly. For example, if the smaller array had three elements and the larger had nine, the three elements would be put in locations 1,5 and 9. If these three elements contained the values of 0 at location one and 8 at location five , the value at location two would be 2, at location three, 4 and at location four, 6. This is how the two dimensional matrices were planned to be. Stored in the data file, if the user wanted to determine the height field by matrix, would be a 10x10 matrix, no matter what the size of the smaller matrix was (i.e. input by the user, this could be anything from a 2x2 to a 9x9 matrix would be expanded to a 10x10 matrix and this, in turn, would be expanded to a 513x513 in the final reader).

After getting the matrix reader/writer to work, I began work on the equation builder part of the program. This I started with the dialog box design (Fig 2) and then worked on the code. By this time, I had changed all the related height field manipulating code into its own segment and took out the portions I had written in the Dialog.c segment. The new segment is called HFchanger.c. Also, at this point, most of the functions were clearly defined (for complete function definitions see the guide to the programming code, Apendix I).

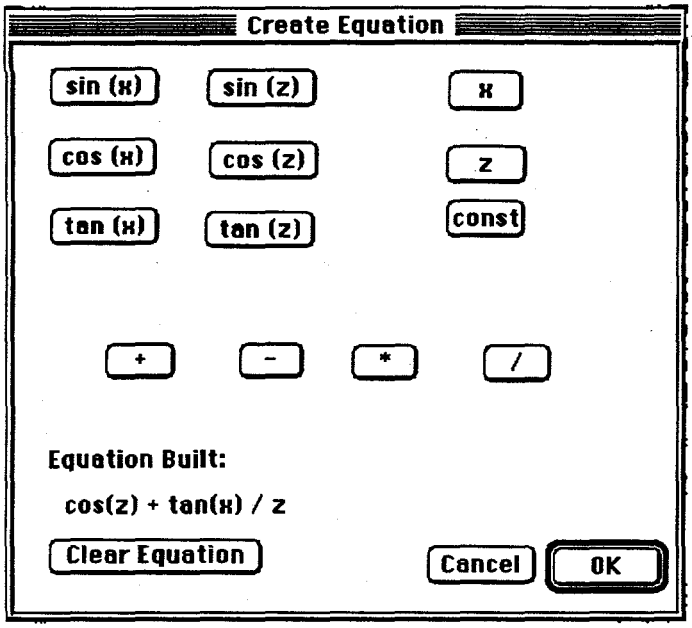

Fig 2. Dialog for equation builder

After designing the dialog boxes, I immediately got the equation display of the dialog to work. Each of the functions and operations available was defined as a specific number and stored in a single dimensional array. The decoder (or reader) would then have to figurre out the equation by the numbers entered in the array. Most of my time spent on this portion was in testing for correct output in both the data file and the final answer.

Generator Output / Reader Input

To be able to extract a final answer, I was also working on the reader at the same time. For this, I had to standardize the output to the data file throughout the program. The current output of the program is of the form:

Integer: between one and five. One through three indicates a simple preset equation. Four is a built equation, and five is a matrix.

Integer: If the first number is a four, then this number will be present as well. This number indicates the number of entries in the array to store the different functions and operations.

Floats: If the first number is one to four, they will then be followed by four real numbers: the bottom boundary of the x axis, the top boundary of the x axis, the bottom boundary of the z axis, and the top boundary of the z axis.

Data: If the first integer is a four, what then follows is the single dimensional array which indicates the sequence of functions and operands chosen. If the first integer was a five, what follows is a 10x10 matrix (either original or converted) which will later be converted to the 513x513.

The reader program is then to interpret the data as it is given and produce the two dimensional array (as seen in the Fortran code of Fig 1) which will control the height field. An initial entry of one through three sends the evaluation to a specific equation (equation chooser method), four to the equation builder, which decodes the array to produce the input equation, and five to the matrix expander.

Conclusions and Future Work

This project focused on a much needed function for WireMan, however, I was not able to complete all the work nessasary on this project. Still missing from the program code are the definitions of the cancel buttons in the dialogs, and the portions of the program which will actually "tie in" the changes to wireman. My mentor has suggested to "tie in" the file which will record the height field changes, to place it at the

end of the .fly file of wireman. Future programmers could add some notation to indicate that the values for the height field will be stored in another file should a height field exist in the set of objects. This change also has to be made with the object file as well. Currently, if a user saves an object file (or .wm file) , the changes for the height field are not included. In other words, when you bring up a saved .wm file, if a special height field were saved, the stardard has now taken its place.

Another addition to this portion of the program which should be made is adding a wire figure of the height field. This could be accomplished by adding a "view height field" option to the height field menu which would display the wire figure after altering it. Representing the height field by a plane in wireman is appropriate, but there should be someway you can look at the figure before you send it up to the NES because of the amount of work and time the ratracer needs to complete its work.

I hope these and other changes can be made to the WireMan program, it is a program which could expand into a very complex application with some hard work and dedication from its programmers.

Apendix 1(i)

Function Name	Operation preformed
HandleEqRngDialog	handles the dialog which appears when "Set Matrix By Equation" is chosen off the menu. Branches to range or equation setting dialogs
HandleRangeDialog	handles the range dialog called by the previous function
Set_Ranges	called by the HandleRangeDialog, it sets the values of the bottom and top boundaries of the range for x and z
Adjuster	called when ranges are entered by user rather than selected from the dialogs. It makes sure the smaller value is the lower boundary
WriteNewRange	this function writes the new range to the output file once a change is set
HandleEquationDialog	handles the equation dialog as called by HandleEqRngDialog
HandleEqChoiceDialog	handles the dialog for the equation builder, also creates the array which determines how the reader will build the equation later
GetWarning	issues a warning if incorrect or too many elements are put into the equation builder
WriteNewEquation	for preset equations, writes changes to the output file
HandleKonstDialog	when entering a constant for the equation builder, a dialog pops up.

Apendix 1 (ii)

Function Name	Operation preformed
	This handles the constant dialog
HandleTheGrid	Handles the 10x10 dialog box which appears when "set equation by matrix" is chosen from the menu
GetRowBox	Handles the dialog which appears to ask what size of dialog (10x10 or smaller) the user will be entering
DoMatrixStuff	called by HandleTheGrid, it organizes the sequence of events which the nxn to 10x10 matrix will follow
RetrieveMatrix	First function called by the previous, it gets the nxn matrix from the dialog according to the "n" entered in GetRowBox
PlaceTemp	Second function called by DoMatrixStuff, it places the nxn matrix in the appropriate locations throughout the 10x10 matrix
FinishMatrix	Finishes the 10x10 by directing the filling in of the rows and collumns
MatrixSetRow	Fills in the rows of the 10x10 matrix
MatrixSetCol	Fills in the collumns of the 10x10 matrix
HandleInfoDialog	Handles the dialog which appears when selecting "Get Height Field Info" off of the Height field menu

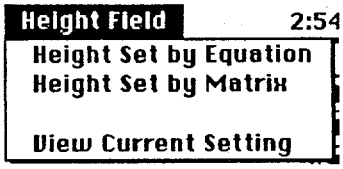

fig 2.1 height field menu

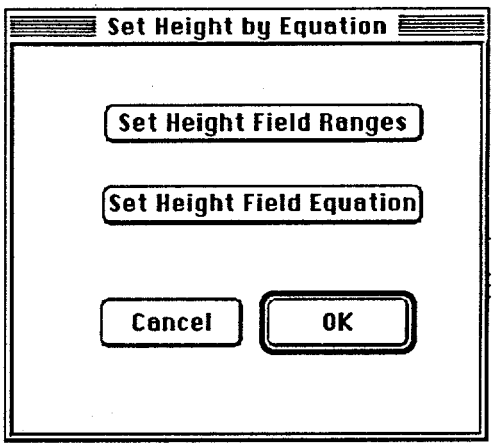

fig 2.3 Range and Equations dialog

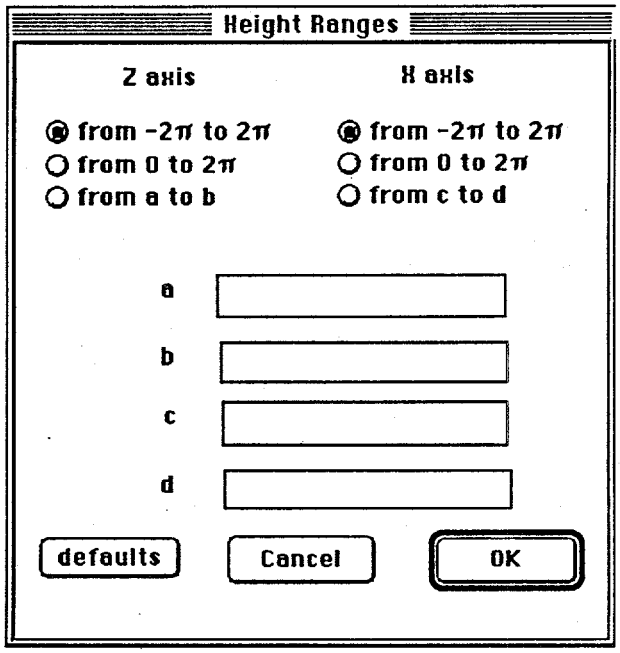

fig 2.2 set ranges dialog box

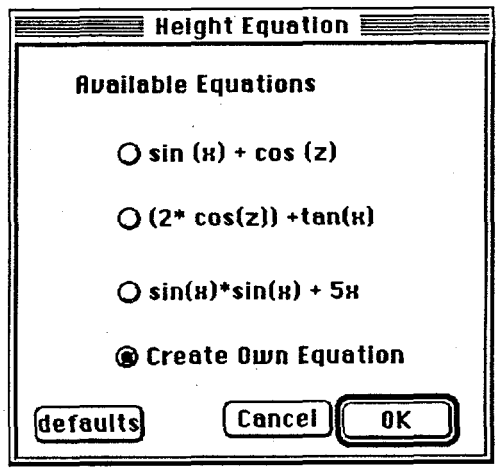

fig 3.3 set equations dialog box

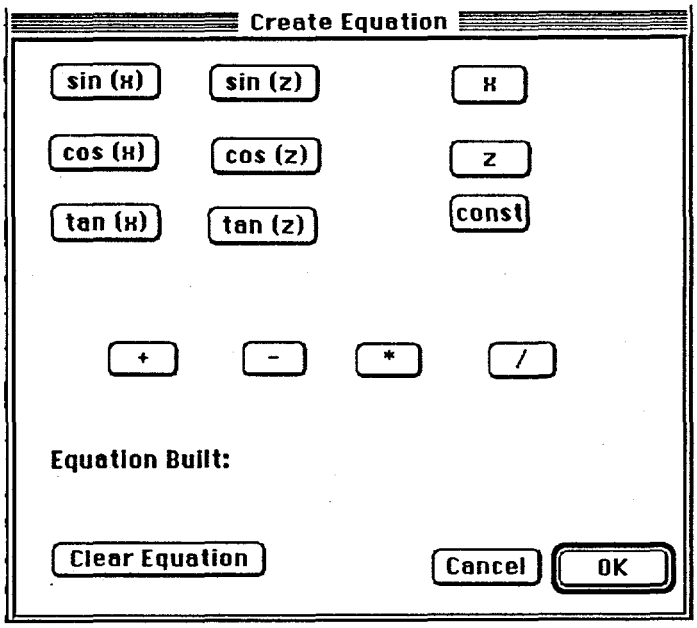

fig 2.4 build equation dialog box

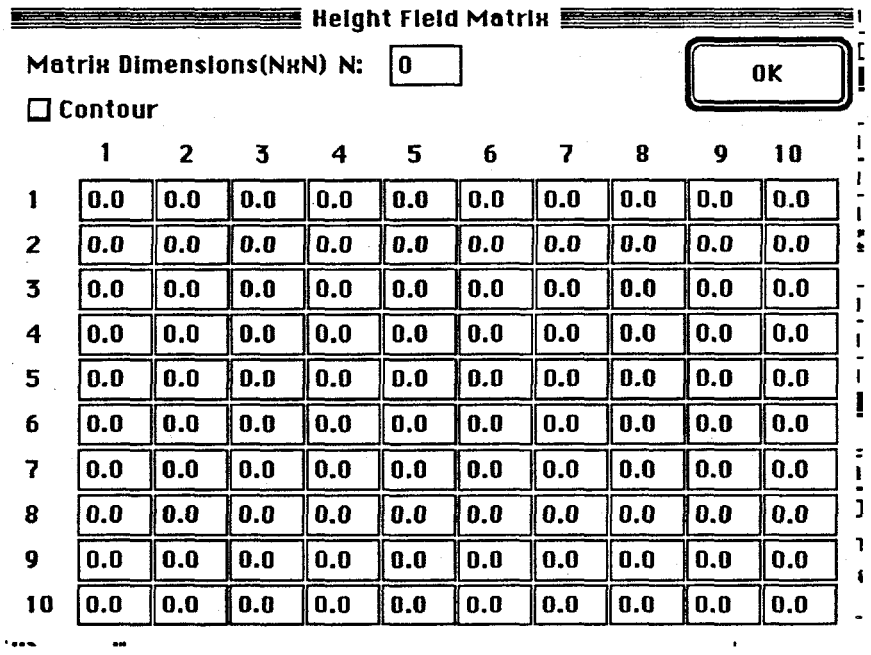

fig 2.5 set matrix dialog box

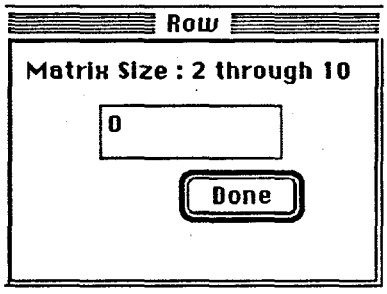

fig 2.6 get n for nxn matrix (2x2 to 10x10)

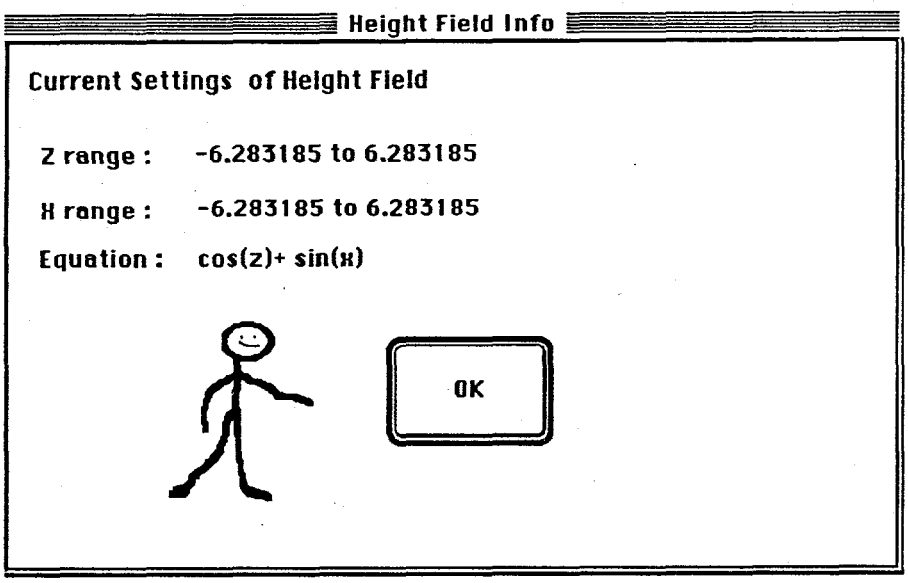

fig 2.7 get height field information dialog

Lead in Food and Food Containers*

Anna O. Chu

University of California at Berkeley

Lawrence Livermore National Laboratory
Livermore, California 94550

December 17, 1993

Prepared in partial fulfillment of the requirements of the Science and Engineering Research Semester under the direction of Patrick Epperson, Research Mentor, at the Lawrence Livermore National Laboratory.

* This research was supported in part by an appointment to the U.S. Department of Energy Science and Engineering Research Semester (hereinafter called SERS) program administered by LLNL under Contract W-7405-Eng-48 with Lawrence Livermore National Laboratory.

Lead in Food and Food Containers

Anna O. Chu

ABSTRACT

We investigated food and food containers suspected of containing high levels of lead. Food containers investigated were bought in Northern California and were linked to several cases of lead poisoning in children and adults.

Coffee mugs and Mexican pottery were leached with acetic and citric acid, respectively. The amount of lead leached from the lip and rim area of eleven coffee mugs ranged from non detectable to 79 ppm. Lead leached from Mexican potteries ranged from non detectable to 584 ppm of lead.

Although there are no regulations pertaining to the amount of lead in the lip and rim area of ceramic ware, under California Proposition 65 vendors are required to warn consumers of the presence of toxic materials in consumer products.

Foods analyzed for lead content were candy and beans. A sample of tamarindo candy taken from the center of its storage container, a Mexican clay pot, was found to contain 1.0 ppm of lead, while the candy in contact with the glaze contained 16 ppm of lead. Beans cooked in Mexican clay cooking pots contained lead ranging from 2.8 to 9.2 ppm.

Two-thirds of the food containers investigated and the food analyzed did not meet the Provisional Total Tolerable Daily Intake level set by the U.S. FDA, assuming a reasonable amount of liquid and food was ingested.

Introduction

Lead and its compounds have long been known to be toxic (1), yet leachable lead is still found in glazed ceramics that are used to store and prepare food (2). In cooperation with the Food and Drug Branch of the California Department of Health Services, we investigated food and food containers suspected of containing high levels of lead. The results of this project support an investigation by DHS into a possible link between imported food containers and several cases of lead poisoning.

Food containers analyzed included 11 imported coffee mugs from China and 10 pieces of imported Mexican pottery.

A 4% glacial acetic acid leaching test was performed on the interior and the lip and rim area of the coffee mugs. A leaching test was performed on the lip and rim area of the coffee mugs because lead was suspected to be present in the brilliant decals.

A similar leaching test was used on 10 pieces of Mexican pottery, the difference being that Country Time® Sugar Free Pink Lemonade was used instead of 4% glacial acetic acid. This leaching procedure was developed to simulate realistic lead dose levels received while using these pots. The Mexican tableware and cookware were both glazed and unglazed.

Tamarind candy stored in a Mexican clay pot and beans cooked in Mexican cooking pots were also analyzed for lead. There was a suspicion that foods cooked and stored in glazed Mexican pottery could be contaminated with lead.

The samples were analyzed for lead by flame atomic absorption spectroscopy (AAS) and by inductively coupled plasma-mass spectroscopy (ICP-MS).

Methods

Materials. Redistilled nitric acid and redistilled, 6 M, hydrochloric acid was purchased from GFS Chemicals, Inc. 'Baker Analyzed'® glacial acetic acid was purchased from J. T. Baker, Inc. Deionized water was used in all experiments. Standards were diluted from SPEX Plasma Standard Solution for lead with a concentration of 1,000 µg/ml. Platinum crucibles were used for the dry ashing of the foods. Nitric acid, 5%, was used to leach residual lead from the crucibles.

Leachable Lead from Coffee Mugs. Eleven coffee mugs and six plastic food containers with lids were rinsed with deionized water and then air dried. A 4% glacial acetic acid leaching test (3) was first performed on six of the eleven mug interiors. 100 ml of 4% glacial acetic acid was poured into the mug and allowed to stand at room temperature for 24 hours. A watch glass was placed over the opening of the mug and a piece of aluminum foil placed over the watch glass. This extraction method was followed according to 973.32C of *AOAC Official Methods of Analysis* with the exception that the solution volume was not adjusted to the original volume of acetic acid used after leaching had occurred.

The leaching procedure for the lip and rim area of the mug was ASTM test method C927-80 (4). The lip and rim area of the mug was leached by inverting the mug into the container, placing 200 ml of 4% acetic acid into the plastic container, and covering the container with the plastic food container lid. The mug was leached in the acetic acid for 24 hours at room temperature.

Leachable Lead from Mexican Pottery. Country Time® Sugar Free Pink Lemonade was used as the leaching agent for extracting lead from the Mexican pottery (5). It was prepared per instructions on the

canister, i.e., the contents of one tub was emptied into a plastic container and mixed with 8 cups of deionized water. The pottery was leached for 24 hours at room temperature without stirring. the pottery was covered with its lid or with aluminum foil if the pot had no lid to prevent airborne contamination.

Lead in Beans. Three one gallon Mexican cooking pots were filled with 3000 ml deionized water. A line was scratched with an X-acto knife at the 3 L mark on the inside of the pot. This line was used as a reference to keep the water volume constant at 3 L while the beans were cooking. The water in the pot was then poured out and another 3000 ml of deionized water was put into the pot. 500 g of pinto beans were weighed out and placed into the pot. The beans were cooked at 75 to 85°C for two six hours periods over two days. The beans were not stirred except when deionized water was added to replace water that evaporated.

The blank for the Mexican cooking pots was beans cooked in a beaker. Extractable lead from the beaker was removed by washing the beaker three times with 4% acetic acid and then rinsing it five times with deionized water. 3000 ml of deionized water was
placed into the beaker using the 3 L mark on the beaker as a reference line. 500 g of pinto beans was placed into the beaker and the beans were cooked in the manner stated above. A watch glass was used to cover the beaker.

AOAC method 972.23D was used to prepare the bean sample for analysis on the AA (6). This method was modified in that the sample was not dried for two hours at 135-150°C prior to ashing in the furnace. 25 g of cooked beans was dry ashed at 500°C for 8 hours in a furnace. The furnace temperature was raised two degrees Centigrade per minute up to

400°C and held there for 3 hours. From there, the temperature increased at four degrees Centigrade per minute up to 500°C. Cooked beans consisted of 4 parts beans and 1 part bean liquid. A nitric acid ashing was performed to obtain a clean, practically C-free ash. Hydrochloric acid, 1 N, was used to dissolve the ash and to bring the bean sample to a final volume of 25 ml.

Lead in Candy. Two samples of tamarind candy were taken from each of two Mexican candy pots. Candy from the center of the pot and candy in contact with the clay and glaze of the same pot were analyzed for lead content. Analysis of the candy from different parts of the pot were done to determine if lead was in the candy before being stored in the container or if lead was in the candy as a result of storing it in the container.

Digestion of the candy sample was similar to that of the beans. 25 g of candy taken from the center of the pot and 25 g of candy in contact with the clay and glaze taken from the same pot was dry ashed at 550°C for 8 hours. The furnace temperature was raised two degrees Centigrade per minute up to 450°C and held there for 3 hours. From there, the temperature increased at four degrees Centigrade per minute up to 550°C. A nitric acid ashing was performed to obtain a clean, practically carbon free ash. Hydrochloric acid, 1 N, was used to bring the candy sample to a final volume of 25 ml.

Leachable Lead from Candy Pot. The inside of two pots used to store the tamarind candy was cleaned with deionized water and then allowed to air dry. 110 ml of 4% glacial acetic acid was poured into one candy pot and was allowed to stand for 24 hours at room temperature. The candy pot was covered with a watch glass in this time period. The

other candy pot was placed in a plastic food container, and 4% glacial acetic acid was poured into the container just until the leaching solution came halfway up the neck of the pot. The lid was put on the container, and the acetic acid was allowed to stand at room temperature for 24 hours.

Determination of Lead. Lead concentrations were determined by AAS and ICP-MS. A Perkin-Elmer Model 5000 atomic absorption spectrophotometer using an air-acetylene flame and the lead 283.3 nm resonance line was used for AAS measurements. A PQ1 inductively coupled plasma mass spectrometer manufactured by VG Instruments was also used for a small number of lead measurements as a check on the AA results and to measure the trace levels of lead in the reagent blanks because of the greater sensitivity of the ICP-MS. Lead values by the two methods agreed within 10%. Values reported in tables are from the AA measurements.

Results and Discussion

Reagent Blanks. The concentration of lead in the 1 N HCL used in the dry ashing step was 0.0005 ppm. The 4% glacial acetic acid leaching solution contained 0.00007 ppm of lead.

Leachable Lead from Coffee Mugs. The colorfully adorned coffee mugs being tested for lead were bought in many well-known stores throughout Northern California. These ceramic mugs were glazed and had decals on the outside of the cup only. The decals had brilliant hues of oranges, yellows, greens, reds, and blues, as can be seen in Figure 1.

A non detectable amount of lead was leached from the interior of six coffee mugs. The amount of lead leached from the lip and rim area of the coffee mugs ranged from non detectable to 79 ppm of Pb (Table I).

Because no detectable lead was leached from the interior, the lead leached from the lip and rim area of the coffee mug is presumed to come from the decals and not from the glaze.

Leachable Lead from Mexican Pottery. Table II lists Mexican pottery investigated. Examples of cooking pots, casserole dishes of varying sizes, and a drinking cup investigated are shown in Figure 2. All were glazed except for the drinking cup and a pot. These imported potteries were purchased in stores throughout Northern California with the intention of cooking and storing foods and liquids in them.

The results of the leaching test on Mexican pottery are listed in Table II. To evaluate the significance of the amount of lead in the lemonade, the lead dose for children, adults, and pregnant women were calculated by multiplying the concentration of lead in the sample by an estimated typical volume of lemonade drank per day. The results for the 10 items are listed in Table III. Based on these results, 8 of the 10 pots exceeded the the Provisional Total Tolerable Daily Intake (PTTDI) level (Table IV) for lead set by the U.S. FDA (6) by factors ranging from 2 to 17,000. The Provisional Total Tolerable Daily Intake level is that dose of lead beyond which adverse health effects would be observed in the four groups of people. It is likely that many of these pots can cause adverse health effects in children and adults.

Lead in Beans. The test for lead in cooked beans simulated the typical use of these pots in order to obtain an accurate dose of lead an individual would receive if they were to eat beans cooked in these Mexican cooking pots. The concentration of lead in the beans cooked in the three pots is listed in Table V. Table VI lists the dose of lead received from eating beans from the pot with the highest lead levels for four population

groups and compares the doses to the PTTDI. All of the pots had significant leachable lead that would result in lead doses above the PTTDI for all population groups.

Lead in Candy. Candy from the center of the pot and candy in contact with the clay and glaze of the same pot were analyzed for lead content. Two samples of candy were taken from the same pot to see if the source of lead was the tamarind candy or was the result of contact with the container glaze. The concentration of lead in the candy in contact with the container glaze is approximately 16 times that of the candy from the center of the pot (Table VII).

Leachable Lead from Candy Pot. Significant amounts of lead leached from the interior and the exterior of the candy pots (Table VII). This suggests, along with the data on the concentration of lead in the candy, that the lead in the candy was coming from the candy pot.

Conclusions

Analysis of imported food containers shows that there are regulatory significant amounts of lead present. Food stored and cooked in these containers can cause adverse health effects to humans, particularly in young children and pregnant women.

The results of these analyses support an investigation by the California Department of Health Services into a link between imported food containers and several cases of lead poisoning in California. Because lead has been found to contaminate foods beyond established safety levels, DHS can now take action in prohibiting the sale of these food containers and recommending to the State of California Attorney General that a warning

be posted to alert consumers that these food containers may pose a health threat to children and adults.

Acknowledgments

I would like to thank Robert Lim for his tremendous assistance with this research project, Philip Miller for ICP-MS analyses, Dr. Alfredo Quattrone of the Department of Health Services, State of California for many helpful discussions, and Patrick Epperson for being a truly wonderful mentor.

References

(1) Mahaffey, K. R. *Dietary and Environmental Lead: Human Health Effects*; Topics in Environmental Health, Volume 7; Elsevier: Amsterdam, 1985.

(2) Schroeder, H.A.; Tipton, I. H. *Arch. Environ. Health*, **1968**, 17, 965-978.

(3) *Official Methods of Analysis of the AOAC*; 973.32; Association of Official Analytical Chemists: Arlington, Va, **1990.**

(4) *Annual Book of ASTM Standards*, Vol. 15.02; C 927-80 (Reapproved 1985); American Society for Testing and Materials, **1986.**

(5) Gould, J. M.; et al. *Analytical Letters* **1988**, 21, 2145-2154.

(6) *Official Methods of Analysis of the AOAC*; 972.23; Association of Official Analytical Chemists: Arlington, Va, **1990.**

(7) Bolger, M.; Kerrington, C. *Reg. Tox. and Pharm.* **1992**, 16.

Figure 1. Coffee Mugs Investigated and Leachable Lead from Lip and Rim Area of These Mugs

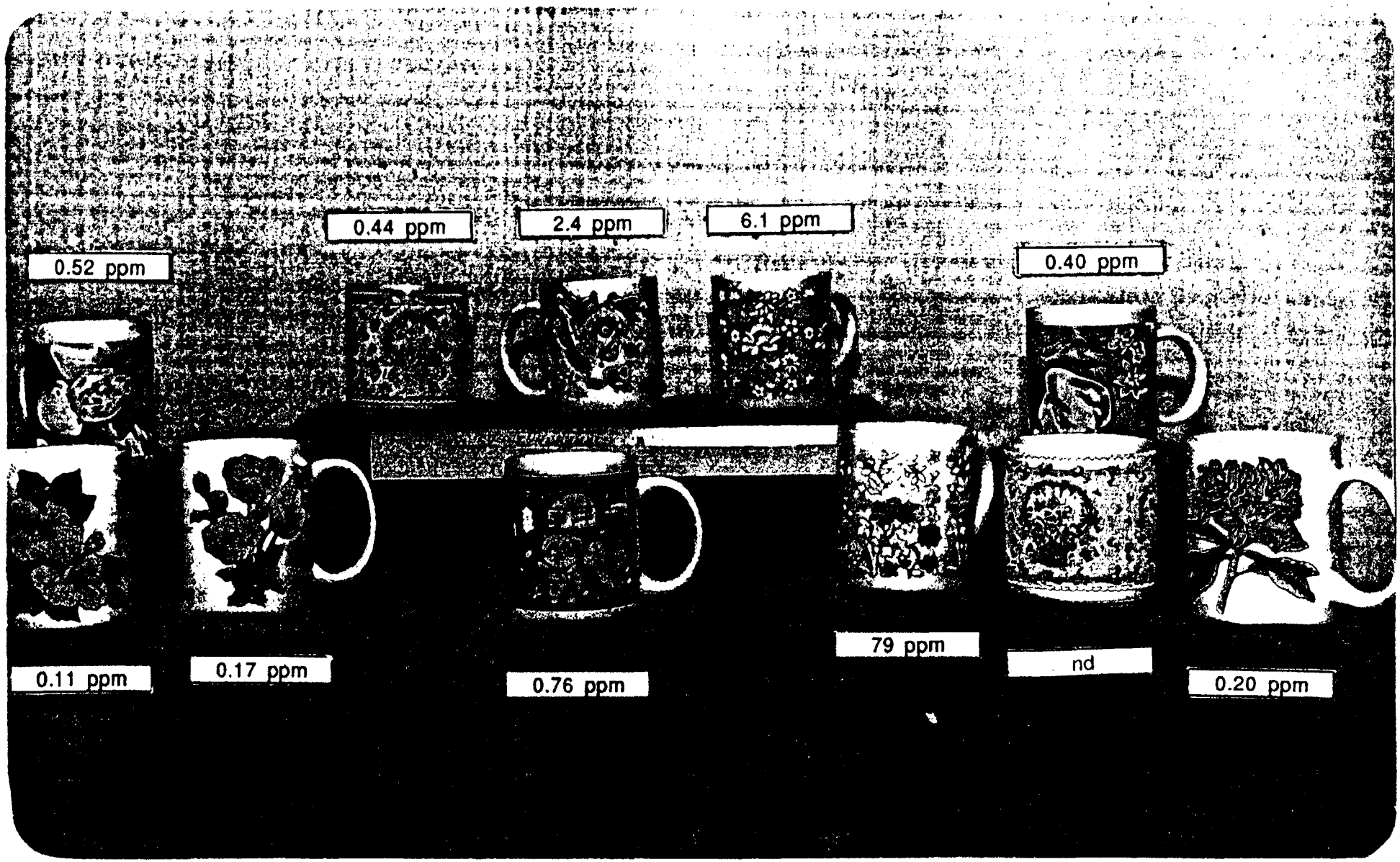

Figure 2. Examples of Mexican Pottery Investigated

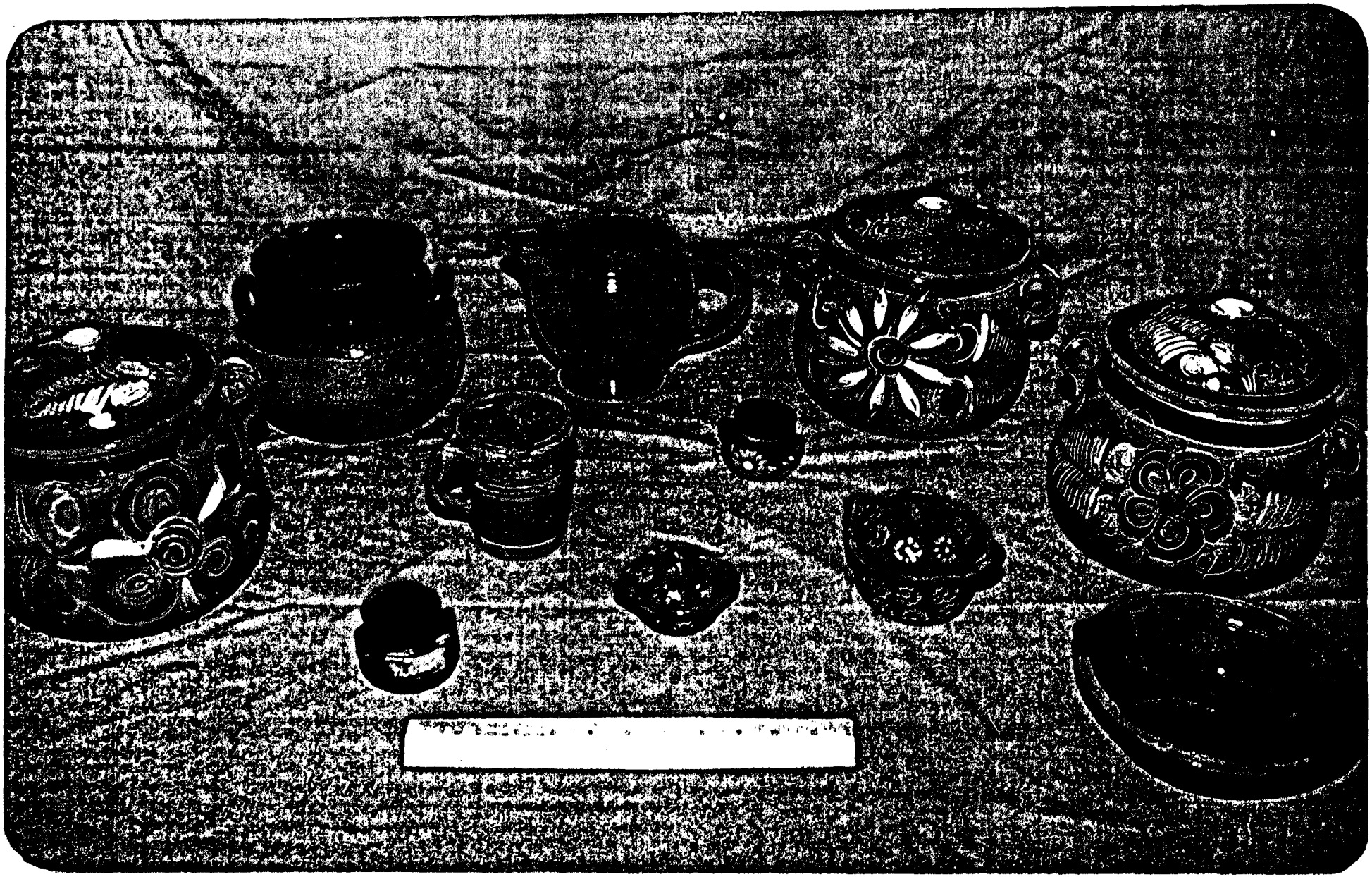

Table I. Concentrations of Lead from Coffee Mugs Determined by Flame AAS

	conc. of Pb (ppm)	
coffee mug	interior	lip and rim area
A	nd	2.4
B	nd	6.1
C	nd	0.52
D	nd	0.40
E	nd	nd
F	nd	0.44
G	na	79
H	na	0.76
I	na	0.17
J	na	0.20
K	na	0.11

nd, not detected; na, not analyzed.

Table II. Description of Mexican Pottery Investigated and Leachable Lead from These Potteries

Mexican pottery	glazed?	conc. of Pb (ppm)
cooking pot #1	yes	220
cooking pot #2	yes	2.6
cooking pot #3	yes	9.7
salsa pot	yes	38.6
drinking cup	no	nd
casserole dish	yes	584
6 oz. casserole dish	yes	56
2 oz. casserole dish	yes	11
pot with handle	yes	0.40
jug	no	nd

nd, not detected.

Table III. Lead Dose from Drinking Lemonade Stored in Mexican Pottery for 24 hours.

Average volume of lemonade drank per day is estimated to be 175 ml (approx. 6 oz) for children 0 to 6 years of age and 350 ml (approx. 12 oz) for children 6-18, pregnant women, and other adults.

Mexican pottery	dose of Pb (μg) for 350 ml/day	dose of Pb (μg) for 175 ml/day
cooking pot #1	77,000	38,000
cooking pot #2	910	460
cooking pot #3	3,400	1,700
salsa pot	14,000	7,000
drinking cup	0	0
casserole dish	200,000	100,000
6 oz. casserole dish	20,000	10,000
2 oz. casserole dish	3,900	1,900
pot with handle	140	70
jug	0	0

Table IV. Provisional Total Tolerable Daily Intake (PTTDI) Level from any Food Source for the Four Groups of People

children (0 - 6 years)	6 μg / day
children (7 - 18 years)	15 μg / day
pregnant women	25 μg / day
everyone else	75 μg / day

Table V. Lead in Beans Cooked in Mexican Cooking Pots

	conc. of Pb (ppm)
beans cooked in pot #1	9.2
beans cooked in pot #2	2.8
beans cooked in pot #3	3.0
blank	0.15

Table VI. Comparison of PTTDI Level and Dose Amount of Lead Received by Children, Pregnant Women, and Everyone Else as a Result of Eating Beans Cooked in Mexican Cooking Pot #1

Group	amount eaten	dose of Pb	PTTDI level
children (0-6 years)	50 g	460 µg	6 µg
children (7-18 years)	75 g	690 µg	15 µg
pregnant women	100 g	920 µg	25 µg
everyone else	100 g	920 µg	75 µg

Table VII. Lead in Tamarind Candy and Leachable Lead from Candy Pot as Determined by Flame AAS

	conc. of Pb (ppm)
candy in contact with clay and glaze[a]	16
candy in center of pot[a]	0.96
interior of candy pot leachate	16
exterior of candy pot leachate	34

[a]Listed concentration is the average of two concentrations.

EXTRACTION OF HEXAVALENT CHROMIUM FROM GROUNDWATER USING ION EXCHANGE RESINS

Research in Support of
Environmental Restoration Division
Lawrence Livermore National Laboratory
Livermore, California

Duncan Cottrell
Georgia State University

Maureen Ridley
Environmental Restoration Division
Lawrence Livermore National Laboratory

Funded by the US Department of Energy's
Science and Engineering Research Semester program
December 1993

Extraction of Hexavalent Chromium From Groundwater Using Ion Exchange Resins

Introduction

A bench top experiment was performed to determine the hexavalent chromium (Cr^{+6}) adsorption capacity of three ion exchange resins. The resin types tested were Purolite A300, A500, and A600 which are commercially available. This experiment is part of an effort to better characterize resin efficiencies at removing Cr^{+6} from ground water extracted from wells at the Lawrence Livermore National Laboratory. The information obtained from these laboratory scale tests will aid in the determination of the preferred resin for an onsite ground water treatment facility.

Background

The study area is the US Department of Energy's Lawrence Livermore National Laboratory (LLNL) in Livermore, California. Chlorinated solvents, principally trichloroethylene (TCE) and perchloroethylene (PCE), have been detected in ground water beneath and downgradient of the laboratory site in concentrations exceeding Federal or State Maximum Contaminant Levels (MCLs) or State Recommended Drinking Water Action Levels. It is believed this contamination originated in the 1940's when the site was a Navy aviation-training base. In the process of characterizing the ground water for remediation efforts, hexavalent chromium (Cr^{+6}) was found to occur in a limited number of monitor wells in concentrations somewhat above its MCL (see Figure 1). Cr^{+6} is known to be toxic to plants, fish and mammals, and the US Environmental Protection Agency has recently declared Cr^{+6} to be carcinogenic as well.

The volatile organic compounds (VOCs) will be removed to carbon cannistors by air stripping the ground water after pumping it to the surface. It is desired to discharge the treated water to the surface storm drainage system. In order to do so the effluent must meet NPDES Surface Water Discharge Limits of 11 ppb for Cr^{+6}, a level determined by the sensitivity of fish to this chemical species (the drinking water standard for Cr^{+6} is 50 ppb). Therefore the air-stripped water must be treated to lower the Cr^{+6} concentration below regulatory discharge limits. Because of the

low initial concentration of Cr^{+6} (1-160 ppb) and the low discharge limit required, the treatment option of ion exchange was selected over filtration or reduction of Cr^{+6} to Cr^{+3} by addition of a ferrous salt.

Chromium concentrations found in the ground water at LLNL and surrounding areas are likely the result of geological characteristics of the region. Surface and subsurface sediment samples contain 10 to 80 ppm chromium as Cr^{+3}. A chromium mine and chromite deposits exist near the study area. The clay-silt fractions of the subsurface tend to have two to three times more chromium than those in the non-clay sediment. The clay-silt fractions also contain manganese dioxide (MnO_2), a natural catalyst to convert Cr^{+3} to Cr^{+6} (Bartlett and James, 1979; Eary and Ral, 1987; Malati and Sear, 1989). A possible mechanism for Cr^{+6} production by MnO_2 has been suggested as (Ridley and Martinelli, 1992):

$$Cr^{+3} + 1.5\ MnO_2 + 6\ H^+ = Cr^{+6} + 1.5\ Mn^{+2} + 3\ H_2O$$

Cr^{+6} in the ground water is stable and does not reduce to Cr^{+3} due to the high level of dissolved oxygen, an Eh range of ~+350 to +400 mv (see Figure 2), a high pH (averaging 7.8), and moderate to high levels of carbonates. High ground water chromium concentrations are found upgradient of any known anthropogenic sources. The high concentrations of chromium in the ground water do not consistently correlate to the possible anthropogenic sources. However, possible anthropogenic additions of chromium exist from 1) chromic acid waste discharges to an unlined waste pit and leach field by a local manufacturing company and from 2) blow down release to the storm drain system from cooling towers at LLNL using chromate solution as a bacterial inhibitor.

Ion Exchange Chemistry

An ion exchange resin is comprised of a polymer matrix (usually polystyrene cross-linked with 3 to 8% divinylbenzene for structural stability) to which charged functional groups are attached by covalent bonding. There are four basic categories of functional groups: strongly acidic (e.g., sulfonate), weakly acidic (e.g., carboxylate), strongly basic (e.g., quaternary amine), and weakly basic (e.g., tertiary amine). Associated to the fixed functional groups by electrostatic attraction are mobile counterions of the opposite charge (e.g., Na^+ balances the SO_3^- affixed at the ion exchange site). This is depicted in Figure 3. When water with unwanted ions is run through a bed of ion exchange resin, the unwanted ions adhere to the matrix by displacing the mobile counterions.

This exchange has been long used for water softening by replacing calcium ions in the water with sodium ions from the resin. Water to be treated is continually run through the resin bed until the unwanted contaminant appears at an unacceptable concentration in the effluent. This is the point of contaminant "breakthrough" and the adsorbent is said to be "exhausted." Ion exchange reactions are reversible and the resin can be regenerated by flushing with a solution containing an excess of the original ion, allowing the matrix to be used many times before being discarded due to irreversible fouling. The exchange capacity of the resin is the number of fixed charge sites per unit volume or weight of resin. Porosity refers to the degree of openness of the resin's polymer structure and is called microporous, gel, or macroporous. According to Clifford (1990) regarding chromate affinity, macroporous resins perform better than gel types and hydrophobic polystyrene resins are better than hydrophilic polyacrylic types.

The resins under investigation in this study are strong-base anion (SBA) exchange resins. In SBA resins the quaternary amine functional group is so strongly basic that it is ionized and is therefore useful as an ion exchanger over a pH range of 1 to 13. SBA resins most often come in either the hydroxide form or the chloride form, where OH^- or Cl^- respectively are the mobile counterions associated with the quaternary amines. The chloride form of SBA resins is investigated in this study in order to avoid the pH extremes in the effluent associated with OH^- which could exceed regulatory discharge limits.

The ion exchange reaction procedes from left to right according to the following equation, where R signifies the resin matrix and the overbar indicates the solid (resin) phase (Clifford, 1990):

$$\overline{R_4N^+Cl^-} + K_2CrO_4 \leftrightarrow \overline{(R_4N^+)_2\,CrO_4^{-2}} + 2KCl$$

Ion exchange resins do not prefer all ions equally. The variability of preference is expressed quantitatively as a separation factor α_{ij} from chemical engineering separation practice (Clifford, 1990):

$$\alpha_{ij} = \frac{\text{distribution of ion } i \text{ between phases}}{\text{distribution of ion } j \text{ between phases}} = \frac{y_i/x_i}{y_j/x_j}$$

where y_i = equivalent fraction of ion i in resin
x_i = equivalent fraction of ion i in water

The order of preference is described in the "selectivity sequence" as shown in Figure 4, where the most preferred ions, i.e., those with the highest separation factors, are listed at the top of the table and the least preferred ions at the bottom. For example, the $\alpha_{Br/Cl}$ value of 2.3 means that at equal concentrations in the aqueous phase, bromide is preferred by the resin 2.3/1.0 over chloride.

As can be seen from the table of relative affinities in Figure 4, chromium as chromate is an excellent candidate for removal from water using SBA exchange resins. Complications arise and the resin's effective exchange capacity is decreased when other anions such as sulfate and nitrate occur in the water in huge concentrations and compete with chromate for exchange sites. In the ground water studied, sulfate concentration was 18.4 ppm and nitrate concentration was 9.3 ppm compared to a chromate concentration of 0.032 ppm. The reason for this resin study was to determine the actual exchange capacity of the resins with high sulfate and nitrate concentrations in the water. Two aspects of this capacity will influence the selection of the resin for use in the treatment facility. First, the quantity of chromium absorbed by each resin before exhaustion will be determined and compared. Second, the regeneration efficiency, or percentage of resin capacity that is renewed after flushing with a sodium chloride solution, will be significant in overall resin capacity. Of concern is the quantity of chromium-contaminated regenerant solution required to achieve resin regeneration, since this must be disposed of as hazardous waste.

Typical Chemical and Physical Characteristics of Resins

The three ion exchange resins studied are commercially available from The Purolite Company. All come in the form of spherical beads. Resin A300 is described as operating best on waters having a high percentage of strong acids and as having high regeneration efficiency. Resin A500 is isoporous and resists organic fouling because of its large pore structure. It is particularly effective in applications where there is intense chemical and physical shock. Resin A600 has excellent physical stability and a high capacity for silica removal. The manufacturer's literature says nothing about chromate removal but does supply the information given in Table 1.

Methods

Experimental apparatus and set-up (Figure 5) was identical for each resin column. In the beginning, a gravity feed system was used to deliver

the influent water containing Cr^{+6} to the columns through the influent path which included Tygon tubing, a plastic sample port and a PTFE/glass flow control valve. Later in the test a peristaltic pump was acquired and used to deliver and control flow rate of the influent water. The pump has a multi-channel head, allowing influent delivery to all resin columns from a common reservoir. Each resin column was packed in a 10 mL plastic syringe barrel with approximately 7 cc of resin held in place by Pyrex glass wool plugs at each end. The influent side had a second glass wool plug which served as a filter to remove particulate matter from the water before contacting the resin. All resins were hydrated with nanopure filtered water prior to pouring the columns. Post column effluent water was collected in 1 liter fractions within plastic containers.

Ground water collected from monitor well 361 (MW361) was delivered to the metals lab room in a 55 gallon interior-coated drum. This water was used to fill the 10 liter influent reservoirs for each resin column. After the peristaltic pump was put into service, a single influent reservoir was used in common for all resin columns. A new batch number was assigned each time the reservoirs were refilled. Influent, effluent and drum samples of every batch were collected and sent to an offsite analytical laboratory for general minerals analysis. An analysis of the influent groundwater is shown in Table 2. Also see Table 5 for a comparison of minerals absorbed by the resin during the first bed volumes of water treated at the initialization of column use.

Before flows through the resin columns were started, the influent water was air-stripped of the volatile organic compounds (VOCs) in solution by bubbling air through the reservoir in the ratio of 25:1 air to water. This simulated the air-stripping to be performed at the water treatment facility for VOC removal. Following air-stripping the pH of the influent water was adjusted down to ~7.90 by bubbling CO_2 into the reservoir. This procedure lowers the pH, while bubbling compressed air into the water was used to increase pH when necessary. Influent water was kept below a pH of 8.0 to eliminate the formation of carbonate precipitates. Influent water was kept above a pH of 7.0 to avoid mobilization of chromium off the resin column. Influent and effluent pH was monitored on a daily basis after starting the water flow through the resin columns.

After adjusting the pH, the influent water flow was initiated. It was calculated that a flow rate of approximately 2-3 mL/min. would match the specified flow of 2-3 gallon per minute per cubic ft. of resin for the treatment facility. Flow rate with gravity feed was very difficult to control and varied from 0.25 to 4 mL/min, which prompted use of a peristaltic

pump for influent delivery. With the pump a constant flow rate of 2.4 mL/min was utilized. A continuous flow was maintained throughout the test except over weekends and while refilling influent reservoirs.

Chromium analysis of the effluent water was performed using an atomic absorption spectrophotometer (AA) equipped with a graphite furnace and set up to measure absorbance of the 357.9 nm wavelength of light. Ten-microliter aliquots of each 1 liter fraction and occasional grab samples were injected into the AA and the peak height of absorbance was read. Previous investigations had shown that all the chromium in the groundwater exists as Cr^{+6} and this was verified by analyzing samples both by AA for total chromium and by EPA Method 7196, Colorimetric Determination of Hexavalent Chromium. Concentrations were the same by both methods. Weekly samples were collected from each influent reservoir, the 55 gallon drum water and an acid bath used to leach out lab ware prior to use.

A minimum of 4 replicates of each sample were analyzed and the mean light absorbance was calculated and compared to a calibration curve to derive ppb values. Calibration standards were obtained by diluting a 1000 ppm certified potassium dichromate standard obtained from Fisher Scientific into a 1% nitric/nanopure water solution to make a 1 ppm working stock. From this stock, standard concentrations of 2.5, 5, 10, 25, and 50 ppb were prepared and used to determine the calibration curve equation. At least one standard was analyzed daily along with the samples to confirm the continued validity of the calibration curve. A new curve was developed when necessary.

After each column reaches exhaustion at the appearance of 11 ppb of chromium in the effluent, the amount of chromium on the resin will be calculated by mass balance. Then the resin will be regenerated by flushing with a 2 molar NaCl solution in a ratio of 500 gallons/30 ft^3 at the manufacturer's recommended rate of 0.2 to 0.5 gal per min/cu ft. The chromium in the waste regenerant will be measured and a mass balance calculated. Then a second NaCl flushing will be done, followed by chromium measurement and mass balance. The adsorption capacity of the resin for its second service cycle can then be calculated.

A postmortem will be performed on each resin column after effluent Cr^{+6} concentration has exceeded the determined 11 ppb limit. This examination should reveal any cracks, fractures or air pockets in the column's packing that could lead to channeling of influent water resulting in reduced surface contact with the resin.

Results

During the period of research covered by this paper, one resin column (A600) arrived at exhaustion (11 ppb Cr^{+6} in the effluent) and a second resin (A500) closely approached that limit. (The study will be continued by others since this researcher is leaving). The results of chromium adsorption to December 14, 1993, are shown in Table 3. For purposes of comparison, Table 4 shows the two resins still in process at the point where equivalent amounts of water (58 liters) had been treated by both.

Table 3 also shows a fourth resin column of A600 resin. In this study the chromium concentration of the influent was only one third that of the other columns. Otherwise the water was identical to that provided to the other resin columns, also originating from MW361. This allows the effectiveness of the resin on lower chromium concentrations to be compared with that on higher concentrations.

Figures 6, 7 and 8 show for each of the three resins the amount of chromium leaking into the effluent as a factor of the quantity of water treated by the resin.

Table 5 shows the effluent concentrations of anions in competition for exchange sites during the first few fractions of water treated. Chromate concentration was less than detection levels in all cases. The fractions sampled were: 0 to 250 mL, 250 to 500 mL, 500 to 1000 mL, and 1000 to 2000 mL. For A600 the mineral content of liter number 13 is also shown.

Discussion

A600 reached the regulatory limit of 11 ppb Cr^{+6} in its effluent at 6849 bed volumes (BV) of water treated. A300 and A500 continue to treat more water than A600, indicating a larger native capacity than A600. Either of these resins may be a better choice than A600, depending on the comparative regeneration efficiencies. At 9444 bed volumes A500 is leaking 10.5 ppb Cr^{+6} in its effluent, so it is essentially exhausted. At this point, then, A500 shows a 38% larger Cr^{+6} adsorption capacity than A600.

Data on A300 is too incomplete to allow a judgement of how it compares to A500. The comparison in Table 4 shows differences that are

not significant given the cumulative level of error. A300 started leaking Cr^{+6} into its effluent a little earlier than A500. This could indicate that chromate has a harder time replacing sulfate and/or other anions already loaded onto the resin's exchange sites than it does on A500.

With only one-third as much Cr^{+6} in the influent, A600 treated much more water but adsorbed much less chromate before reaching the same level of leakage compared to any of the other resins at a higher Cr^{+6} input level. This is probably because the chromate ions are so overwhelmingly outcompeted by the other anions for exchange sites. At lower levels of chromate input the resin may need regeneration less frequently.

The analysis of competitive anions shown in Table 5 indicates that nitrate and sulfate (present at 9 and 18 ppm respectively in the influent) are readily adsorbed onto the resin. Carbonates (449 ppm in influent) exhibit the same pattern. Chloride, which is at 115 ppm in the influent, is augmented by chloride being displaced from exchange sites. Chloride concentration reaches equilibrium by the time the first quarter of the water has passed through the column. Analyses of later effluent fractions (not available at this writing) will further illuminate the patterns of various anions' adsorption and desorption.

Regeneration of resin columns has not been undertaken at this writing. The information provided by that investigation will be very significant in evaluating the resins' overall performance.

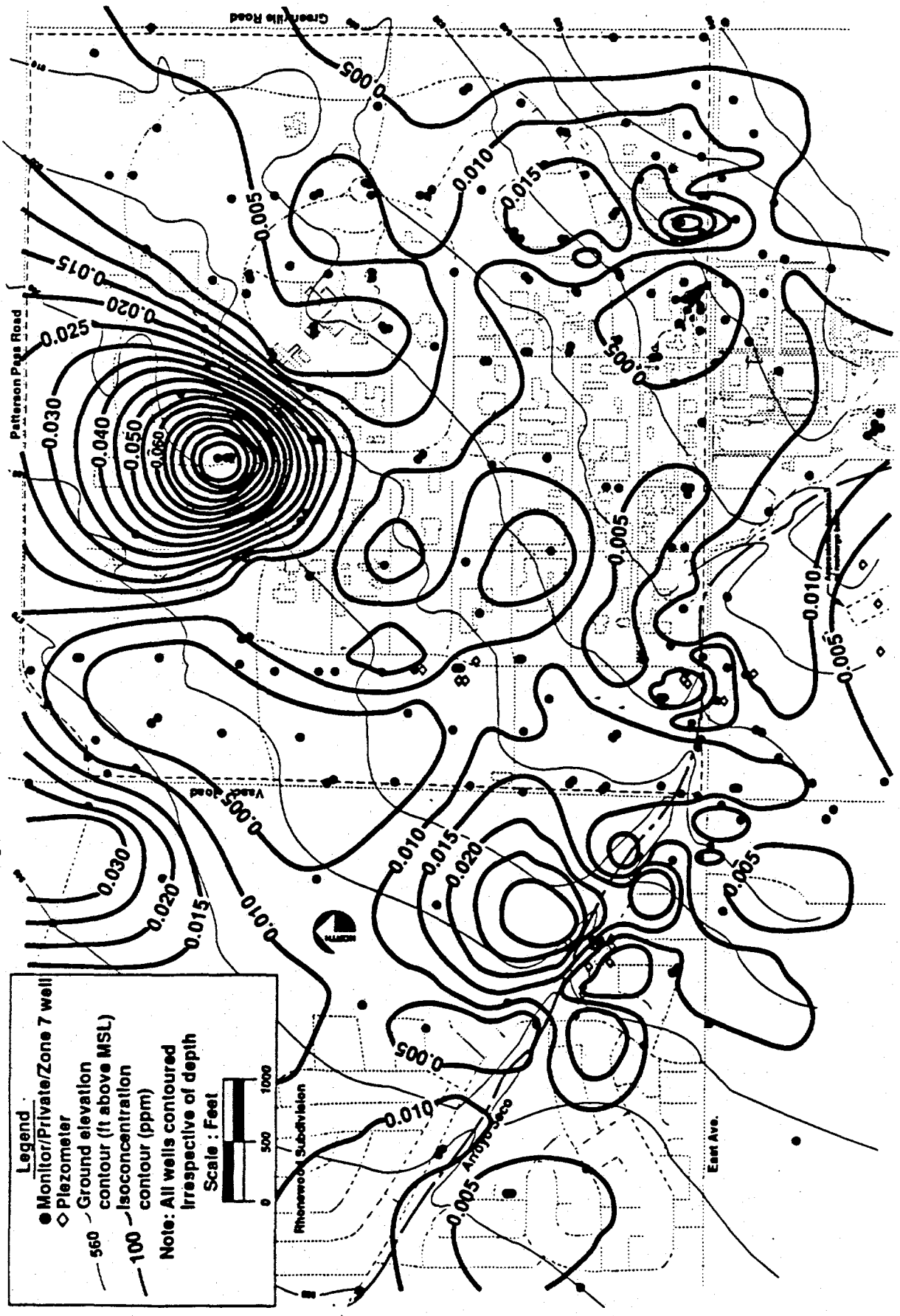

Figure 1 Total chromium in ground water LLNL Area.

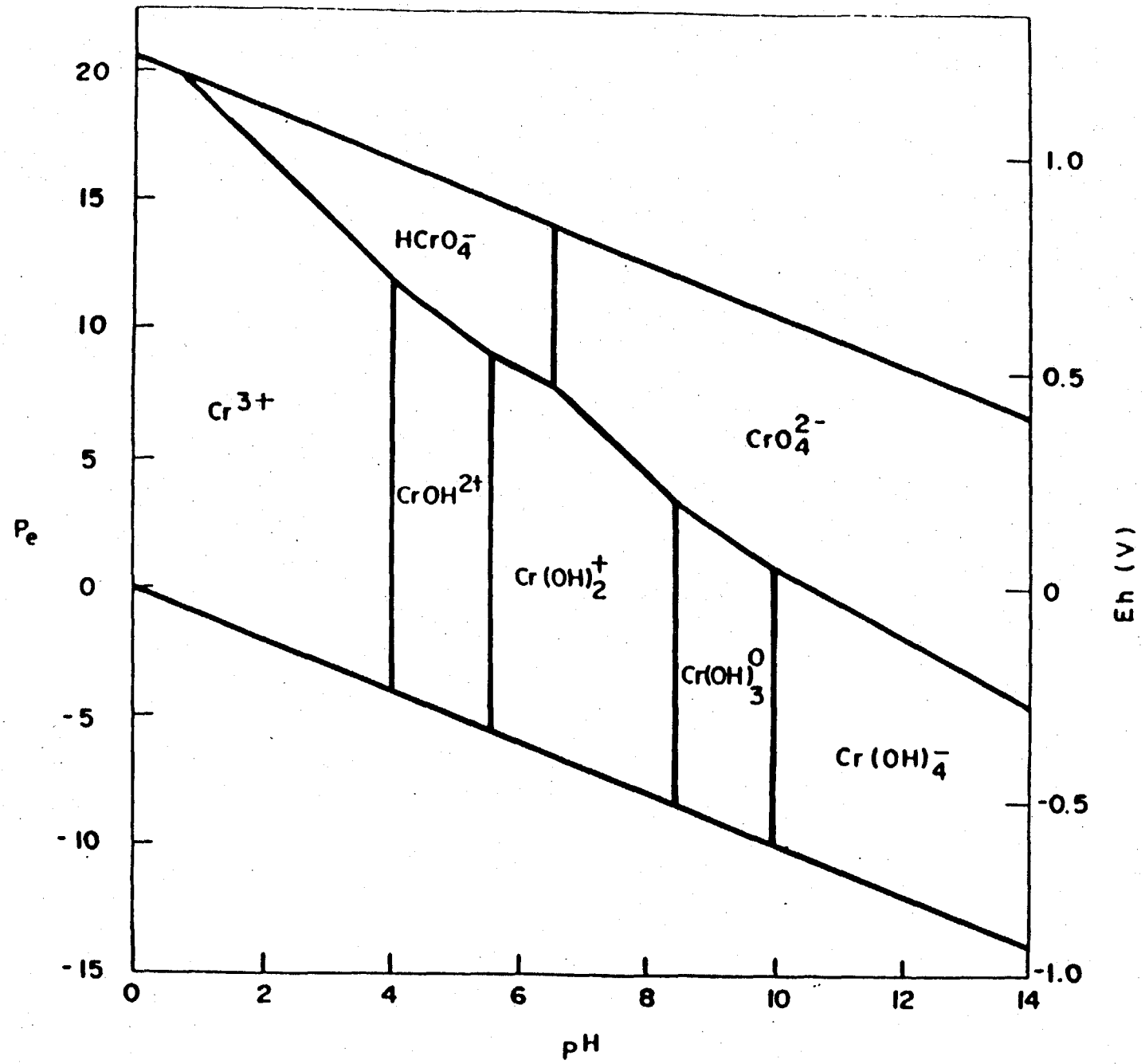

Figure 2 Areas of dominance of dissolved chromium species at equilibrium in the system $Cr + H_2O + O_2$ at 25°C and 1 atm. (Data from Baes and Mesmer, 1977; Hem, 1977)

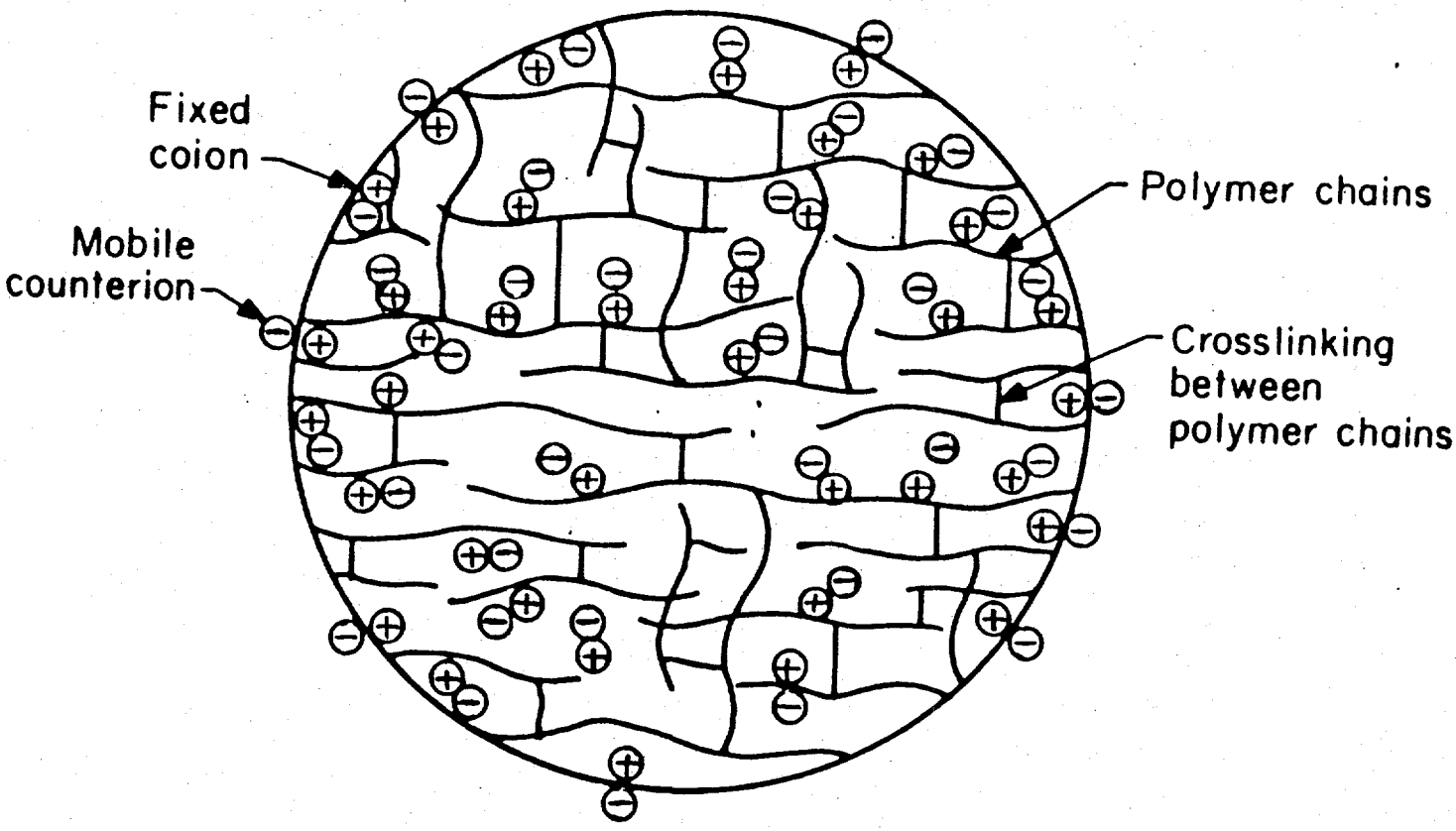

Ion-exchange resin bead made of polystyrene polymer cross-linked with divinylbenzene. Fixed coions (plus charges) are quaternary amines covalently bonded to the polymer. Exchangeable counterions (minus charges) are chloride ions .

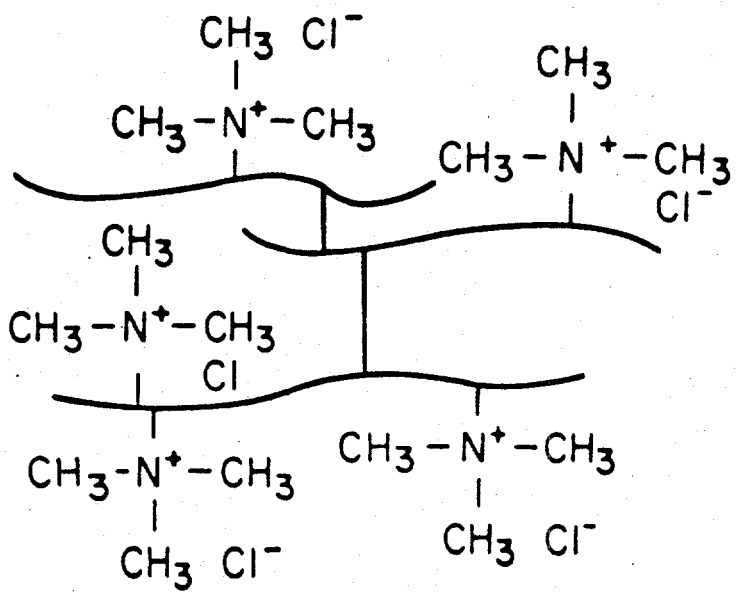

Close-up view of ion exchange sites.

Figure 3

Figure 4: Relative Affinities of Ions for Strong-base Anion Resins

Anion I	α_{I/Cl^-}
CrO_4^{2-}	100.0
SeO_4^{2-}	17.0
SO_4^{2-}	9.1
HSO_4^-	4.1
NO_3^-	3.2
Br^-	2.3
$HAsO_4^{2-}$	1.5
SeO_3^{2-}	1.3
HSO_3^{3-}	1.2
NO_2^-	1.1
Cl^-	1.0
HCO_3^-	0.27
CH_3COO^-	0.14
F^-	0.07

Figure 5 Column Setup

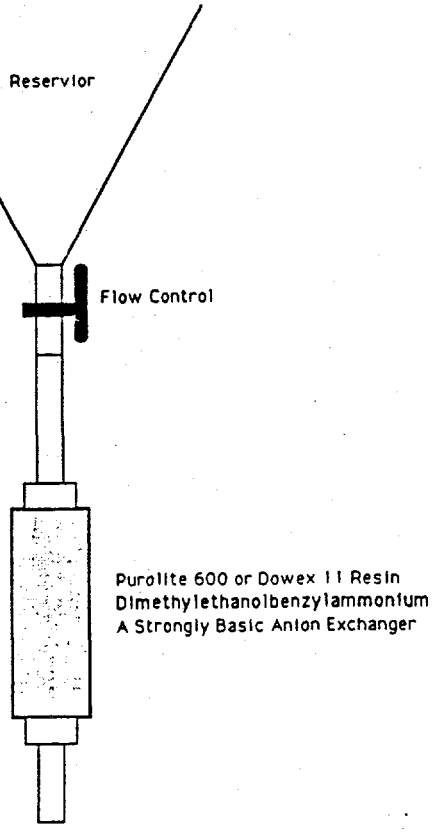

Figure 6

Cr in Effluent of Resin A600

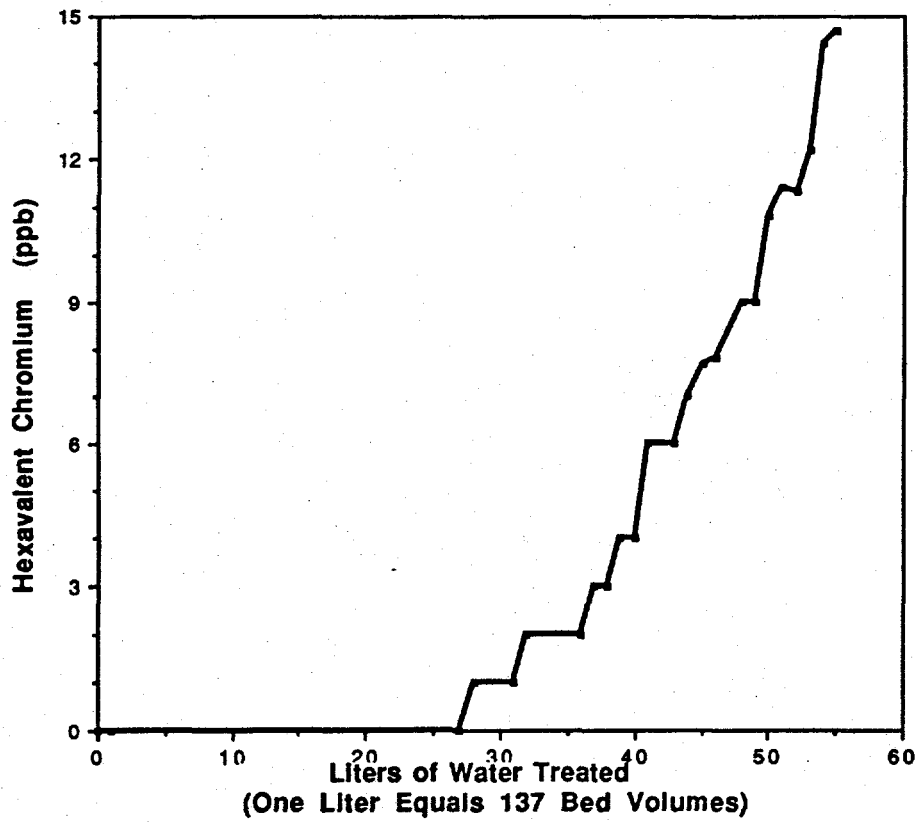

Figure 7

Cr in Effluent of Resin A500

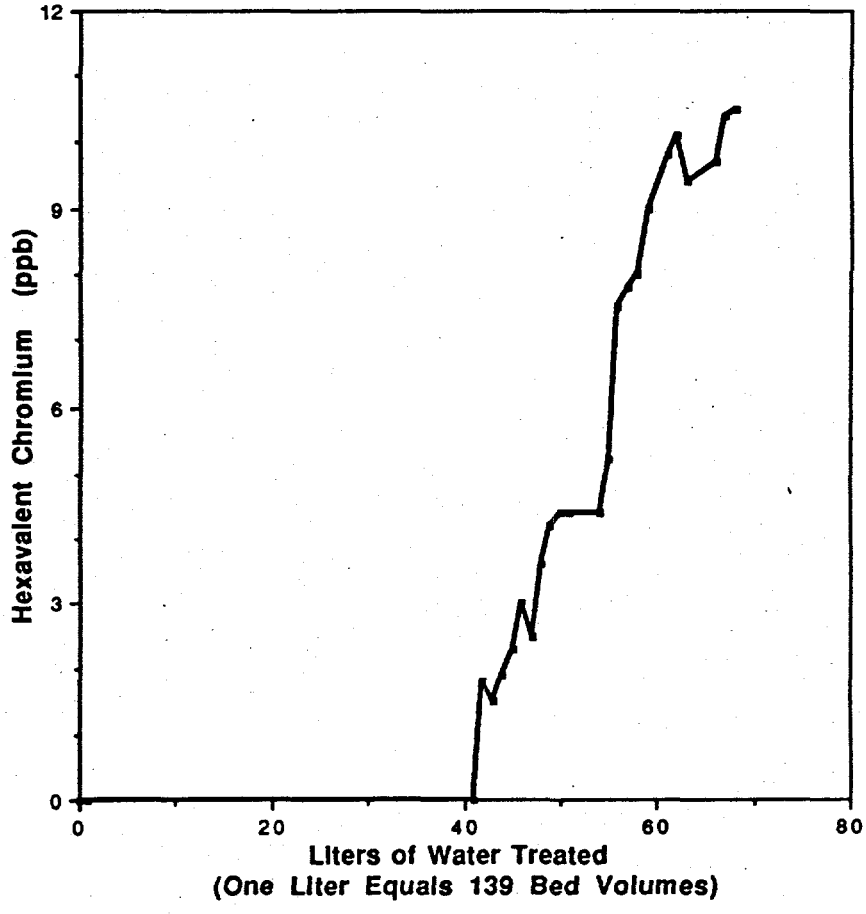

Figure 8

Cr in Effluent of Resin A300

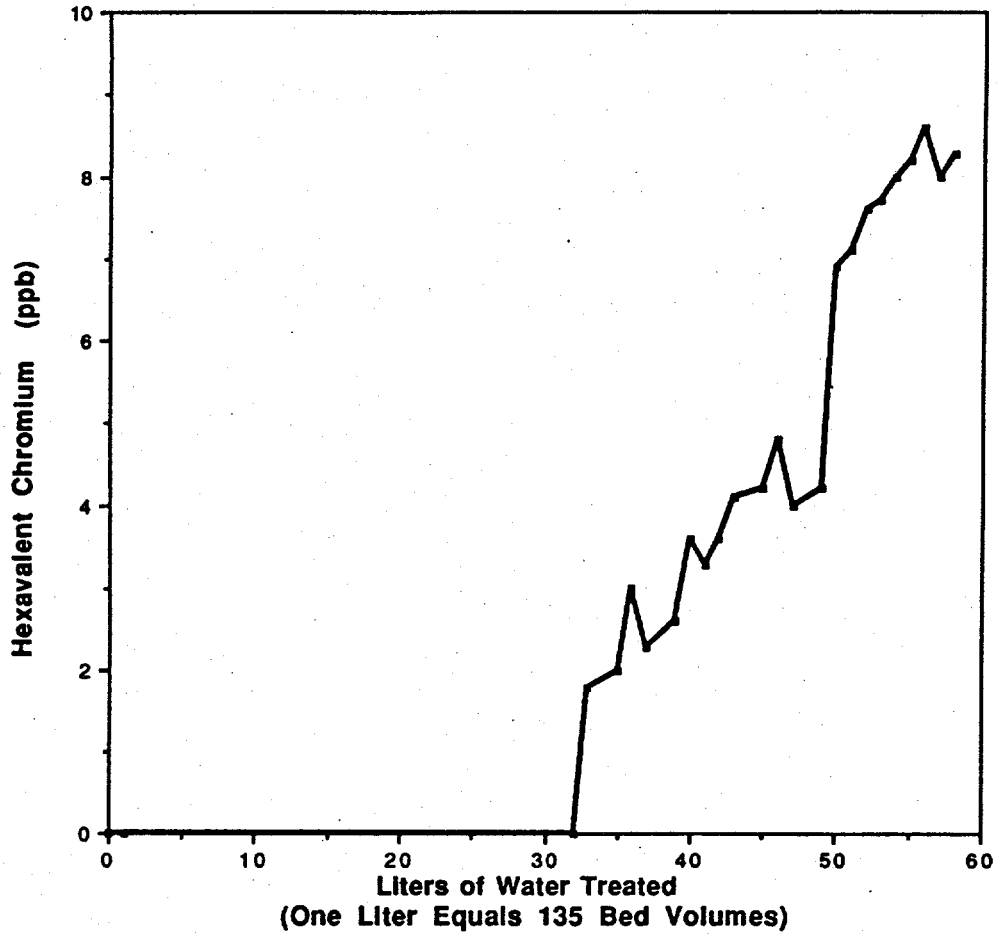

Table 1

Typical Chemical and Physical Characteristics of Resins

	A300	A500	A600
Type Resin	Type II Gel Strong Base	Type I, Macroporous Strong Base	Type I, Macroporous Strong Base
Polymer Structure	-----Polystyrene crosslinked with divinylbenzene-----		
Functional Groups	$R(CH_3)_2 (C_2H_4OH)N^+$	$R(CH_3)_3N^+$	$R(CH_3)_3N^+$
Ionic Form	Chloride	Chloride	Chloride
Screen Size (US std mesh)	16-50	16-50	16-40
pH Limitations	none	none	none
Temperature Limitations (deg F)	170	212	212
Total Capacity, minimum			
meq/ml Volumetric	1.45-1.6	1.15	1.5
meq/gm Weight	3.5-3.7	3.9	3.7
Water Retention, %	40-45	53-58	43-48
Regenerant	NaCl	NaCl	NaCl

Analyte	Code	Results (mg/L)	Rep. Limit (mg/L)	Method
Total Alkalinity (as CaCO3)	0300	530	1.0	310.1
Bicarbonate Alk (as CaCO3)	1125	530	1.0	310.1
Carbonate Alk (as CaCO3)	1850	ND	1.0	310.1
Hydroxide Alk (as CaCO3)	5250	ND	1.0	310.1
Aluminum	0313	ND	0.20	200.7
Calcium	1700	73	0.50	200.7
Chloride	1950	120	0.50	300.0
Copper	2800	ND	0.050	200.7
Fluoride	4825	0.38	0.050	340.2
Hardness, Total (as CaCO3)	4940	330	1.0	2320B
Iron	5350	ND	0.10	200.7
Magnesium	5500	35	0.50	200.7
Manganese	5550	ND	0.030	200.7
Nickel	5850	ND	0.10	200.7
Nitrate	5895	10	0.50	353.3
pH	7000	8.1	NOTE 1	150.1
Potassium	7050	2.0	1.0	200.7
Sodium	7850	120	1.0	200.7
Specific Conductance	8000	1100	NOTE 2	120.1
Sulfate	8025	20	1.0	300.0
Surfactant	8150	ND	0.50	425.1
Total dissolved solids (TDS)	7300	690	1	160.1
Zinc	9050	ND	0.050	200.7

Note 1: Units for pH are standard pH units.
Note 2: Units for specific conductance are umho/cm @ 25 degrees Celsius.

ND = Not detected at or above indicated Reporting Limit
Rep. Limit = Reporting Limit unless otherwise indicated in parentheses.

Table 2: General Minerals Analysis of Influent

Table 3: Chromate Absorption Capacities of Resins

	A300	A500	A600	A600
Resin Column Bed Volume (cm^3)	7.4	7.2	7.3	5.5
Influent Cr (ppb)	30	30	32	10
Bed Volumes to first Cr breakthru	4324	5694	3699	4545
$\mu g/cm^3$ Cr on resin at first breakthru	132	179	124	45
Bed Volumes to 11 ppb breakthru			6849	
$\mu g/cm^3$ Cr on resin at 11 ppb breakthru			204	
Bed Volumes to Current Date	7027	9444	6849	15,273
$\mu g/cm^3$ Cr on resin at Current Date	197	262	204	111
Data @ Liter #	58	68	50	84
Cr in Effluent at Current Date (ppb)	8	10	11	8

Table 4: Chromate Absorption Capacities of Selected Resins at Comparable Throughvolumes

	A300	A500
Resin Column Bed Volume (cm^3)	7.4	7.2
Influent Cr (ppb)	30	30
Bed Volumes to first Cr breakthru	4324	5694
$\mu g/cm^3$ Cr on resin at first breakthru	132	179
Bed Volumes to Current Date	7027	8056
$\mu g/cm^3$ Cr on resin at Current Date	197	234
Data @ Liter #	58	58
Cr in Effluent at Current Date (ppb)	8	8

Table 5: Initial Mineral Content of Resin Column Effluent

A300

Liter sampled	0.25	0.50	1.0	2.0
Carbonates	29	120	230	290
Chloride	320	280	210	160
Nitrate	ND	ND	ND	ND
Sulfate	ND	ND	ND	ND

A500

Liter sampled	0.25	0.50	1.0	2.0
Carbonates	76	230	310	330
Chloride	300	240	170	140
Nitrate	ND	ND	ND	ND
Sulfate	ND	ND	ND	ND

A600

Liter sampled	0.25	0.50	1.0	2.0	13.0
Carbonates	24	160	300	320	310
Chloride	370	290	190	160	110
Nitrate	ND	ND	ND	ND	ND
Sulfate	250*	ND	ND	ND	ND

* Probably anomaly or erroneous analysis

References

Bartlett, R.J., and Kimble, J.M. 1976. *Behavior or Chromium in Soils: I. Trivalent Forms.* J. Environ. Qual. 5:379-382.

Bartlett, R.J., and Kimble, J.M. 1976. *Behavior of Chromium in Soils: II. Hexavalent Forms.* J. Environ. Qual. 5:383-386.

Bartlett, R. and James, B. 1979. *Behavior of Chromium in Soils: III. Oxidation.* J. Environ. Qual. 8:31-35.

Clifford, D.A. *Ion Exchange and Inorganic Adsorption.* in Pontius, F.W., ed. Water Quality and Treatment. 1990. McGraw-Hill: New York.

Das, M., Sarkunan, V., Misra, A.K., and Nayar, P.K. 1990. *Chromium Oxidation in Soils.* J. Indian Soc. Soil Sci. 38:161-163.

Eary, L.E. and Ral, D. 1987. *Kinetics of Chromium(III) Oxidation to Chromium(VI) by Reaction with Manganese Dioxide.* Environ. Sci. Technol. 21:1187-1193.

Malati, M.A. and Sear, A. 1989. *Oxidations By Manganese(III)--II. Oxidation of Chromium(III).* Polyhedron. 8:1874-1875.

Ridley, M. and Martinelli, R.E. 1992. *Chromium Characterization and Treatment at Lawrence Livermore National Laboratory.* Unpublished. Lawrence Livermore Lab.

Thorpe, R.K., Isherwoood, W.F., Dresen, M.D., and Webster-Scholten, C.P. May 1990. *CERCLA Remedial Investigations Report for the LLNL Livermore Site.* UCAR 10299. Lawrence Livermore National Laboratory.

Development of Photopolymerization for the Fabrication of Optically Sensitive Polymers for pH Measurements*

Jennifer N. Fisher

University of Central Florida

Lawrence Livermore National Laboratory
Livermore, California 94550

December 15, 1993

Prepared in partial fulfillment of the requirements of the Science and Engineering Research Semester under the direction of Fred Milanovich, Research Mentor, in the Lawrence Livermore National Laboratory.

*This research was supported in part by an appointment to the U.S. Department of Energy Science and Engineering Research Semester (hereinafter called SERS) program administered by LLNL under Contract W-7405-Eng-48 with Lawrence Livermore National Laboratory.

Development of Photopolymerization for the Fabrication of Optically Sensitive Polymers for Measurements

Jennifer N. Fisher
University of Central Florida
Environmental Sciences Division

ABSTRACT

The Department of Energy is currently supporting the development of a fiber optic pH sensor. This sensor is being developed to monitor contaminants, which were created during the weapons development era. These contaminants are being stored in large vats while decomposition occurs. These vats have proven to be very pH sensitive, and need to be monitored. An optical sensor would be inherently safer than the traditional electric pH sensors for this task.

The optical sensor is being developed using the dye fluorescein. This dye fluoresces with varying intensity when exposed to different pH environments. The dye is chemically bonded to the end of the optical sensor. Ultraviolet light is used to activate a reaction, between fluorescein and other chemicals, to create the sensor. Then a device, a fluorimeter, is used to measure the pH of a given solution.

A wide range of parameters are being tested to determine how to create the best sensor, i.e. the one with the largest range over the pH scale and the fastest response time. Some of the parameters under consideration include wether to include an acid bath in the cleansing process. Also, during the photopolymerization process, limiting the wavelengths of light, the exposure time and the light intensity must be considered. Lastly, oxygen interference and the photopolymerization solution's age have been examined.

Then, a number of handling techniques have been learned. For example, the sensors require conditioning. With so many factors, the sensors have proven to to be unreproducible. Understanding what effects this photopolymerization process, and how, is the key objective of this project. Without reproducible results, no sensor, no matter how good it may be, is useless.

Development of Photopolymerization for the Fabrication of Optically Sensitive Polymers for pH Measurements

1. The problem.

The Department of Energy has recently undertaken the enormous task of cleaning up the waste created during its cold war weapons development era following World War II. Much of this waste is radioactive and is being stored in large vats as it slowly decays. Unfortunately, these storage containers cannot withstand any pH even slightly acidic. A solution pH greater than 9.5 would be ideal. It is therefore necessary to develop a pH sensor that can measure the acidity of the waste in these containers, despite the caustic environment, without generating any explosion hazard.

The idea of developing an optical pH sensor developed out of this need. Since this device only uses light to make measurements, there could be no spark. Also, the detector attached to the end of the fiber optic cable could be a safe distance away from the storage vats. Fiber optic cable is able to carry its signal, undiminished, for a long distance. A fiber optic cable of up to one kilometer can be used in the proposed measuring set-up without the signal fading.

2. Background.

Before this idea is put into practice, one must understand, basically, what a fiber optic cable is and how it works. An optical cable consists of three components. There is the central glass core that actually carries the light down the cable. This is surrounded by the cladding, which is further surrounded by an insulating buffer. The fiber operates by internally reflecting light down its length. The cladding and the glass core both have an index of refraction associated with them. The cladding material is selected such that total internal reflection occurs, thus keeping the signal moving down the cable undiminished. The index of refraction associated with the glass core is higher than the index for the cladding. See Figure 1. (Young, 5-9).

Originally, fiber optic pH sensors were created by embedding a fluorescent dye into a glass bead, which was attached to the end of the fiber. Unfortunately, these sensors proved to be unstable and fragile. Now, the idea of chemically depositing the dye onto the end of the fiber is being developed. During this process, the glass fiber is cleaned with sulfuric acid and functionalized with 3(trimethosysilyl) propylmethacrylate. It than has the polymer attached to the tip. This polymer contains the dye itself, fluorescein, as well as ethylene glycol dimethacrylate, to bond

Figure 1

Schematic (to scale) of surface amplified fiber sensor.

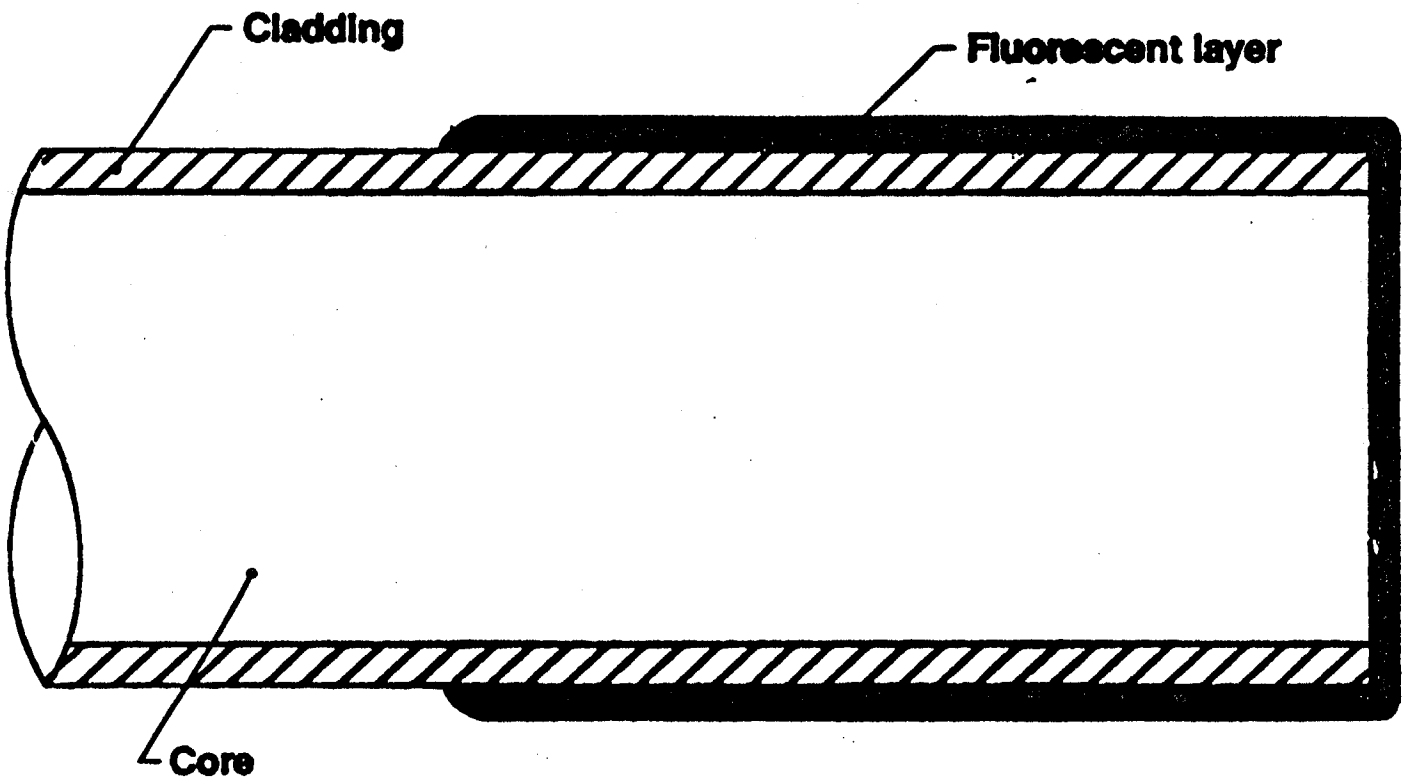

the polymer together, and 2-hydroxyethyl methacrylate, to encourage ion transfer during pH sensing. See appendix A.

3. Polymerization process.

During the polymerization process, ultraviolet light is coupled through the fiber. The unpolymerized dye solution is placed onto the tip. Chemically bonding the dye to the fiber tip requires ultraviolet light. Unfortunately, if light of other wavelengths is let in, the dye is bleached, and the signal the sensor would have produced is reduced. Therefore, a band pass is used to filter out unnecessary and harmful light. The polymerization equipment currently uses a filter that passes light around the 350 nm wavelength, with a band width of about 100 nm.

It is also critical to align each fiber individually. Each fiber is unique, despite careful polishing of the connector end. A power meter is used to measure the light energy passing through the fiber. Each fiber is aligned to pass a given amount of energy for a batch of experiments. Without this alignment, the results would not be compatible.

4. Fluorimeter.

Once the fiber has been affixed with the dye tip, a fluorimeter is used to measure the response the sensor generates in a pH buffer solution. A technique called fluorescein intensity detection is used. This dye fluoresces at different intensities according to the pH of the surroundings. The fluorimeter uses a tungsten-halogen lamp. These lamps do not gradually fade as they age, but provide a constant intensity throughout 90% of their lifetime. This is crucial for comparing results obtained over a period of time. (Willard).

The fluorimeter uses a series of band passes and dicroic filters (beam splitters) to separate out unwanted light while measuring the sensor's response. The first filter is placed in front of the light source. This band pass only passes light around the fluorescein dye's excitation wavelength of approximately 490 nm. (See Figure 2). The light then passes through a beam splitter that passes light under 500 nm. The rest of the spectrum is reflected, and thus separated out. The light travels through the fiber and to the tip. Remember that the dye fluoresces with different intensities in different pH solutions. The emitted light is carried up the fiber and to the beam splitter. There, light below 500 nm is filtered out, with the rest of the light being reflected out of the way. The emission wavelength of fluorescein is around 515 nm. The light then travels through another band pass which passes light only around the emission wavelength. This limits the energy traveling to the detector. The detector then converts the power to a voltage readout. See Figure 3. These readouts

Figure 2

FLUORESCEIN

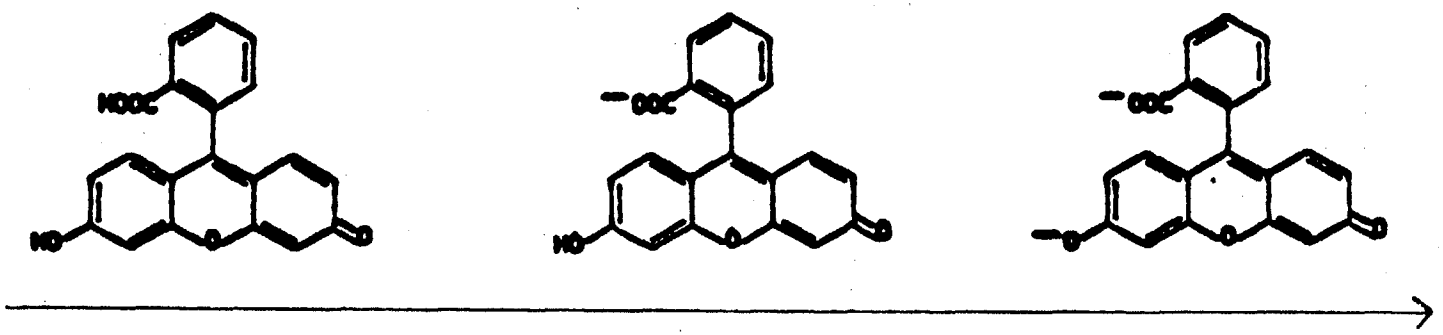

INCREASING pH

FLUORESCEIN EXCITATION/EMISSION SPECTRA

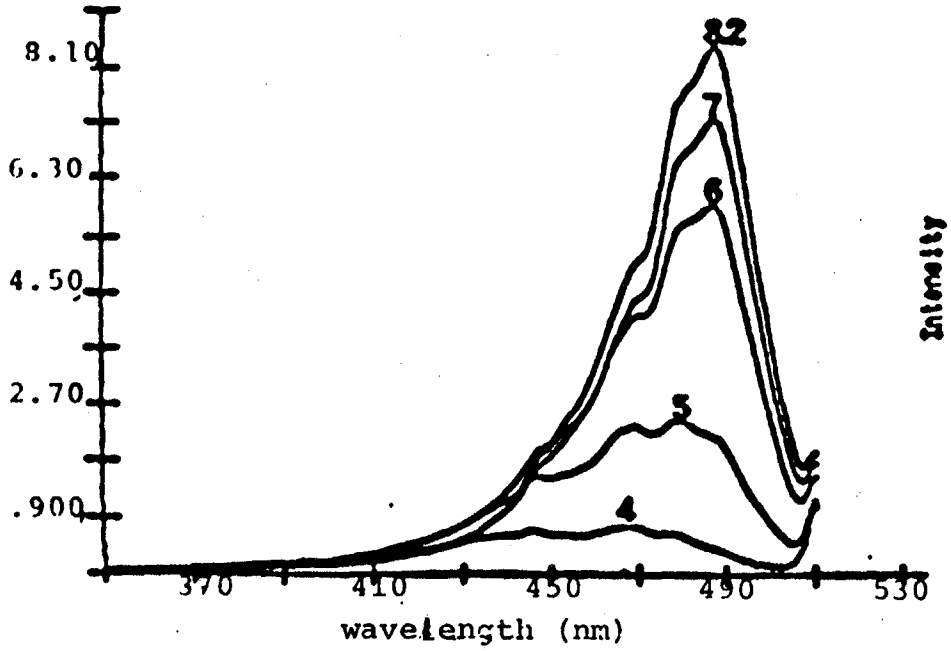

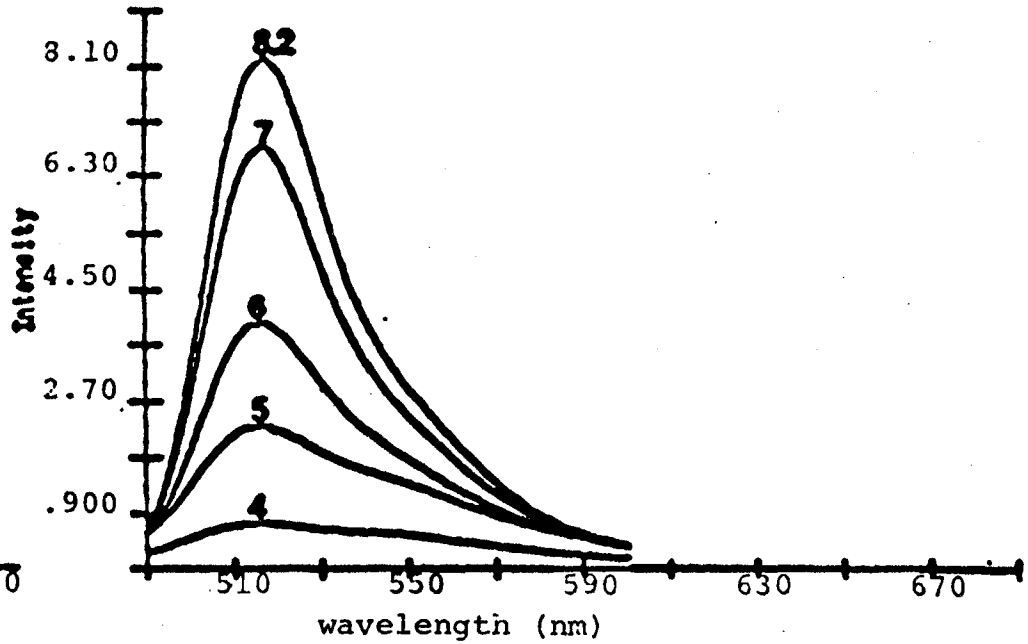

Figure 3

Schematic of Single-fiber Sensor Concept

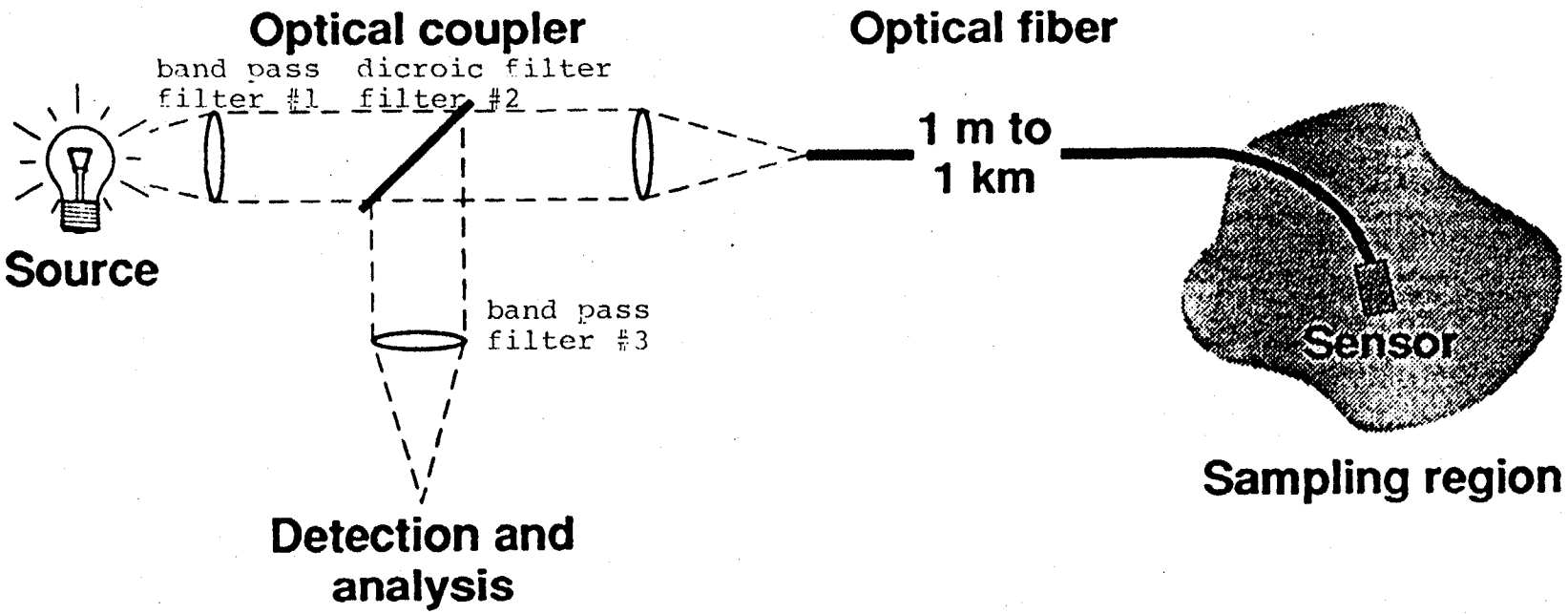

can be used to calibrate a pH curve for any sensor.

When testing the sensors, pH buffer solutions are used. With buffers, the solution can be made to a specific pH. Also, these solutions can withstand large amounts of water dilution before the pH shifts. The buffers used had constant ionic strength whenever possible. McIlvaine constant ionic strength buffer solutions were made (Elving, Markowitz, Rosenthal, 1179). The effects of ionic strength on these sensors have been considered. Since the sensor reacts to hydrogen and hydroxide ions, it is reasoned that if other ions are in the pH solutions, this will affect the sensor reading. (Do Optical Sensors Really Measure pH?). Using pH buffers of constant ionic strength eliminates this variable from these studies, although a thorough investigation should consider this factor. For many applications this affect is negligible.

Before any fibers were fabricated, a control group was run. The fluorescein dye was diluted with pH buffer solutions ranging from pH 4 to pH 10. Then a bare fiber was used to measure the response with the fluorimeter. There were two general conclusions. First, the signal increased with increasing pH. This trend continued with the sensors where the dye was polymerized onto the fiber tip. Second, there was a linear response region. The response increased linearly with solutions containing between 1% and 17% dye. Thus, sensors fabricated with differring dye concentrations could be compared.

5. Experimental parameters.

A series of parameters were then tested to see under which conditions the fiber response, in both response time and range, would be optimal. One of the first parameters tested was the necessity of the sulfuric acid bath. Since this is an over night step, it would be advantageous if it were unnecessary. The difference in fibers produced with and without the acid bath was small, but this step was continued for cleanliness. It is thought that the sensor life span would be reduced without this step because the polymer would not bond properly with the fiber tip. This has not been followed up on, but any excess dye left unpolymerized could also make the sensor change over time. Eventually, this dye would be washed away.

Various optical filters were used to limit the wavelengths of light flowing through the optical cable during polymerization. First, a filter with a very narrow band pass centered around 335 nm was used. It blocked out too much of the ultraviolet wavelengths, and had a low percentage of transmission at the 335 nm wavelength. This filter was then abandoned for another with a band pass of 350 nm and with a band width of around 100 nm. This filter also has a 90% transmittance

rate at the 350 nm wavelength. This filter has been used to create fibers with substantially larger responses ranges. This change provided for greater sensor sensitivity. Sensors created with this filter also had a larger magnitude of response than sensors made with no filter. This evidence supports the theory that excess light allowed into the photopolymerization process bleaches the fluorescein dye.

The central parameter throughout this experiment is exposure time. The longer the polymerization solution is exposed to light, the further the reaction will progress. This produces a large range of signal response. However, the polymer can become too thick, increasing the response time. With a thick polymer, the diffussion rate of new pH environments slows down. It takes longer for the ions to flow in and out of the pourous polymer tip. Thus, an exposure time that produces a good range and a fast response must be determined.

With the wide band pass filter, the threshold between fast response and wide range was between 12 and 15 seconds. This change is too small a window. With the series of steps needed to produce the sensor, there is too much room for human error. For example, after the fiber with the applied polymerization solution has been exposed, it is rinsed off with water to remove any unpolymerized solution. This could take a second or two, a critical amount of time if the exposure time is so short already. Thus, neutral density filters were incorporated into the process. By decreasing the power going through the fiber, it was hoped that the exposure time would increase. First, a filter of neutral optical density 1, which reduces the intensity to 10% of its original strength, was used. Even at long exposure times of two minutes, there was no polymerization occurring. Thus, it was reasoned that the process required some amount of activation energy to break bonds. Once these bonds are broken, the reaction must progress at an exponential rate. This hypothesis would explain the small window of exposure time, where on one side the response time is fast, but with a small range, and on the other side the reverse occurs. Then, another filter of optical density 0.3, or approximately 50% of the original intensity, was used. This did not provide enough blockage, for this threshold was centered around a short exposure time again. Finally, a filter of 0.5, or approximately 32% of the original intensity going through the fiber, was used, and satisfactory results were reached. The threshold, with the wide band pass filter being used, is believed to be around 20 seconds.

Then, it was decided that a capillary should be used during the polymerization process. The reagents used in this process react well with air, particularly the oxygen in it. At first, the solution was applied to the fiber tip, and

then left in the open air during polymerization. It was thought that the process occurred quickly enough that this was not a major problem. However, by using the capillary to hold the solution, and then slipping the capillary over the fiber tip, oxygen could not get in the way. In fact, the polymerization solution is nitrogen gassed for an hour before used so as to remove any oxygen from the mixture. With the capillary, sensor response improved.

Another consideration is the age of the solution. The reagents store well before mixing. After mixing, however, they age. After a three to four week shelf life, the acryleylfluorescein, and the resulting polymerization solution it is used to make, must be mixed fresh. Sensors made with old solution showed no change in response from pH 4 to pH 9.5. At pH 10 though, the signal suddenly dramatically increased. The sensor response was analogous to a high-tech litmus paper response. The sensor being developed must respond to a range of pH solutions.

6. Sensor conditioning and stability.

All of these factors came together to produce a satisfactory sensor. The conditions during the fabrication of the sensor were 20 seconds exposure time, a filter of optical density 0.5, use of a capillary, and the wide band pass filter. See Figure 4. When testing the sensor, a few more handling procedures were discovered. First, there seems to be a conditioning or hydration period associated with the sensor before it gives consistent results. This conditioning includes exposing the sensor to a range of pH solutions. A range of pH 5 to pH 8 was regularly used.

Secondly, the fiber still cannot give consistent results day by day. See Figure 5. The results from this test were taken a week after those for Figure 4. It was hoped that with rinsing the fiber tip after the exposure, the sensor would give consistent results over a period of time. Some of the earlier fibers left some unpolymerized solution on the fiber tip. This was before the rinsing step was included in the polymerization process, directly after the exposure. Thus, the sensor readings deteriorated over a few days until all the unpolymerized solution was rinsed away. However, this satisfactory sensor was made with the rinsing step included in the fabrication process. The aging process is not fully understood. One theory is that the 2-hydroxyethyl methacrylate sites, which encourage ion transfer, become clogged. These sites may permanently bind with ions in solution, thus destroying the sensor.

Another handling issue is how measurements are taken. Currently, the sensor is dipped into small viles that contain pH buffer solutions. Depending on how far the sensor is inserted, the reading will change. When the buffer is stripped,

Figure 4

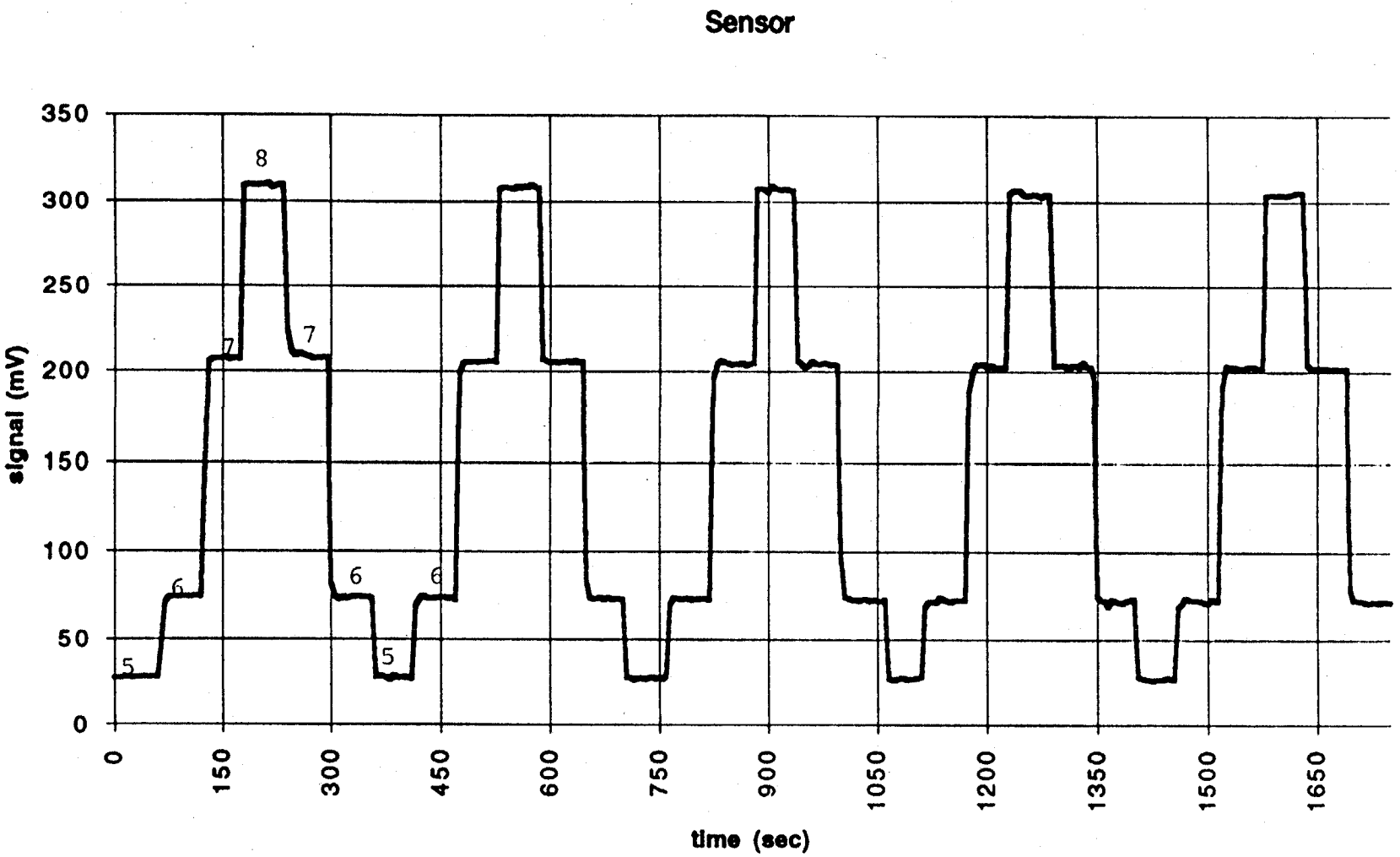

pH ranges 5,6,7,8,7,6,5,repeat

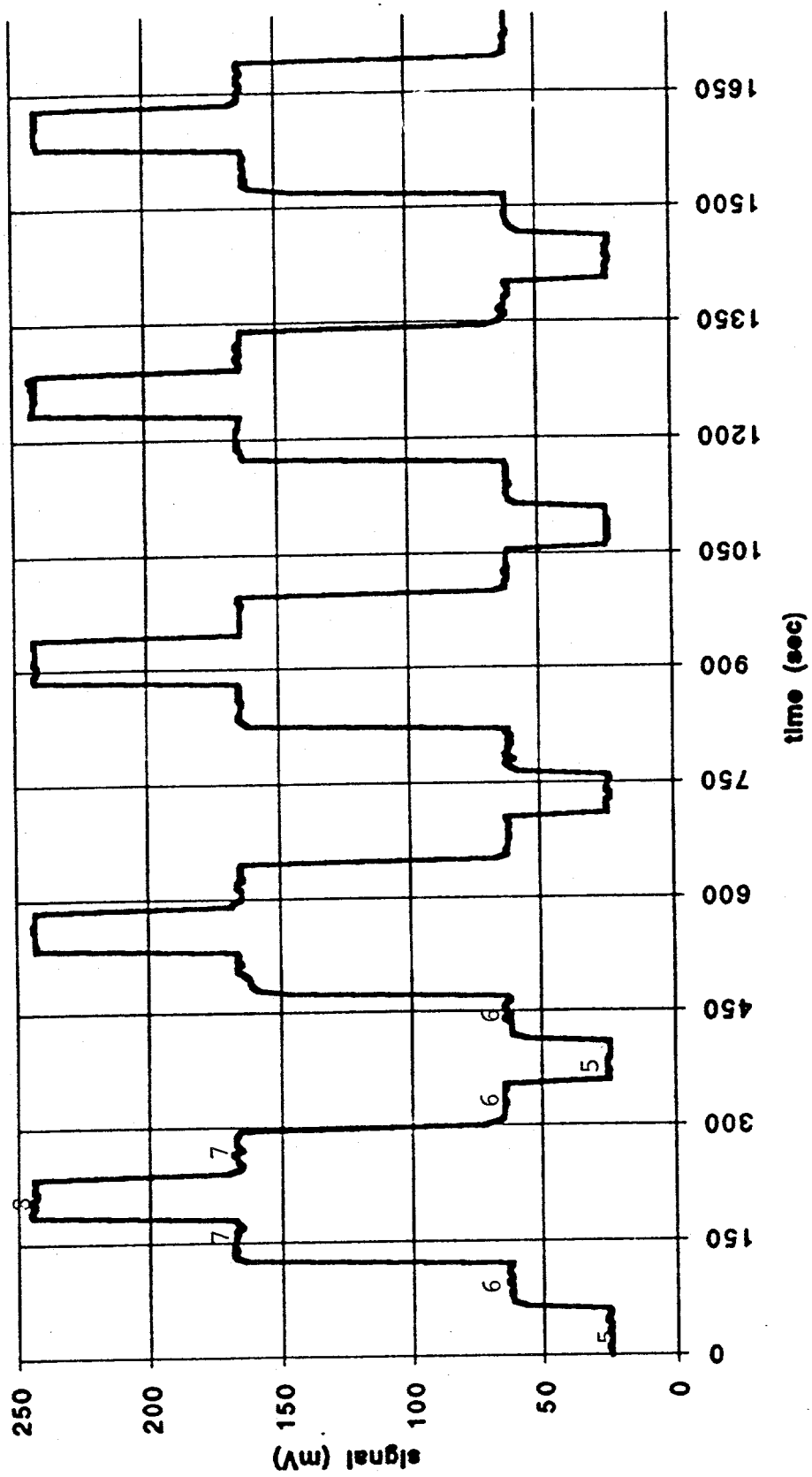
Sensor Retest
signal (mV)
250
200
150
100
50
0
time (sec)
0
150
300
450
600
750
900
1050
1200
1350
1500
1650
5
6
7
8
7
6
5
6
7
6
5
pH ranges 5,6,7,8,7,6,5,repeat

Figure 5

a small length of cladding is left exposed. This varied in length, for the problem was not readily realized. At the connector end, light is trapped into the cladding layer. If the area where the cladding is exposed is left open to air, light will not escape. In the pH solution it can. Thus, as the sensor was dipped deeper into the solution, more light was lost, and the sensor response declined. In order to eliminate this discrepancy, the sensors were tested in the same manner. The entire length of exposed cladding was emersed in solution when measurements were taken.

Perhaps the most important handling tip is being careful not to bump the sensor on anything. The polymer tip can be knocked off quite easily. A method of hanging and protecting the sensors is recommended.

7. Reproducibility.

As might be expected with so many variables, this fiber has proven to be irreproducible. Therefore, several modifications are being made to take out the human error. An electronic shutter has been installed so that there is no error in cutting off the light source after a given amount of exposure time. Previously, a block was manually placed in front of the light source. Also, a fiber holder has been made to hold the fiber at the exact same location while power output is being checked. Remember that the same amount of light must be flowing through the fibers from exposure to exposure if the results are going to be compatible. Lastly, the light source used during the polymerization process is rather old. It has a tendency to have hot spots. Since the source is an arc lamp, these spots will jump around, perhaps during the polymerization process itself. Thus, a new lamp is being looked into. In the mean time, the location of the light source is checked before and after each sensor is made. If the light source did not shift, the sensor is considered to be acceptable. If the source moved, the sensor is removed from consideration.

8. Conclusion.

An optical sensor is an ideal solution to the pH measurement problem. Unfortunately, developing such a sensor is fraught with questions and uncertainties. Many important variables in this process have been investigated, but there is much more work to be done.

It is hoped that once a pH sensor has been developed, the same technique can be used to create other fiber optic sensors. For example, a carbon dioxide fiber optic sensor. Such a sensor would be small. It would also provide instantaneous measurements. This would eliminate taking samples, and sending them off to a lab to be analyzed. Thus, the experiment was not only centered around pH sensors, but about how to develop fiber optic sensors in general.

9. Acknowledgments.

Many scientists and engineers helped with this project. In particular, Eugene Mizusawa, Jim Richards, Fred Milanovich, Kevin Langry, Steve Brown, and Tom Vess provided vital expertise and skill. Also, the research group at Tuffs University provided critical guidance and insight.

10. References.

1. Elving, Philip P.; Markowitz, Joseph M.; Rosenthal, Isadore. "Preparation of Buffer Systems of Constant Ionic Strength." Analytical Chemistry. Vol. 28, No. 7. July 1956. p. 1179-1180.

2. Janata, Jiri. "Do Optical Sensors Really Measure pH?." Analytical Chemistry. Vol. 50, No. 9. May 1, 1987. p. 1351-1356.

3. Munkholm, Christiane. Polymer Immobilization Chemistry for the Preparation of Fiber Optic Sensors. 1989.

4. Willard H. Instrumental Methods of Analysis. 1988.

5. Young, Matt. Optics and Lasers, Including Fibers and Optical Wave Guides. Fourth Edition. 1992. p. 5-9.

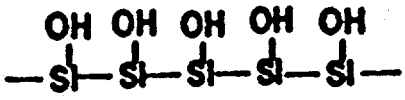

Fiber surface after the sulfuric acid bath

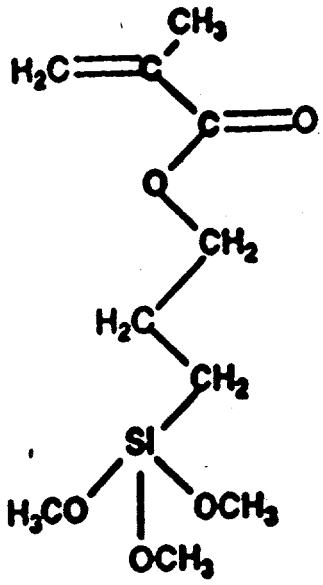

3 (Trimethoxysilyl) propylmethacrylate

Fiber surface + 3 (Trimethosysilyl) propylmethacrylate $\xrightarrow{\text{acetone}}$ Functionalized Fiber Surface

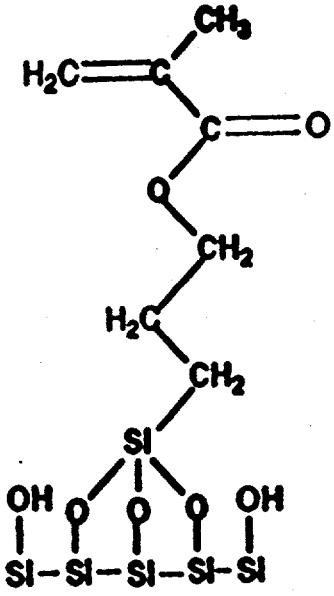

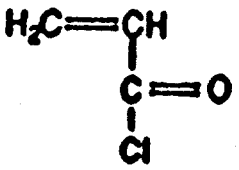

Acryloyl Chloride

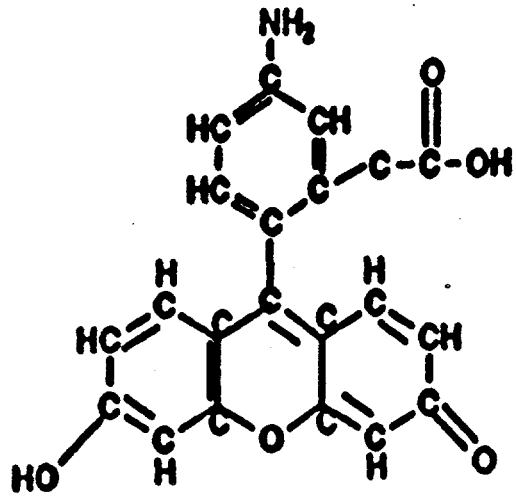

Fluoresceinamine Isomer 1

Fluoresceinamine Isomer 1 + Acryloyl Chloride $\xrightarrow{\text{acetone}}$

Acryleylfluorescein

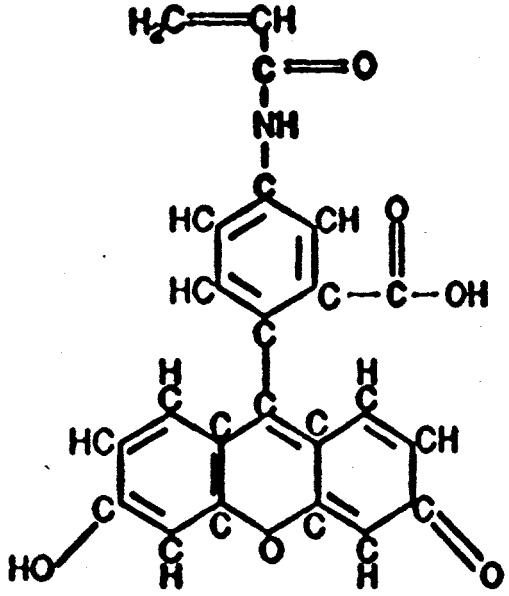

STEP 3

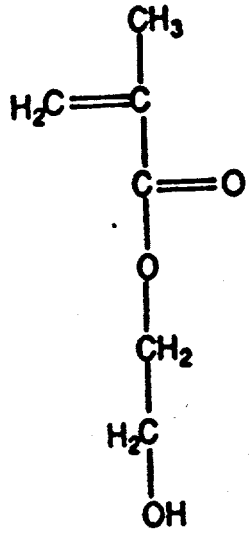

2-Hydroxyethyl Methacrylate

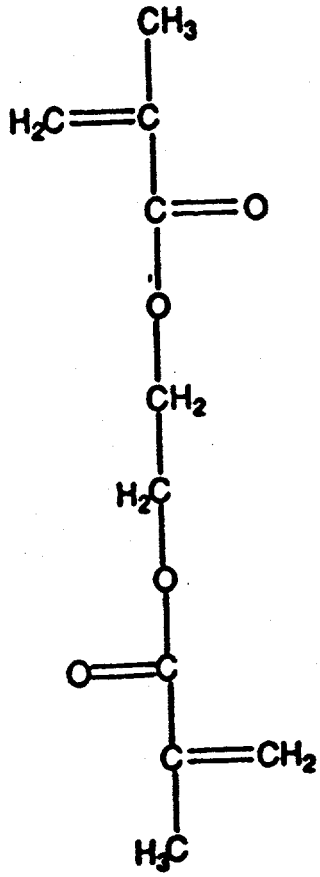

Ethylene Glycol Dimethacrylate

STEP 3

Functionalized fiber surface + Acryloylfluorescein +

2-Hydroxyethyl methacrylate + Ethylene glycol dimethacrylate $\xrightarrow[E = h\nu]{\text{Benzoin ethyl ether}}$

polymer, sensor

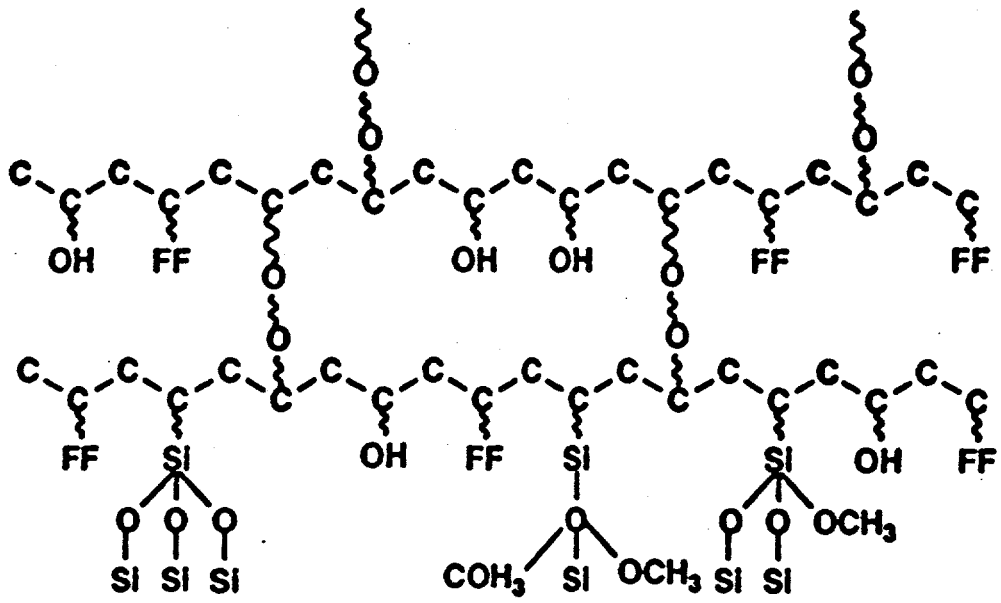

Ethylene Glycol Dimethacrylate

2-Hydroxyethyl Mathacrylate

Acryloylfluorescein

Replacing Chlorofluorocarbons(CFCs) in the Metal Cleaning Process*

Sophia Hsu

Indiana University

Lawrence Livermore National Laboratory
Livermore, California 94550

December 15, 1993

Prepare in partial fulfillment of the requirements of the Science and Engineering Research Semester under the direction of Mike Meltzer and Dave Miscovich, Research Mentor, in the Lawrence Livermore National Laboratory.

*This research was supported in part by an appointment to the U.S. Department of Energy Science and Engineering Research Semester (SERS) program administered by LLNL under Contract W-7405-Eng-48 with Lawrence Livermore National Laboratory.

Replacing Chlorofluorocarbons(CFC's) in the Metal Cleaning Process

Sophia Hsu
Indiana University
Lawrence Livermore National Laboratory
U.S. Dept. of Energy
Livermore, California 94550
Dec. 15, 1993

Abstract

The Montreal Protocol requiring industries to phase out the production and use of ozone depleting compounds(ODC), i.e. Freon TE, has prompted Lawrence Livermore National Lab(LLNL) to identify high performance environmentally benign cleaners that could replace Freon TE. My project; with the mentor ship of Ralph Hershey, Mike Meltzer, and Dave Miscovich; is to identify high performance alternative solvents that could replace Freon TE, which is a CFC-113, in metal cleaning and plastic processes, specifically printed board assemblies(PBA). All the alternative solvents we chose for our project can adequately remove flux and contaminants from PBAs via ultrasonic cleaning. Also, we wanted to know the efficiency of these cleaners on the PBAs compared to Freon TE if aged a simulated 15-20 years. This paper will briefly discuss the Alternative Testing Program at LLNL followed by a description of the methods used in my project. However, any conclusive results cannot be made until more extensive research is done.

The Alternative Testing Program

For decades, humans have used hazardous solvents such as freon and 1,1,1 trichloroethane, carbon tetrachloride and isopropyl alcohol for many cleaning applications. Industries and the public now understand what the consequences of their previous actions can do to the ecosystem and themselves. Freon and other chlorinated cleaners have the ability to destroy the stratospheric ozone layer, which is the primary reason why the Montreal Protocol was developed and implemented.

The purpose of the Alternative Solvents Testing Program is to identify high performance environmentally benign cleaners which ensures employee safety while minimizing industrial waste and cost. In order to achieve this goal, we need to test the alternative cleaners and compare them with the traditional solvents. We can replace the traditional solvent if the alternative performs "equally to or better than existing cleaning technology".

As a result of our program, many divisions at LLNL have already switched to alternative cleaners. For example, the Lasers program now uses Brulin 815GD to cleaning their vacuum pumps and laser glass. Brulin 815GD is a fully aqueous industrial cleaner which is biodegradable, does not require an air quality permit, and is not a volatile organic compounds.

My Project

My project is to identify alternative solvents that can replace Freon TE in the metal cleaning process specifically printed board assemblies (PBAs). Freon TE, a member of the halogenated hydrocarbon/alcohol family, has been used for many decades and is an accepted cleaner in the metal cleaning process. We want to ensure that the alternatives will

perform equally or better. In addition to identifying alternative cleaners which clean equally or better than Freon TE, we want to know if these solvents will detrimentally degrade the PBAs electrical performance in 15-20 years.

High performance alternative cleaners are identified by testing and comparing them to the traditional cleaners. The first stage of the alternative solvents testing program is to establish a cleanliness baseline for a particular contaminant, substrate, and cleaner. The cleanliness baseline is then used on the PBAs with the alternative cleaners. To determine the cleanliness of the PBAs, one needs to use a combination of visual, chemical, and electrical test methods.

For the PBA alternative cleaner test, we chose the following:

Contaminant:	Rosin mildly activated solder flux
Substrate:	Printed Board Assemblies(19 total)
Baseline Cleaner:	Freon TE
Alternative Cleaners:	1. Four PBAs were cleaned with Axarel 32
	2. Two with Armakleen E2000
	3. Two with Kyzen 101
	4. Two with H20002E
	5. Two with Rosin X
	6. Two with 815 PCX
	7. One with Purasolv ELS

Note: We also tested two uncleaned boards

Procedure Overview

I used the following key steps in the PBA project:

+Fabricate the PC boards
+Conformity/shorts testing
+Assemble the PC boards
+Clean the PC boards
+Humidity and calibration system(environmental test chamber)
+Analyze the environmental test chamber data
+Analyze the PC boards
    -microscope
    -ionograph
    -reflective surface infrared spectroscopy

Procedure

Bare copper printed boards were designed specifically to be used to determine the insulation resistance between conductivity patterns. Insulation resistance experiment indicates the change in resistance between the conductivity patterns when exposed to a high humidity and high temperature environment. Our industrial partner TRW fabricated and assembled (components only) four out of the 19 PBAs. LLNL fabricated the remaining 15 PBAs and I assembled them.

Before assembling the printed boards, I tested them with a Fluke Mutimeter to insure the absence of shorts and that the PBAs were functional. I recorded any pattern which had shorts. The very few PC boards which did have some shorts were still functional enough for our experiment.

The PBA consisted of soldering the components to the surface of printed board. I then soldered the wires to the board, including the TRW boards. I soldered the nine ceramic chip components; three 1210s, three 1206s, and three 0805s; onto the PBA to determine if contaminants from

underneath them could be removed by cleaning (see fig 1.1). Each board consisted of over 80 wires, which connected the boards to a pair of card connectors. The card connectors connected to a ribbon cable which was then connected through the wall of the environmental test chamber to the data acquisition and control system (see fig 1.2).

Our cleaning process for the boards consisted of a vapor degreaser and an immersion bath using ultrasonics. Two boards were cleaned with Freon TE in the vapor degreaser for a baseline comparison. We cleaned the others in a 50 megahertz immersion bath. We used the manufacture's instructions for the solvents' concentration and agitation temperature. We agitated the PC boards for five minutes and rinsed them twice, five minutes apiece. The boards were then air dried.

Note: Since Axarel 32 is extremely oily, we ended up cleaning four boards. The agitation temperature was low(42°C-48°C) for the first set and high(65°C-70°C) for the second set. The first set of boards we rinsed twice, five minutes a piece, and the other two we rinsed *four* times(at 65°C), five minutes apiece. See fig 2.1 for a detailed report on how the other boards were cleaned.

Fig. 1.1

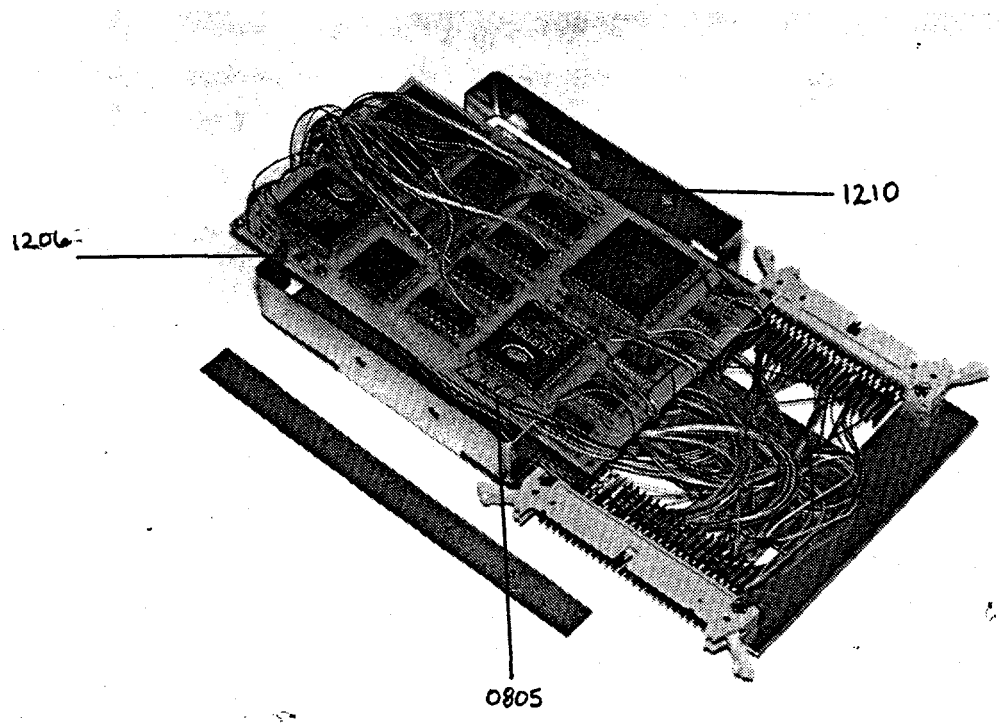

The Display of the Printed Board Assembly's Wires and Components

Fig. 1.2

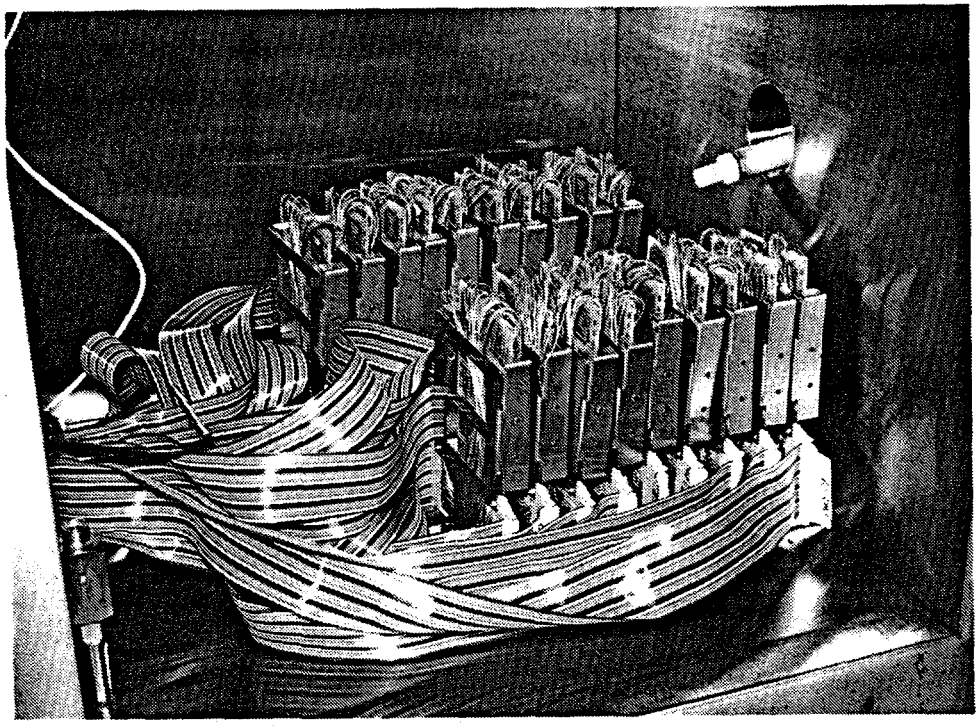

The card connectors connected to a ribbon cable which was then connected though the wall of the environmental test chamber and to the data acquisition and control system

Fig. 2.1

Solvent	Manufacturer	Concentration	Agitation Temperature	Observations
Armakleen E2000	Church &	10%	28° C	The agitation temp. was too low so they were re-rinsed at 40° C
	Dwight			
Axarel 32	DuPont	100%	42°-48° C	
Axarel 32	DuPont	100%	65°-70° C	Four rinses at 65° C
Freon	DuPont	100%	n/a	Vapor Degreaser-spray application
H2002E	O.C.S	10%	26° C	The agitation temp. was too low so they were re-rinsed at 40° C
	Manufacturing			
Kyzen 101	Kyzen Corp.	8%	40° C	
Purasolv ELS	PURAC	100%	40° C	
Rosin X	Brulin	20%	44°-50° C	
815 PCX	Brulin	30%	45° C	

Environmental Test Chamber

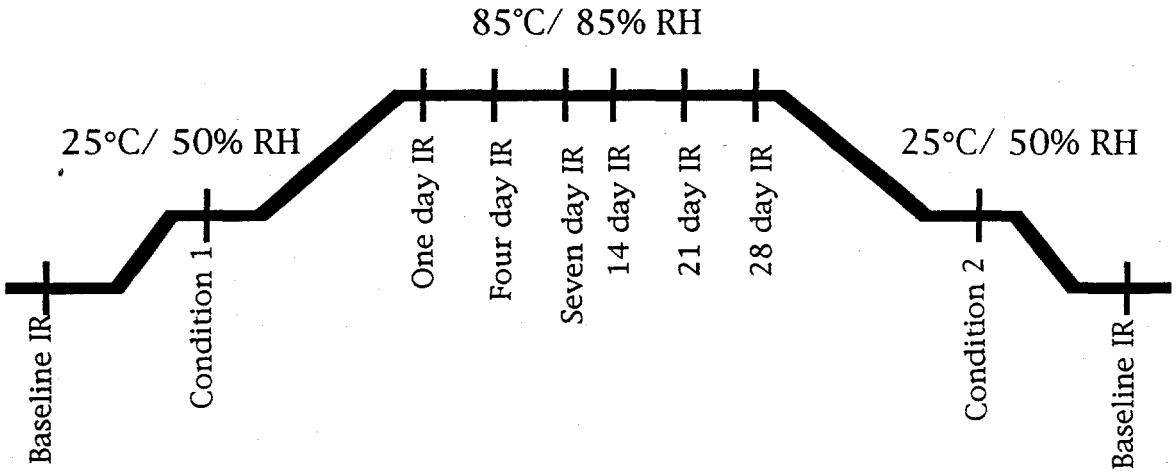

After cleaning the PC boards we put them through an elevated temperature and humidity test chamber to simulate a 15-20 year aging process. The test chamber has accurate temperature and humidity controls to control the environment in order to measure insulation resistance leakage current. To establish insulation resistance(IR), the boards are first conditioned for one day at 25°C/50% relative humidity(RH). Then the boards are exposed to a 85° C/85% RH environmental stress strain for 28 days and then ramped down to 25° C/50% RH for another day of conditioning reading. For the each different test condition (10 total, see above figure), I took an IR current reading. The baseline IRs were taken of the electrical test system at ambient conditions without being hooked up to the PC boards.

Analysis of IR data

The raw data from the test chamber came out as leakage current(in micro amps). Because of the test chamber's highly sensitive controls, any

slight disturbance will cause the data acquisition equipment to record measurements as negative. If a negative data value emerged and was approximately equal to the other data readings, then I took out the negative sign. If the current measurement was above 2.00E-7 amperes(IPC specification), then I recorded the pattern as shorted. Anything above the IPC Spec. would infer a low resistance path or high current levels. As a data acquisition function check, an 10 MOhm resister was placed on the ninth channel of each boards. If running correctly, the ninth channel on each board should consistently register a leakage current close to 4.45 E-6.

No quantitative data is available at this time because we are in the process of investigating the data since an inconsistency of the data exists between day one IR, day four IR, day seven IR, day 21 IR, and day 28 IR.

The IR test does not statistically determine to the cleanliness of the PC boards. The IR test only provided a means of evaluating whether or not the alternative cleaners disrupted the PC board's electrical performance. The alternative solvents may leave ionic residues which the RI test cannot detect. We can look for visual evidence of contaminates(e.g. flux, solvent crystallization, corrosion) through a microscope while quantitative data can be acquired by an ionograph and reflective surface infrared spectroscopy. The ionograph measures the amount of residual ionic contaminants left on the PC board. The reflective surface infrared spectroscopy measures the thickness of hydrocarbon contaminants remaining on the PBAs and also identifies the contaminants. This data is not available at this time.

Conclusion

The purpose of the alternative solvents testing program is to identify high performance solvents, compare them with the traditional cleaners, and then replace them if they perform equally or better. These alternatives are safer to the workers and the environment in addition to minimizing cost and industrial waste. My project is to identify high performance solvents to replace CFC's in the metal cleaning process. I discussed the procedures I used and procedures I would have used, given more time. However at this time, further investigation needs to be done on the project to make any conclusive results. Many of the alternative cleaners are already being used at LLNL, which not only makes the alternative solvents testing program successful but also displays people's willingness to use them.

LifeMan*

Brant Lindhorst

Northeastern Illinois University

Lawrence Livermore National Laboratory
Livermore, California 94550

December 15, 1993

Prepare in partial fulfillment of the requirements of the Science and Engineering Research Semester under the direction of Brain Lindow
Research Mentor, in the Lawrence Livermore National Laboratory.

* This research was supported in part by an appointment to the U.S. Department of Energy Science and Engineering Research Semester program administered by LLNL under Contract W-7405-Eng-48 with Lawrence Livermore National Laboratory.

LifeMan

Brant Lindhorst
Northeastern Illinois University
Computations

ABSTRACT

My project involved creating a simple predator/prey model. It is actually an extension of the game of LIFE. The game of LIFE is a computer simulation that was developed by John Conway to test a theory of J. Von Neumann. The game involves simple objects and rules governing those objects. The rules determine if an object lives, dies, or is born. The game starts with an initial pattern, user defined or random. Each iteration applies the rules to the objects, and the objects are displayed on the screen. Will the pattern remain constant, die off, or possibly evolve? We want to extend this system. The objects become species, and the rules become changeable. The user can define many different species, each of which has its own rules. In doing this, LIFE becomes a simple subset of our proposed simulation. The ultimate purpose is to see how various systems change over time and to demonstrate that making small changes in a system can drastically change outcomes.

Introduction

My project is called LifeMan. LifeMan is a predator/prey simulator. Its predecessor is the Game of LIFE. LifeMan is based on, and expands upon the Game of LIFE. Although LifeMan is superset of the Game of LIFE, it has a different purpose.

The Game of LIFE

The Game of LIFE is a computer program devised by John Conway to test a theory of J. Von Neuman. Von Nueman was a prominent scientist who wanted to know if machines could build more complex machines. Conway basically restated this to say: can simple and random systems evolve into more complex and organized systems?

Conway devised the Game of LIFE to test this restated theory. In the Game of LIFE, there is only one type of obejct and a simple set of rules governing the objects. The objects are displayed on the screen as pixels. An object is born if it has three neighbors. An object remains alive if it has exactly two neighbors. And, an object dies if it has less than two or more than three neighbors.

William Poundstone, in his book that examines the above theories, The Recursive Universe, argues that given enough time and space, random systems can evolve into organized systems that can reproduce. This implies that Von Neumans original theory is correct.

Expanding the Game of LIFE to LifeMan

The game of LIFE is interesting and fun to watch, but rather simple. A more complex system based on LIFE, might be even more interesting. This new system should allow more than one type of object, and each object should have its own set of rules. My mentor, Brian Lindow, has decided to call it LifeMan. In LIFE, there is only one type of object. In LifeMan, there can be multiple objects that we call *species*. In LIFE, the rules governing the single object are fixed. In LifeMan, the rules can be modified, and a species can be affected by another species rules. LIFE simulated the "evolution" of an object to determine if it could develop into more and more complex systems, given enough time and space. LifeMan simulates how how different species interact.

Because LifeMan is changeable, we can set up scenarios. For instance, we can let species one represent bears, species two can represent wolves and species three can represent rabbit. We can then set rules to reflect births, deaths due to under and overpopulation, and species preying on other species.

We could then enter our own starting pattern or let the computer fill in a random pattern. We can watch each generation, or enter the number of generations to be performed and only see the final one. Maybe we don't like the results, the wolves have started to take over. We could kill a few off, add in some more bears, or possibly put in a new predator - mountain lions that like to hunt wolves. We can then rerun the simulation to see how our changes have affected the outcome.

It should be noted that the Game of LIFE is a simple version of LifeMan. In LIFE, there is only one species, the particle or pixel, and the rules concerning the particle do not change.

The LifeMan Program and Future Work

The LifeMan Program is mainly intended as an educational game. Young students can experiment with adding different species and changing the rules of those species. The program gives fast, visual results, so that students can see how the changes they have made affect outcomes.

LifeMan uses a similar interface to WireMan, so that users of WireMan can easily use LifeMan. LifeMan is being developed using Symantecs ThinkC, and is currently available on the Macintosh.

Additional work needs to be done. First, more precise rules could be added. For example, death occuring only when a species has a predator directly above and below it. The user should also be able to choose a color for a species, instead of one being assigned. Icons might represent species instead of colors only. Next, each generation could be made into a movie file for processing on the CRAY and the output played using the movie program. And finally, an IBM version can be added.

LifeMan Users Guide

The Menu

Under the start pattern menu, there are four choices.

The First choice is random, which will enter a random pattern using all of the current species. There are varying densities, from .1 to .9. If you select .1, then any cell of the field has a one in ten chance of being a species.

The second choice, clear the grid, simply clears the grid of all sepcies.

The third and fourth choices, save and restore pattern, go together. Save pattern saves the current field. Restore pattern restores the saved field if the original field has been altered.

Under the grid size menu item, you can set the grid size to 40x40, 80x80, or 100x100.

Under the rules menu item, you can set how your rules are applied.

If field wrap around is checked, the left and right side of the grid, as well as the top and bottom, are connected. If field wrap around is not checked, the field is cut off at the edges of the grid.

If the species born over other species box is checked, a species can be born on top of another, thereby replacing it. Otherwise, species cannot be born over others.

Parameters Dialog

The number of generations can be changed using the left and right arrows for small changes, or by clicking the box itself and typing in a number.

The show generations check box should be checked if you want to see every generation. When the grid size is large, and there are many generations, showing each generation is slow. If the box is not checked, only the last generation will be shown.

The generate button starts the generate cycle. Generations will be computed until the number of generations specified in the generate box is performed, or until the stop button is pressed.

Species Dialog

In the species dialog, you can add species using the Add button, or remove all of the current species using the delete all button.

Rules for a species can be added or edited by hilighting the species using the mouse, and then clicking on it. A dialog will appear requestng information on the species.

Editing the field

To edit the field in the LifeMan window, simply highlight the species you want to add. If there is already species in the cell you want, click it, and it will be removed. If the cell is empty, a click will place the hilighted species in the cell.

The Program

Due to the large size of the program, I am including only one copy of the files where I have done a considerable amount of work : generatete.c and dialog.c. The complete program and its files are on disk.

Detection of Micronuclei in the Germ Cell Line of Male Mice using Multi-color Fluorescence *in situ* Hybridization

Marek Ma

University of Michigan

Lawrence Livermore National Laboratory
Livermore, California 94550

December 15, 1993

Prepared in partial fulfillment of the requirements of the Science and Engineering Research Semester under the direction of Andrew J. Wyrobek in the Lawrence Livermore National Laboratory.

*This research was supported in part by an appointment to the U.S. Department of Energy Science and Engineering Research Semester (hereinafter called SERS) program administered by the LLNL under Contract W-7405-Eng-48 with Lawrence Livermore National Laboratory.

Detection of Micronuclei in the Germ Cell Line of Male Mice using Multi-color Fluorescence *in situ* Hybridization

Marek Ma

Abstract

The ability to detect genetic abnormalities in germ cells helps further our understanding of the effects of toxicants on congenital defects during birth and development. We are currently developing a method to detect one such genetic abnormality, the micronucleus in the male germ line. A micronucleus, a chromatin piece or whole chromosome separated from the main nucleus, is an indicator of a chromosomally abnormal gamete. Our goals are to detect and determine the type of micronuclei in round spermatids, the haploid precursors of sperm, and to investigate the effects of exposure of mice to germinal mutagens.

To make microscope slide preparations of spermatid micronuclei, seminiferous tubules were teased apart, treated with collagenase and trypsin, centrifuged in testis isolation medium, dropped on glass slides, and air dried. Micronuclei were evident when DNA was stained with DAPI. Also, to determine their chromosomal origin, DNA probes for the pan-centromeric regions and the X chromosome were labeled with digoxigenin and biotin by nick translation and the signals were detected using a combination of rhodamine and FITC. Two types of micronuclei can be discerned by these multi-probe procedures; one carries a chromosomal fragment missing a centromere, while the other contains a whole chromosome.

The developed methods are now being applied to a current study. The effect of the aneugen chloral hydrate on the development of the germ cells of male mice is being investigated with the micronuclei and fluorescence *in situ* hybridization methods. By sampling mice shortly after exposure, we investigate the sensitivity of the meiotic phase of spermatogenesis, whereas sampling mice at a longer time interval will reveal effects on spermatogonial cells in mitosis. Such information may have important consequences for human males exposed to this anesthetic agent.

Introduction

The ability to detect genetic abnormalities in germ cells helps further our understanding of the effects of toxicants on congenital defects during birth and development. We are currently developing a method to detect one such genetic abnormality, the micronucleus in the germ line of male mice. A micronucleus, a small chromatin piece or whole chromosome separated form the main nucleus, is an indicator of a chromosomally abnormal gamete (Figures 1 and 2). My main tasks were to help develop the micronuclei detection protocol and to optimize the efficiency of the labeling of the centromeric probes. I also applied the modified protocols to the chloral hydrate study.

Background on Spermatogenesis

The mouse serves as a model in our search for the micronuclei in male germ cells. Spermatogenesis is the development and differentiation of stem cells into elongated spermatids. Through many cycles of mitosis, stem cells become spermatogonia, then primary spermatocytes. Through a complete cycle of meiosis, the primary spermatocytes become secondary spermatocytes, then spermatids. In the process of acrosomal cap maturation and nucleus elongation, round spermatids become elongated spermatids. This entire cycle lasts a total of 58 days.

There are advantages to using spermatogenesis as our model of cell differentiation. The stages are well defined and easily distinguishable morphologically (Figure 3). Another benefit of spermatogenesis is the regularity of its stages. We can predict with some certainty that a cell in one stage was in an earlier stage "X" number of days earlier. For instance, a round spermatid in stage five would have been in diakinesis four days earlier. We can expose a mouse, and wait for the cells at a particular stage when exposed, to develop into round spermatids, where the micronucleus is most visible.

Micronucleus

There are two types of micronuclei; one carries a chromosomal fragment missing a centromere. This micronucleus could arise as a consequence of a DNA breakage event during spermatogenesis. The other type of micronucleus contains a whole chromosome due to an error in chromosomal segregation. Because the centromeres are at the end of the chromosomes, their presence indicates the presence of an entire chromosome. The exact mechanism of micronuclei formation is not yet known.

Methodology

Our three goals were to detect micronuclei in round spermatids in stages 1 through 7, determine if the micronucleus contains a centromere, and to investigate the effects of exposure of mice to germinal mutagens on micronucleus induction. The micronuclei protocol can detect, but is unable to differentiate between the two types of micronuclei. To make microscope slide preparations of round spermatids, seminiferous tubules were teased apart, treated with collagenase and trypsin, centrifuged in testis isolation medium, filtered through bridal veil, dropped on glass slides, and air dried. The centrifugation helps remove the lighter elongated spermatids, while filtration removes the heavier parent cells of round spermatids. Micronuclei were evident when the DNA was stained with DAPI. M.E.A.B. van Beek and I worked on a set of criteria defining what were round spermatids and micronuclei. A round spermatid was distinguished mostly based on the size, texture and shape of its nucleus. To qualify as a 'definite' micronucleus, the structure must be obviously separate from the main nucleus.

The existence of a centromere in a micronucleus can be determined by centromeric probes visualized by fluorescence *in situ* hybridization. DNA probes for the pan-centromeric regions and X chromosomes were chosen for several reasons. Because the pan-centromeric probe labels all chromosomal centromeres, it gives us

the most complete coverage of centromeres. The Y chromosome does not have the complementary sequence and is not labeled. The X chromosome probe, used in addition to the pan-centromeric one, provides three unique advantages. First, because only a single chromosome is labeled, an accurate efficiency value can be determined. Efficiency is the percentage of round spermatids carrying a specific probe. Next, the X chromosome is involved in genetic diseases like the Klinefelter's syndrome. These chromosomal abnormalities are readily expressed phenotypically in humans. Finally, in somatic cells of women, it has been shown that an increase of micronucleus formation correlates with age, and that 80% of those micronuclei contain an X chromosome (Tucker lab, LLNL). It appears that the X chromosome preferentially forms a micronucleus.

These DNA probes were labeled with digoxigenin and biotin by nick translation and the signals were detected using a combination of rhodamine and FITC. This process is known as fluorescence *in situ* hybridization. To get a high efficiency for the X and pan-centromeric probes, we had to experiment with variations of the fixing method which is employed after the slides are air-dried but before they are hybridized.

Results

Over the semester, I have scored approximately 8000 round spermatids (Figure 4). My frequencies of micronucleated spermatids for mouse strains agree with published data. For example, scoring about 4500 cells, I obtained a frequency of 0.9 per thousand cells, which is comparable to the 1.2 value found by Collins et al. (1992).

I have had some success with the probe labeling efficiency. Scoring 500 cells, we found the X efficiency to be 52% while the pan-centromeric was 100%. These values compare well with the theoretical values of 50% for the X and 100% for the pan-centromeric. We expect half of the gametes to carry the X, while the

other half, the Y. The above method of fixation included baking at 80° C for thirty minutes, then treatment with 0.1% Tween-20 followed by an ethanol series. Similar conditions have not always produced consistent results.

Method Application to Chloral Hydrate Study

The developed methods are being applied to a current study. The effect of the aneugen chloral hydrate on the development of the germ cells of male mice is being investigated with the micronuclei protocol and DNA probes visualized using fluorescence *in situ* hybridization. Such information may have important consequences for human males exposed to this anesthetic agent.

Various studies have shown that some effects of chloral hydrate on less differentiated cells in spermatogenesis would remain until they become round or elongated spermatids. In round spermatids, we look for micronucleus induction, whereas, in elongated spermatids, we may see an elevated rate of hyperploidy. A colleague of mine, Elizabeth Nutley, is studying this phenomenon in elongated spermatids. Allen et al. (in press) found a statistically significant increase of micronucleus formation in spermatogonial stem cells expose to varying dosages, using a high dose of 165 mg of chloral hydrate/kg of body weight (Figure 5). Studies have also shown an elevated rate of hyperploidy due to chloral hydrate in two later stages, diakinesis and preleptotene.

For the current investigation, we are focusing on three stages, spermatogonial stem cells, preleptotene, and diakinesis. The dosages are 0, 82.7, 165.4, and 413.5 mg/kg. The number of mice in each group ranges from four to six, totaling 53 mice. The animals were injected intraperitoneally with chloral hydrate. Spermatid preps have been done for all 53 mice, and the slides are now ready for hybridization and scoring.

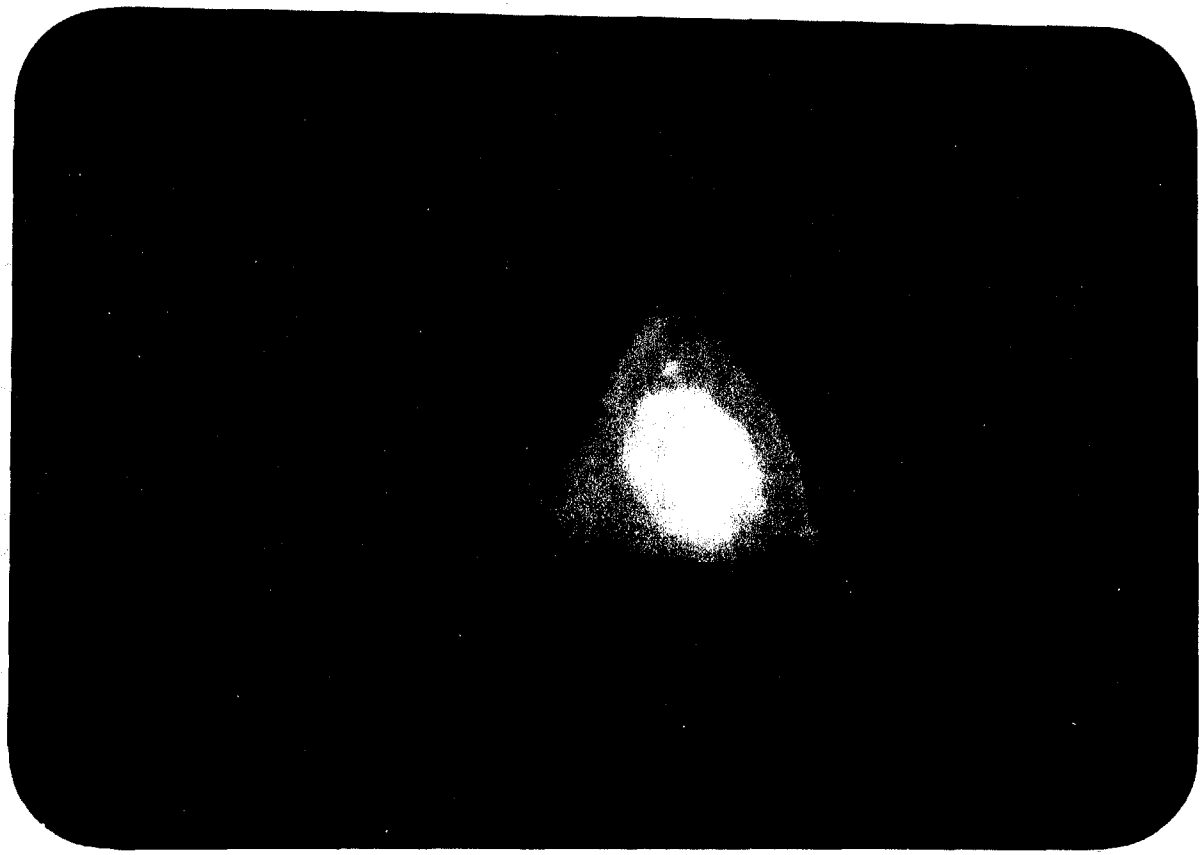

Figure 1
There is a micronucleus above the main nucleus.

Figure 2
The cell in the upper right corner has a micronucleus to the left of its main nucleus. There is an X signal in the center of the nucleus in all three cells.

Spermatogenesis occurs in a predictable manner

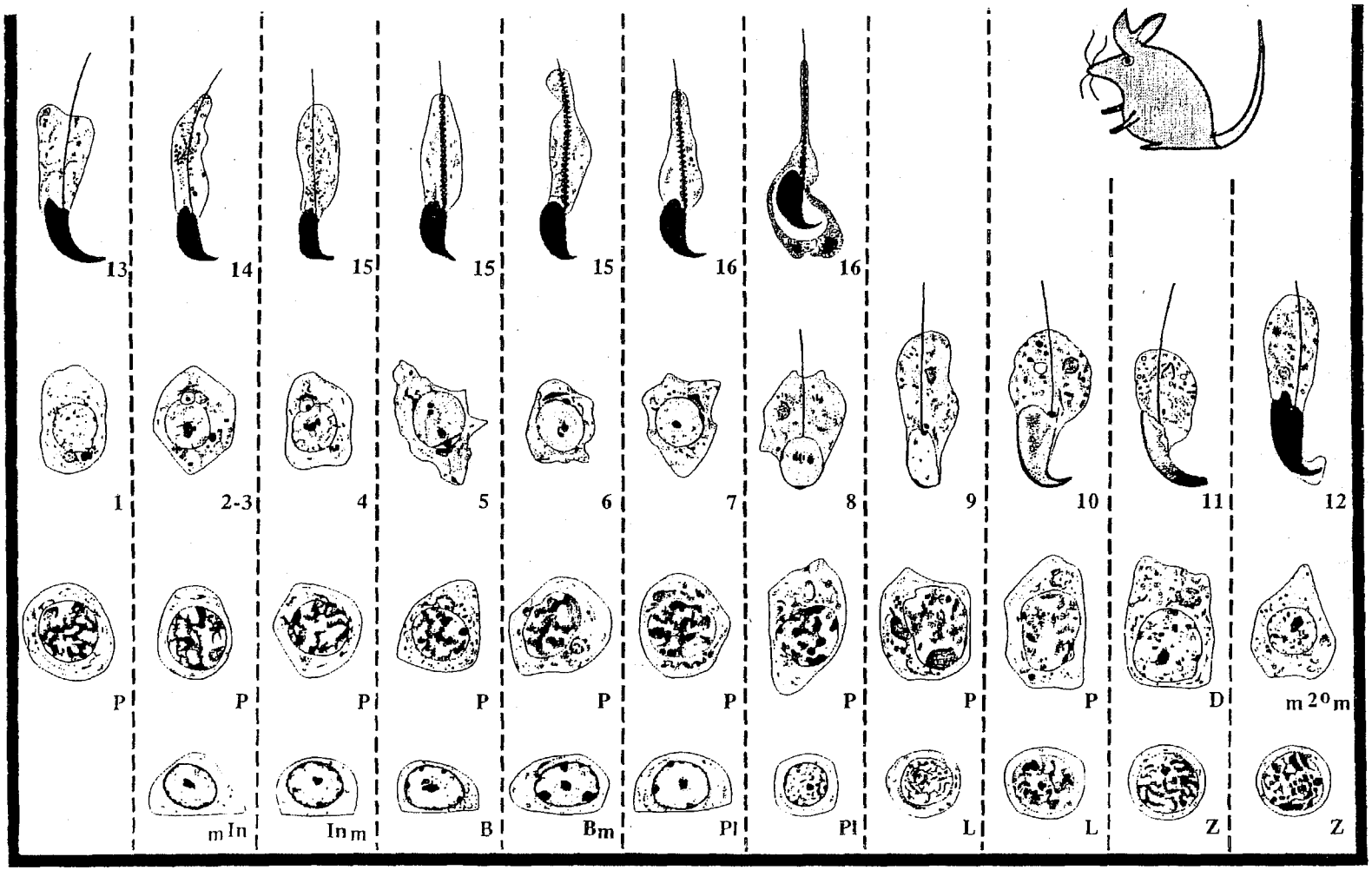

Figure 3

Frequencies of micronucleated spermatids in normal male mice of two genotypes

Strain	Mouse Number	Number of spermatids scored	Number of micronuclei observed	Frequency of micronucleated spermatids (per 1000)
C57BL/6	1	414	1	2.4
	2	1000	2	2.0
	3	1830	1	0.5
	4	1252	0	0.0
	Total/avg.	**4496**	**4**	**0.9**
	Collins et al. 1992	**5000**	**6**	**1.2**
C3H	1	**3400**	**2**	**0.6**
	van Beek, LLNL	**4500**	**2**	**0.4**

Figure 4

Effect of in vivo chloral hydrate exposure on frequencies of spermatid micronuclei in male mice

Allen et al.,In press

Cell Stage Treated	Dose (mg/kg)	% frequencies of micronucleated spermatids	Significance
Spermatogonial Stem Cell (49 days)	0	0.6	NS
	41	3.6	0.05
	83	2.4	0.05
	165	3.8	0.05
Preleptotene (13.5 days)	0	0.6	NS
	41	1.4	NS
	83	2.2	0.05
	165	1	NS
Leptotene-Zygotene (11 days)	0	1.4	NS
	41	0.8	NS
	83	1.6	NS
	165	1.4	NS
Diakinesis-Metaphase I (22 hours)	0	0.6	NS
	41	1.6	NS
	83	1.4	NS
	165	1.2	NS

Current Investigation

Dose (mg/kg)	Number of Mice
0	5
82.7	5
165.4	6
413.5	5
0	4
82.7	4
165.4	4
413.5	4
0	
82.7	
165.4	
413.5	
0	4
82.7	4
165.4	4
413.5	4
Total	**53**

Figure 5

References

Allen, J.W., Collins, B.W., and Evansky, P.A. (in press) Spermatid micronucleus analyses of trichloroethylene and chloral hydrate effects in mice.

Collins, B.W., Howard, D.R., and Allen, J.W. (1992) Kinetochore-staining of spermatid micronuclei: Studies of mice treated with X-radiation or acrylamide, Mutation Res., 281, 287-294.

Russell, L.D., Ettlin, R.A., SinhaHikim, A.P., and Clegg, E.D. (1990) Histological and Histopathological Evaluation of the Testis, Cache River Press, Florida, pp. 52 and 120.

Methods in Determining DNA Conformation*

Eric L. Mayes

Arkansas State University

Lawrence Livermore National Laboratory
Livermore, California 94550

December 15, 1993

Prepared in partial fulfillment of the requirements of the Science and Engineering Research Semester under the direction of Rod Balhorn, Research Mentor, in the Lawrence Livermore National Laboratory.

* This research was supported in part by an appointment to the U.S. Department of Energy Science and Engineering Research Semester (hereinafter called SERS) program administered by LLNL under Contract W-7405-Eng-48 with Lawrence Livermore National Laboratory.

Methods of Determining DNA Conformation

Eric L. Mayes

Arkansas State University

Biology and Biotechnology Research Program

Abstract

While the basic structure of DNA has been known since 1953, there is still a great void in terms of knowing how DNA interacts with its surroundings. Because the structure of biological molecules determines their function, the conformation of DNA is of prime importance in understanding its role in living organisms.

We present two methods of determining some components of DNA's conformation. One uses atomic force microscopy to determine the dimensions of DNA's base pairs, and the other seeks to computationally determine the structure of DNA in different chemical environments.

1 Introduction

While the general structure of DNA has been known since 1953, the structure that DNA assumes in different environments remains largely unknown. Along with that, questions remain about the causes for variability in structure. Many methods (i.e. NMR, X-Ray Diffraction) have been used to attempt to answer some of these questions. The two methods we used to attempt answers are atomic force microscopy (AFM), and computer modeling.

Atomic force microscopy allows, as its name implies, atomic resolution images of a sample. The way that AFM can help answer structural questions, is by making direct measurements of DNA. As it stands, AFM does not allow the imaging of individual base pairs, but it does give good information on the scale of plasmids. The microscope is not diffraction limited like a light microscope, because it uses a very small probe (tip) to physically contact a surface. The tip is attached to a flexible cantilever, and a diode laser bounces from the end of the cantilever to a detector. The sample is mounted on a piezo electric stage that can move in three dimensions with high precision and, by keeping the laser on the same spot on the detector as the cantilever flexes, can obtain topographic information. The resolution of the microscope is, however, limited by the the tip because the resulting image is a convolution of tip geometry and the sample. Another resolution-limiting factor is that, when imaging biological samples, water on the surface sometimes allows the sample to move with the scanning tip. This gives "blurry" images which can be difficult to make measurements from. We were, however, very successful in obtaining double-stranded plasmid images which we could measure (Fig. 1). To answer questions about causes for variability in structure, we

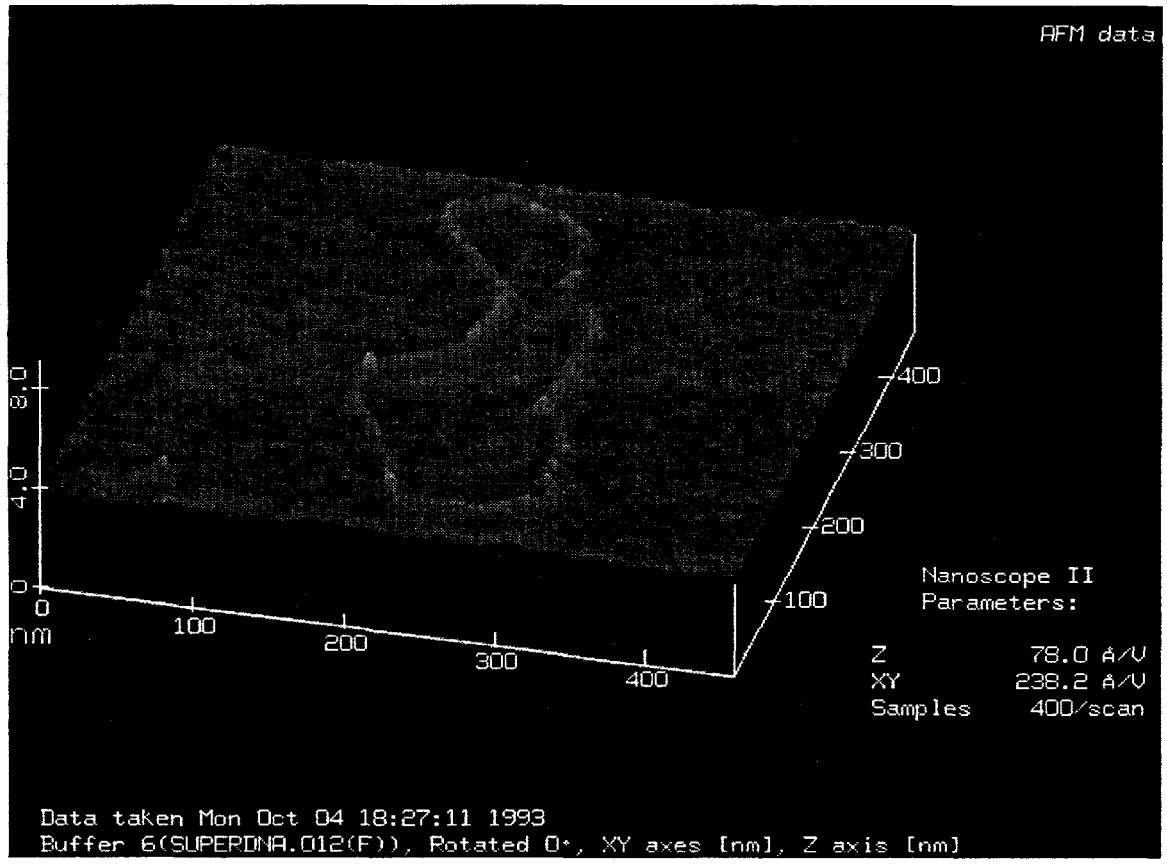

Figure 1: AFM topographic image of pBluescript II KS(+) double- stranded plasmid. The axial base-pair rise for this plasmid is 3.47Å.

used a single-stranded version of the double-stranded plasmid. We found that there was quite a difference in structure based on this change. And, although single-stranded DNA imaging is generally rather difficult [1], we successfully imaged it as well.

Computational modeling allows us to investigate DNA's conformational structure on a much finer scale than large plasmids. We have modeled small DNA fragments (10 bp) in solution with divalent cations to see how the cations affect the structure of the minor groove based on the sequence of the DNA (data pending). Our hope is that this information will give direct structural information about this type of environment.

2 Materials and Methods

DNA and Sample Preparation

The DNA we used is Bluescript II KS+ double-stranded plasmid. The plasmid is 2,961 base pairs long and was obtained from Stratagene (LaJolla, CA). It was supplied at a concentration of 1 mg/ml, and was diluted to 2.5 μg/ml. Freshly-cleaved agar mica squares (Ted Pella, Inc., Redding, CA), 17 mm on a side, were soaked for 24 hours in 33 mM magnesium acetate. This step was performed because DNA binds to the mica's surface better and is less affected by drying conditions when the mica is treated [2]. Treating with magnesium acetate replaces potassium ions on the mica's surface with magnesium ions. This is especially helpful in yielding open, circular plasmid loops which can be measured. The squares were then rinsed in a bath of distilled water for 10 minutes (to remove excess magnesium acetate) followed by drying with nitrogen. Immediately following the drying, 10 μl of DNA solution

was deposited on the mica. The solution was allowed to sit for one minute, then it was rinsed with 100 μl of distilled water. Following another rinse with 100 μl of distilled water, the sample was dried with nitrogen and put in a dessicater for 24 hours prior to imaging.

Both double- and single-stranded samples were prepared with this method. The single-stranded DNA was developed from M13 bacteriophages, as they have been widely used and characterized [3]. Since we prepared a single-stranded version of the Bluescript vector, we could make side-by- side comparisons with the double-stranded plasmids.

Atomic Force Microscopy

AFM imaging was performed under nitrogen using a Nanoscope II AFM (Digital Instruments, Santa Barbara, CA). The imaging tips were etched Nanoprobe Sensors (Digital Instruments, Santa Barbara, CA) with a conical angle of 20°. During the imaging, the force was minimized to the point just before cantilever lift-off which is approximately 1 nanoNewton (nN) [1]. The scan rate was kept to 8.68 Hz, and the images were scanned with an image density of 400x400 points. Integral gain was 2.50, proportional gain was 3.00, and 2D gain was kept to 0.00. The only processing the images received were routines to flatten the images to remove background slope. Following imaging, the images were traced with image processing software to determine plasmid length.

Computer Modeling

For the modeling effort, we used Insight and Discover (Biosym Technologies, San Diego, CA). We prepared input files on Silicon Graphics Indigos using Insight, and sent them to be processed with Discover on a Cray X-MP. The input files that we generated were designed to

explore a particular structural question– are the waters of hydration of a divalent cation the same as the bound waters of DNA's minor groove? Whether or not cations become part of the structure in the minor groove seems to be sequence dependent [4]. So, we prepared input files with decamers of both Poly(dA)·Poly(dT) and Poly(dG)·Poly(dC) DNA. The decamers were put into solution with 10 magnesium cations placed near the minor groove of each molecule. Following a 150 step steepest-decent energy minimization, each DNA fragment will go through a set of molecular dynamics calculations on the Cray.

3 Results and Discussion

AFM Images

The double-stranded images we obtained (Fig. 2) were very clear and we easily made measurements. We found that most of the open loops had a conformation close to B-Form DNA, with an average axial base-pair rise of 3.31Å(B-Form being 3.4Å). Only a fifth of the images we obtained were involved in super-coiling, but even those yielded length measurements close to the average. The single-stranded images we obtained (Fig. 3) were less clear than the double. The single-stranded images were quite "bumpy" and the background was much noisier. The lengths of the single-stranded plasmids were much smaller than the double ($\tilde{0}.35\mu$m), indicating that portions of the plasmids were binding with themselves. We are currently exploring this using RNA secondary-structure techniques to see how much length should be involved in folding. Interestingly, some of the bumps on the single-stranded plasmids are equally spaced and of equal height. In the lower left-hand image of Figure 3,

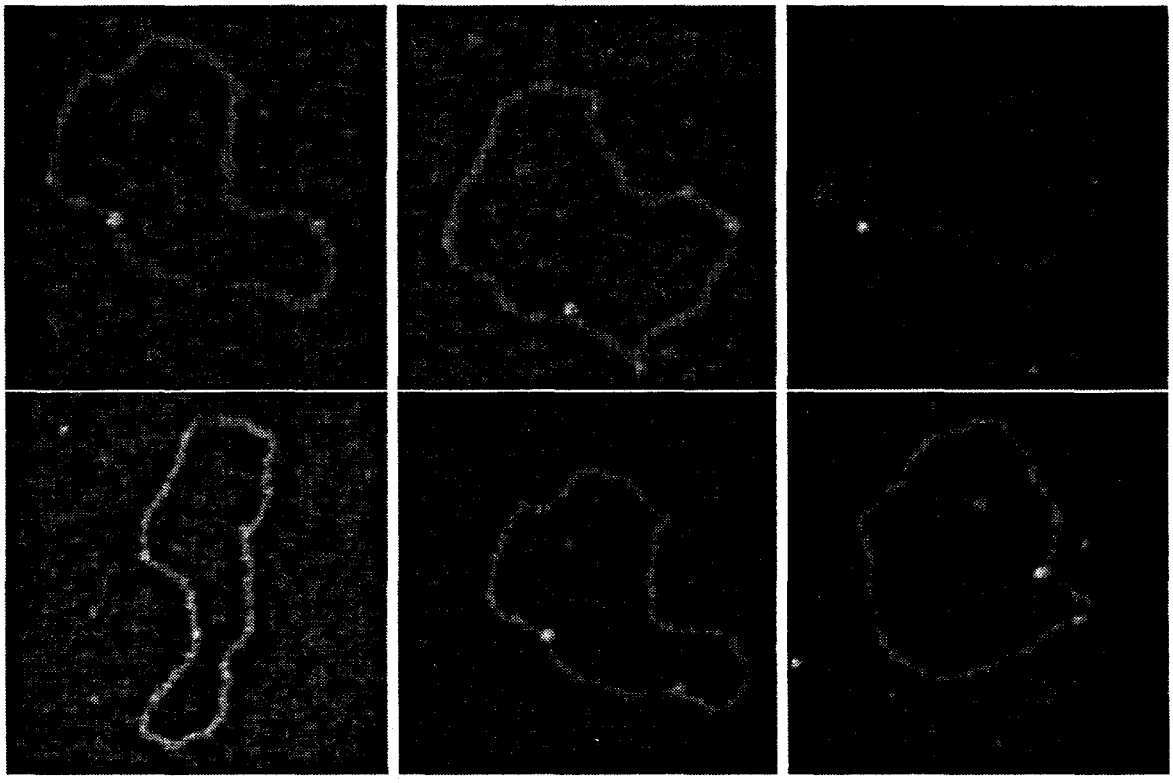

Figure 2: AFM images of 2.96 kb, pBluescript II KS(+) double- stranded plasmids. Clockwise, from top left, the average axial base-pair rise is: 3.14Å, 3.26Å, 3.25Å, 3.21Å, 3.14Å, and 3.47Å. Their respective lengths are: 0.930μm, 0.964μm, 0.962μm, 0.951μm, 0.931μm, and 1.03μm.

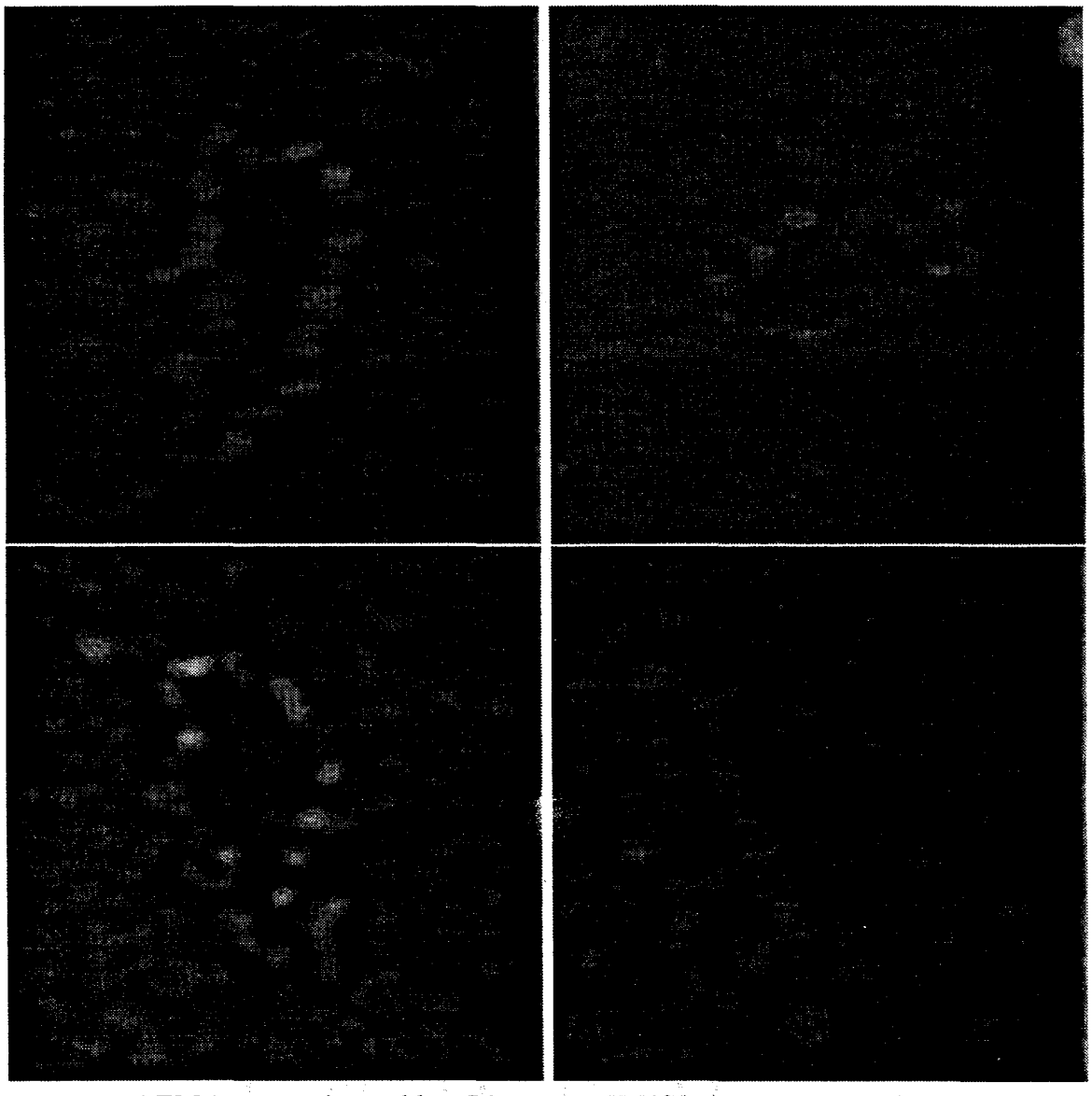

Figure 3: AFM images of 2.96 kb, pBluescript II KS(+) single- stranded plasmids. Clockwise, from top left, the plasmid length is: 0.727μm, 0.495μm, 0.774μm, and 0.627μm. Note the "bumpiness" and the large differences in length.

one can easily observe a diagonal series of these bumps. Whether these bumps are attached proteins or folded features remains to be tested.

Computer Modeling

From input files similar to the one in Figure 4, we are in the process of determining how divalent cations affect the structure of the minor groove of a decamer of DNA. So far, we have found that simple energy minimization shows the cations remaining near the minor groove. However, to determine if waters of hydration are the same as bound waters of the minor groove, long duration molecular dynamics calculations are needed.

4 Conclusion and Further Research

The technique of using AFM to obtain direct structural measurements is extremely valuable in adding to the knowledge of DNA structure. For example, we found that single-stranded DNA was significantly shorter than double-stranded DNA indicating that single-stranded is most likely involved in folding. By binding various proteins to single-stranded DNA, we hope to likewise determine more about what leads to structural variability. We also hope to try different methods of sample preparation that could lead to much clearer images of single-stranded DNA. Computational modeling has not yet proven to provide useful information about structure, but we remain hopeful. Once results are in, we hope to explore structures with more heterogeneous sequences and different cations.

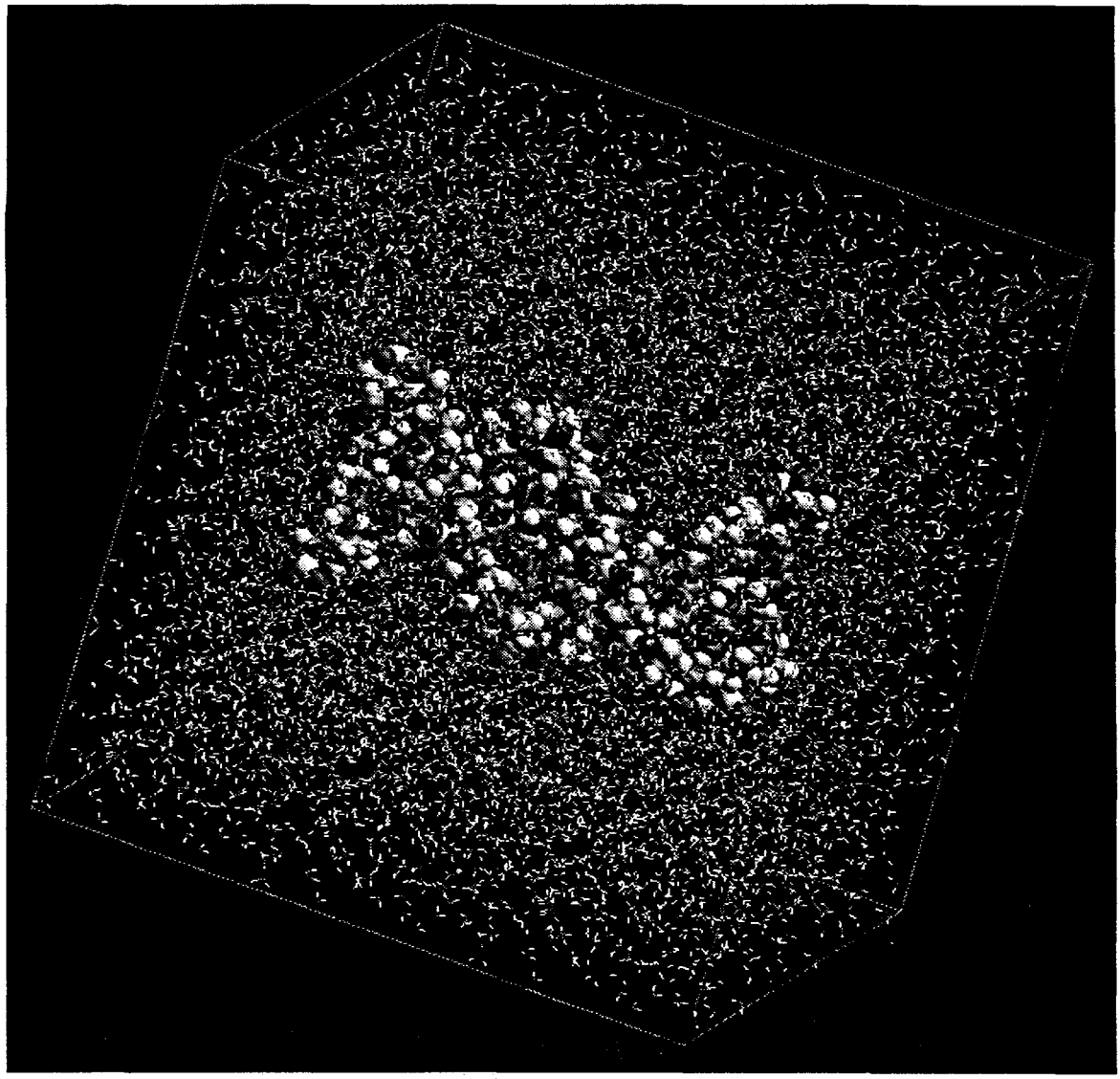

Figure 4: Decamer of Poly(dA)·Poly(dT) DNA in solution. Modeled in HyperChem by AutoDesk Corp.

5 Acknowledgments

We thank R. Balhorn, N. V. Hud, M. J. Allen, J. Lee, J. Kirchner, N. Winter, and A. Riddle for their help and discussions, and J. Kirchner for providing the Bluescript II single- and double-stranded DNA samples. This research was supported in part by an appointment to the U.S. Department of Energy SERS program administered by LLNL under Contract W-7405-Eng-48 with Lawrence Livermore National Laboratory. We are grateful for the support of them all.

References

[1] Hansma, H. G., Sinsheimer, R. L., Li, M. Q., Hansma, P. K. "Atomic Force Microscopy of Single- and Double-Stranded DNA." (1992) *Nucleic Acids Research* **20**, 3585-3590.

[2] Thundat, T., Allison, D. P., Warmack, R. J., Brown, G. M., Jacobson, K. B., Schrick, J. J., Ferrell, T. L. "Atomic Force Microscopy of DNA on Mica and Chemically Modified Mica." (1992) *Scanning Microscopy* **6**, 911-918.

[3] Vieira, J., Messing, J. "Production of Single-Stranded Plasmid DNA." (1987) *Methods in Enzymology* **153**, 3-11.

[4] Fritsch, V., Ravishanker, G., Beveridge, D. L., Westhof, E. "Molecular Dynamics Simulations of Poly(dA)·Poly(dT): Comparisons Between Implicit and Explicit Solvent Representations." (1993) *Biopolymers* **33**, 1537-1552.

"Stimulated Brillouin Scattering as a Function of Bandwidth"*

Alison B. Peck

University of NE at Kearney

Lawrence Livermore National Laboratory
Livermore, CA 94550

Dec. 15, 1993

Prepared in partial fulfillment of the requirements of the Science and Engineering Research Semester under the direction of David Milam, Research Mentor, in the Lawrence Livermore National Laboratory.

*This research was supported in part by an appointment to the U.S. Department of Energy Science and Engineering Research Semester program administered by LLNL under Contract W-7405-Eng-48 with Lawrence Livermore National Laboratory.

"Stimulated Brillouin Scattering as a Function of Bandwidth"

Alison Peck, Univ. of NE at Kearney,LLNL
David Milam, LLNL

Abstract

Stimulated Brillouin scattering (SBS) is a non-linear optical effect which has been of interest to laser scientists for many years. SBS can be extremely useful as a phase conjugator, but it can also cause damage in large lasers by scattering light transversely to the beam. In this experiment, transient SBS has been generated in two materials with a frequency modulated, 13-ns pulse from the OSL Nd:YLF laser, and then compared to SBS generated in the same materials with a narrowband pulse of equal length. Also investigated are the effects of variation of focal volume. Results show that the transient threshold is higher for the broadband pulse than for the narrowband, and that the temporal shape of the pulse transmitted through the cell varies with bandwidth. We also find that the spectrum of the scattered pulse is different from that of the input pulse.

Introduction

Stimulated Brillouin scattering, or SBS, is a non-linear optical effect which occurs when a beam of light passing through a medium excites an acoustic wave in that medium. The acoustic wave then scatters the optical beam. Low amplitude acoustic waves are inherent to all substances, and theoretically occur in every possible orientation, so a small fraction of the incident laser pulse is always scattered. Light scattered from a moving sound wave has doppler-shifted frequency. The frequency of the resultant scattered wave for a narrowband pulse is the difference between the frequency of the incident wave, and that of the acoustic wave. Because the scattered light and the incident laser light have different frequencies, the interference fringes that result from the superposition of these waves will move. The moving interference fringes and the acoustic wave coincide, and through a process known as electrostriction, the intensity pattern causes growth of the acoustic wave[1]. SBS can be very damaging to the optics in a large laser. It was found several years ago, on the NOVA laser, that the transversely scattered light was hitting the lens mounts around the large optics, and causing a shock wave which would then propagate back to the center, and blow up the middle of the lens. But SBS can also be very useful as a phase conjugator.

A number of experiments have been reported which analyze the influence of the bandwidth of the incident pulse on the characteristics of SBS. The work done prior to 1986 has been summarized in a single review.[2] Although neither general closed-form analytical solutions nor completely general three-dimensional numerical codes are available at this time, studies using simplified models have been done for the cases of input phase that varies rapidly relative to the acoustic relaxation time of the medium,[3,4,5] and for SBS induced by a multimode laser emitting discrete narrow modes.[6] For both of these situations, it has been observed that the threshold will not vary with bandwidth when the coherence length of the

input pulse exceeds the length of the SBS gain volume.[7,6,8] For short coherence length, however, the threshold is increased.[9] Studies have also shown that for modest bandwidth, on the order of 0.1 GHz to 10 GHz, the reflected spectra take the same form as the input spectra.[6,7,9]

In the NOVA laser, it was found that transverse SBS was suppressed by the addition of 30-60 GHz of harmonic bandwidth produced by a 3 GHz phase modulator[10], but detailed studies of scattering using pulses with harmonic bandwidth have not previously been done. We have measured the variation of both the SBS threshold and the spectrum of the scattered light as a function of bandwidth and relative coherence length. Data for short coherence lengths are of interest in understanding transverse SBS in large optics. Analysis indicates that transferral of input bandwidth to the scattered pulse is most likely with long coherence length, and demonstration of this transferral is important in determining whether phase conjugation could conceivably be used to correct phase errors in a fusion laser.

Method

For this experiment, tunable laser bandwidth was produced by passing the laser pulse through a 3 GHz $LiNbO_3$ phase modulator. The modulator was placed in a linear cavity which was separated from the rest of the laser chain by the arrangement shown in Fig. 1. We were able to obtain a range of bandwidth by changing the attenuation of the rf field that is applied to this modulator. The laser pulse was kept inside this cavity for two passes by timing the pockels cells, which gave us a range of bandwidth from 26 GHz with 12 db attenuation, to 104 GHz with 0 db attenuation.

To measure the backscattered SBS, a 13 ns, 1053 nm pulse was produced with the OSL Nd:YLF laser and double-passed through this modulating cavity. The pulse

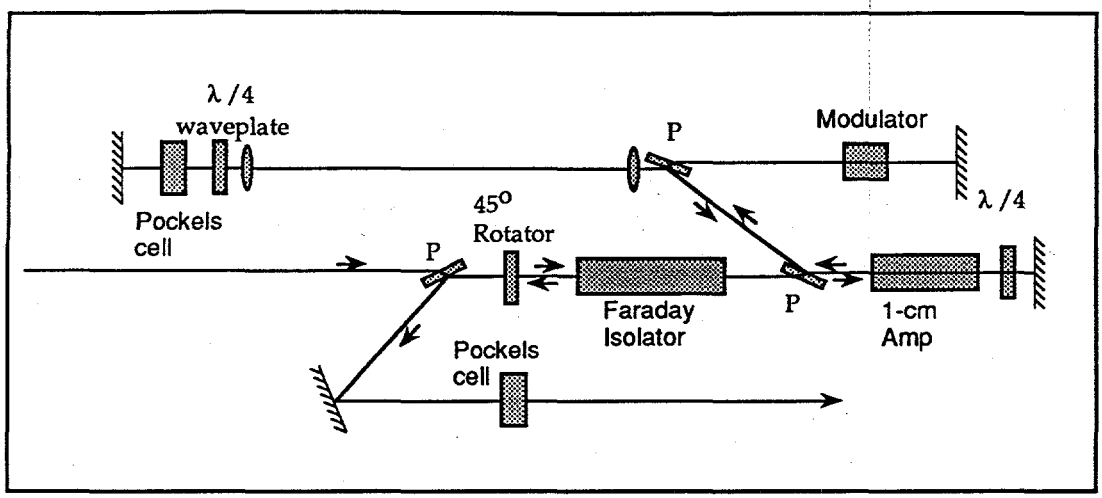

Fig. 1 Arrangement of modulator cavity in laser chain

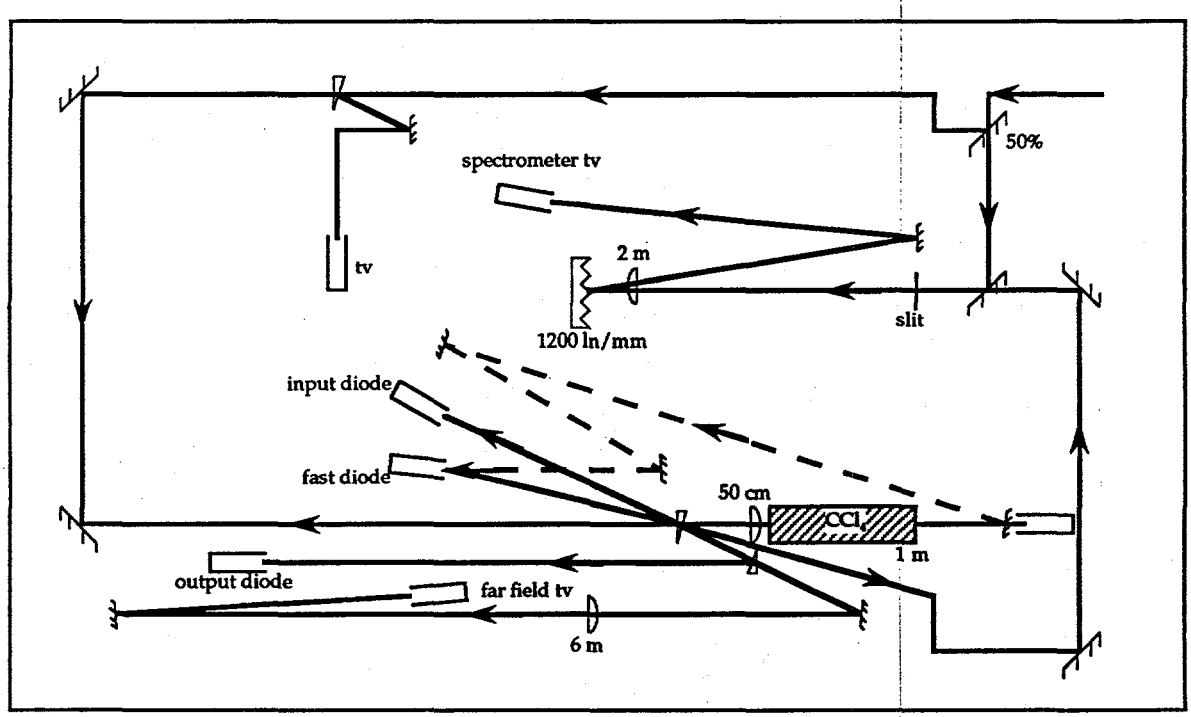

Fig. 2 Layout of SBS experiment

was then amplified and directed through a 50% mirror where about half of the light was diverted to a spectrometer, as shown in Fig. 2. This spectrometer would then measure the bandwidth of the input pulse, and allow us to verify its consistency. Further along the laser chain, a small portion of the light was also diverted to a Cohu camera, so that we could monitor its profile. Following that, the remainder of the pulse was partially reflected by a bare silica window onto a number of input diagnostics, and the rest was transmitted through a 50 cm lens to the 1 m cell of CCl_4. The diagnostics for the incident beam consisted of an input diode, which would measure the input energy of the shot, and a fast photo diode which recorded the temporal shape of the pulse. The output diagnostics included a diode to measure the reflected energy, and a Cohu camera to record the farfield profile of the reflected beam. We were also able to direct the reflected energy to the spectrometer, and record the bandwidth of the backscattered light. We could not record both the input and output spectra for the same shot on our camera, but we were able to double-check the input spectrum by placing a retro-mirror in front of the 50 cm lens. This is also how we aligned most of the other diagnostics. We then directed the light which had passed through the CCl_4 around to the fast photo diode. The waveform of the transmitted pulse indicates when scattering is initiated, and gives, by subtraction of the input waveform, the waveform of the scattered pulse.

Results

Following are the measurements made of the threshold of CCl_4 as a function of bandwidth, using the 50 cm lens. Fig. 3 shows the output energy plotted against the input energy for the full range of bandwidth available. The thresholds were determined by fitting a line curve to this data, and extrapolating back to zero. There is a marked difference in threshold as soon as bandwidth is added, from 1.7 mJ for the narrowband to 4.1 mJ at 26 GHz, then after the initial jump, the rise becomes

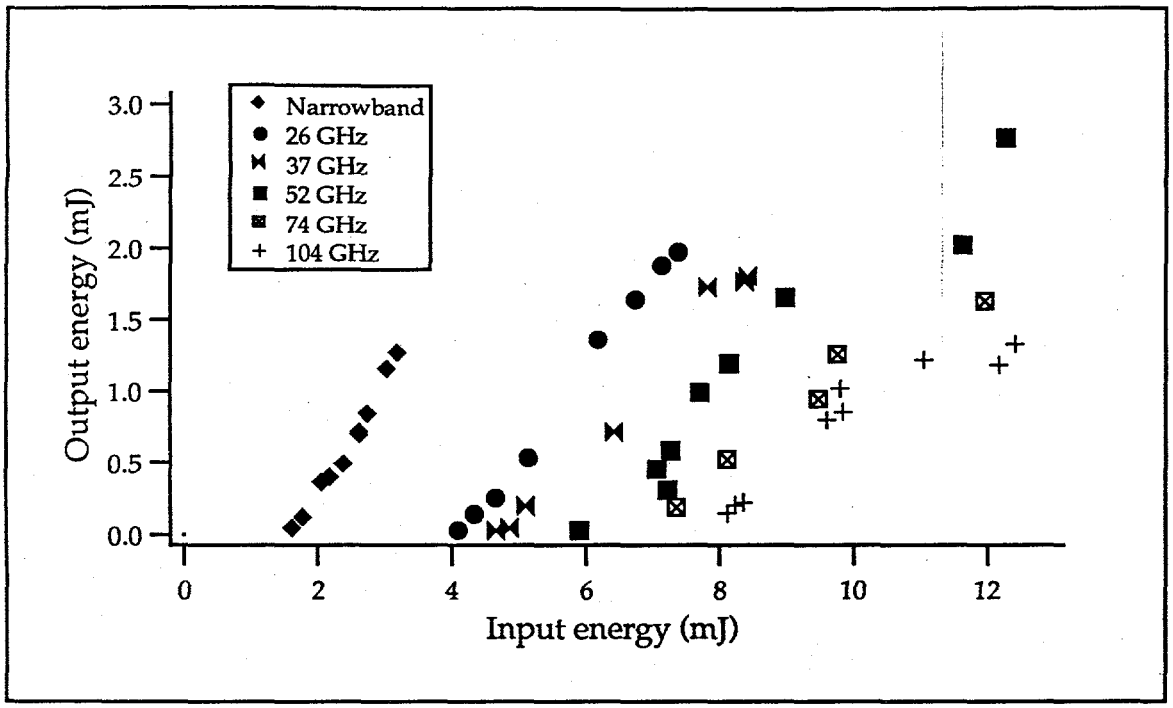

Fig. 3 CCl_4 threshold measurements

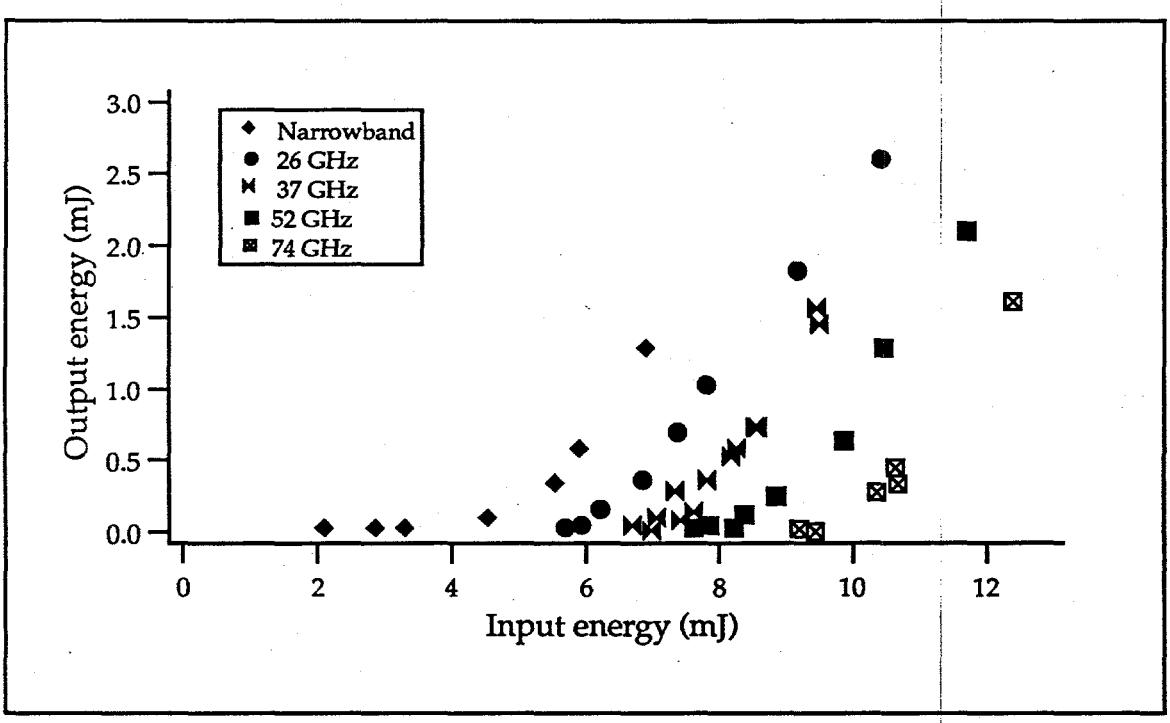

Fig. 4 D-LAP threshold measurements

much more gradual, showing 4.8 mJ at 37 GHz, 6.0 mJ at 52 GHz, 7.0 mJ at 74 GHz, and 7.7 mJ at 104 GHz.. Unfortunately, the data is only reliable up to about 10 mJ of input energy, because we were approaching breakdown in the CCl_4, and at this point we would start to get some sparking within the focal volume in the cell.

Fig. 4 shows the thresholds for D-LAP at the same bandwidths. The SBS gain coefficient for D-LAP is smaller than that for CCl_4, so its narrowband threshold is larger, and the threshold of D-LAP did not change as rapidly with the increase in bandwidth as did CCl_4 We were not able to go all the way to 104 GHz because the threshold for the 74 GHz pulse was already almost 10 mJ, and we were beginning to get breakdown. The thresholds for D-LAP were 5.1 mJ for the narrowband, 6.2 mJ at 26 GHz, 7.1mJ at 37 GHz, 8.3 mJ at 52 GHz, and 9.9 mJ at 74 GHz.

During the course of the experiment, we also changed the focusing lens in front of the CCl_4 cell, to ensure that the focal volume had little effect on the threshold. Fig. 5 shows that although the narrowband threshold, 1.3 mJ, for the 50 mm lens was slightly lower than that of the other lenses, 1.6 mJ and 1.7 mJ respectively, the effect was negligible compared to the effect of added bandwidth.

Also analyzed was the difference in temporal waveform between the input and the output pulses. Fig. 6 shows a typical record of these waveforms. These were measured with the fast photo diode described earlier. The first form is the input pulse as it is reflected from the wedge in front of the SBS target, while the second is the pulse after it has passed through the SBS cell, and been sent back up the table. In this manner, we were able to measure both waveforms for each shot. The onset of strong scattering is indicated by the decrease in transmitted intensity. Subtraction of the input pulse from the transmitted pulse results in the waveform of the reflected pulse. In some experiments with modest bandwidth, we observed a 3 GHz temporal ripple on the transmitted waveform. An example of this is shown in Fig. 7. This intensity modulation was not evident in experiments at 80-100 GHz, possibly due to

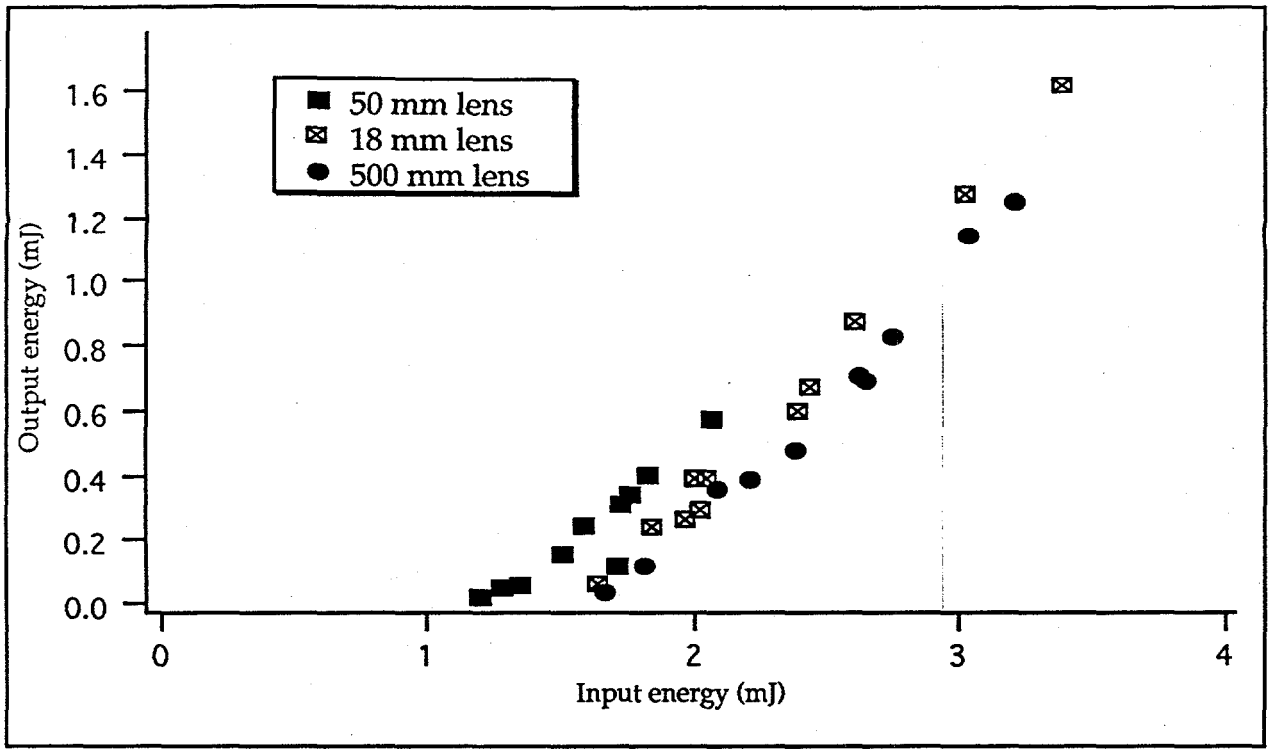

Fig. 5 Narrowband thresholds for three different focal length lenses

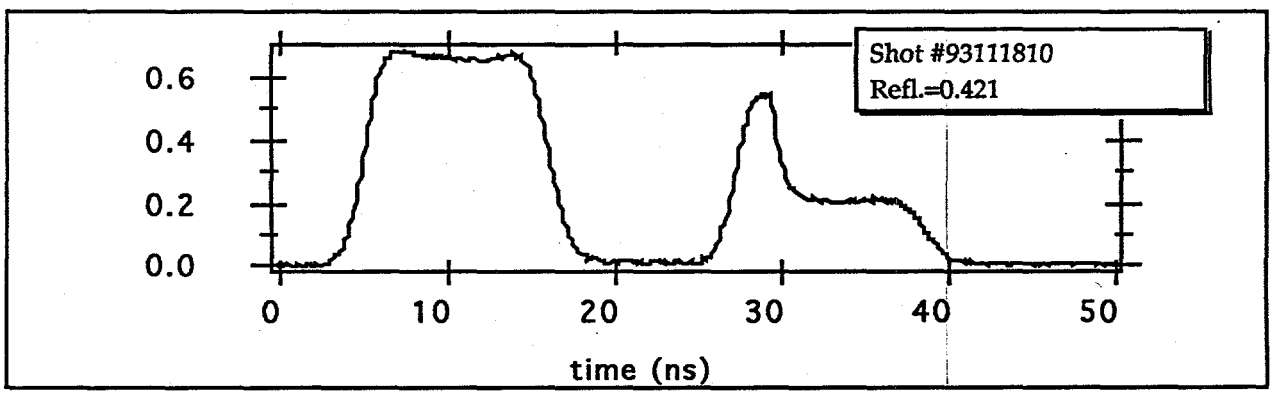

Fig. 6 Typical narrowband waveform for CCl_4

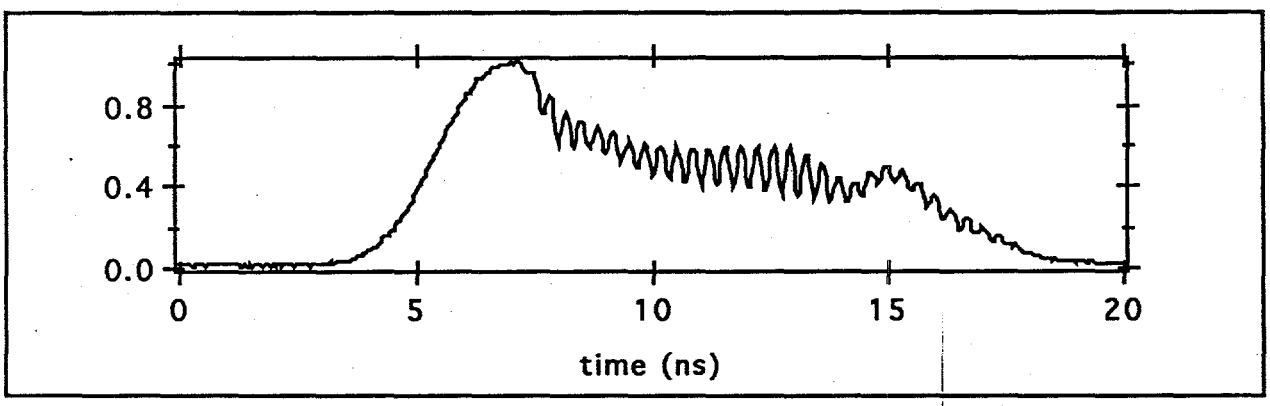

Fig. 7 Transmitted waveform for CCl_4 showing 3 GHz temporal ripple

the 4 GHz limit of the detection system. The responsivity is only 50% at 3 GHz. The temporal ripple did not appear to be present in narrowband experiments.

Lastly, the spectra of the scattered pulses were found to be different from those of the input pulses. Fig. 8 contains spectra of pulses reflected from CCl_4 at input near threshold, and at input of approximately twice threshold for 26 GHz bandwidth. At threshold, the energy of the scattered pulse was concentrated in the blue wing of the spectrum. The spectrum became more complete as the input energy was increased, but never recovered the red wing before we reached breakdown levels. The spectra for D-LAP followed much the same pattern, although at very low energies we were able to see some evidence of the red wing. This effect may have been caused by reflection from the surface of the crystal.

At threshold, with 104 GHz bandwidth, the spectra of the scattered pulses for CCl_4 varied shot to shot from being concentrated in the blue wing to being concentrated in the red wing. It is possible that this random characteristic of the wide spectra is due to the slight shot-to-shot variation in the relative amplitudes of the red and blue wings of the input spectra.

Summary

In this experiment we have measured the stimulated Brillouin scattering threshold for carbon tetrachloride and D-LAP for a range of frequency modulated bandwidths. We have determined that changing the focal volume within the cell has little effect on the threshold. We have also discovered some unusual effects of SBS on the transmitted waveform and on the spectra of the reflected pulses. Following this preliminary report, further analysis of this data will be done, and a more thorough treatment of our results will be written.

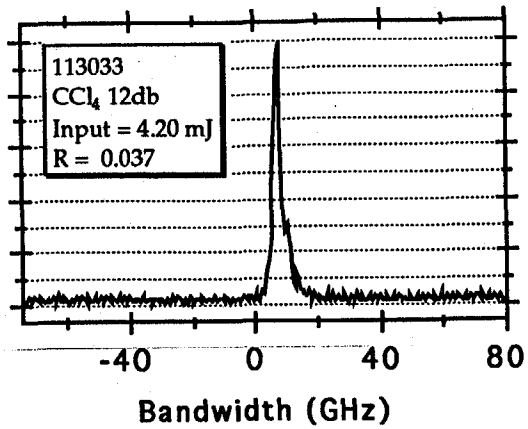

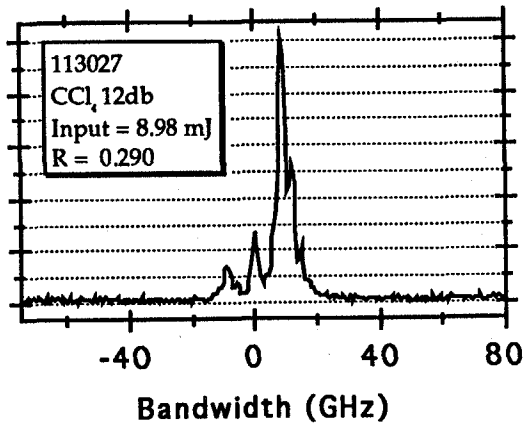

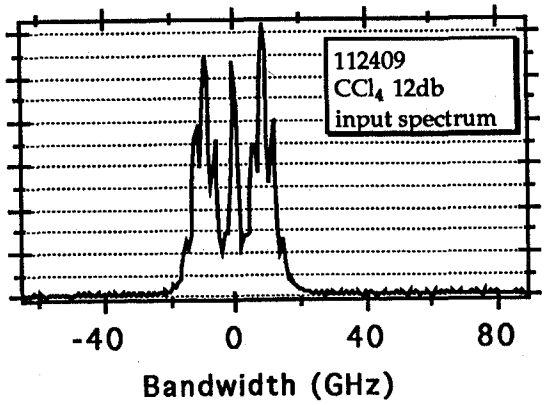

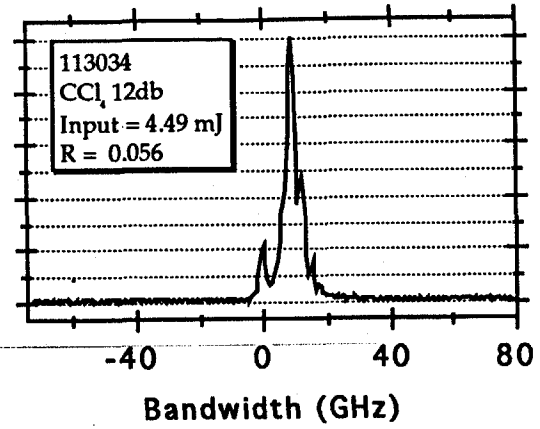

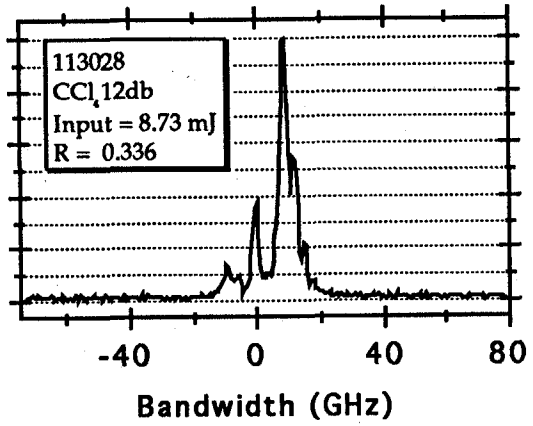

Fig. 8 Top: Reflected spectra with input energy near threshold
Center: Reflected spectra with input energy approximately twice threshold
Bottom: Input spectrum with 12 db attenuation. Bandwidth=26 GHz

References

1. Yariv, Amnon, *Quantum Electronics*, 3rd ed. (John Wiley & Sons,1989.)
2. Valley, G. C., "A Review of stimulated Brillouin scattering excited with a broad-band pump laser," *IEEE Journal of Quantum Electronics*, V QE-22 (1986) pp 704-712.
3. Zel'dovich, B. Ya., Shkunov, V. V., "Theory of phase locking in transient stimulated scattering," *Soviet Journal of Quantum Electronics*, V 9 (1979) pp 1137-1139.
4. Zel'dovich, B. Ya., Shkunov, V. V., "Influence of the group velocity mismatch on reproduction of the pump spectrum under stimulated scattering conditions," *Soviet Journal of Quantum Electronics*, V 8 (1978) pp 1505-1506.
5. D'yakov, Yu. E., "Excitation of stimulated light scattering by broad-spectrum pumping," *JETP Letters*, V 11 (1970) pp 243-246.
6. Narum, P., Skeldon, M. D., Boyd, R. W., "Effect of laser mode structure on stimulated Brillouin scattering," *IEEE Journal of Quantum Electronics*, V QE-22 (1986) pp 2161-2167.
7. Popovichev, V. I., Ragul'skii, V. V., Faizullov, F. S., "Stimulated Mandel'shtam-Brillouin scattering excited by radiation with a broad spectrum," *JETP Letters*, V 19 (1974) pp 196-198.
8. Filippo, A. A., Perrone, M. R., "Experimental study of stimulated Brillouin scattering by broad-band pumping," *IEEE Journal of Quantum Electronics*, V 28 (1992) pp 1859-1863.
9. Zubarev, I. G.,Mikhailov, S. I., "Stimulated scattering of light in a noisy pumping field with a spectrum wider than the frequency shift of the Stokes component," *Soviet Journal of Quantum Electronics*, V 4 (1974) pp 683-684.

10. Murray, J. R., Smith, J. R., Ehrlich, R. B., Kyrazis, D. T., Thompson, C. E., Weiland, T. L., Wilcox, R. B., "Experimental observation and suppression of transverse stimulated Brillouin scattering in large optical components," *Journal of the Optical Society of America B*, V 6 (1989) pp 2402-2411.

SAMPLE SEQUENCING

Christa Prange

St. Mary's College

Lawrence Livermore National Laboratory
Livermore, CA 94550

December 15, 1993

Prepared in partial fulfillment of the requirement of the Science and Engineering Research Semester under the direction of Dr. Gregory Lennon, Research Mentor, in the Lawrence Livermore National Laboratory.

This research was supported in part by an appointment to the U.S. Department of Energy Science and Engineering Research Semester (hereinafter called SERS) program administered by LLNL under Contract W-7405-Eng-48 with Lawrence Livermore National Laboratory.

SAMPLE SEQUENCING

ABSTRACT

The goal of the Human Genome Project is to sequence all 3 billion basepairs of human DNA. At Lawrence Livermore Lab, attention is focused on Chromosome 19, which has been estimated to contain approximately 2000 genes. So far, only 200 have been mapped to specific areas on the chromosome. For this reason, a simple method is needed to predict the most likely locations of the coding regions in the DNA. In addition, there is also a need for unique marker sites (STS's) along the chromosome. Sample sequencing uses standard cloning techniques to prepare DNA for sequencing. Once sequence is obtained, it is analyzed using databases to predict the regions most likely to contain genes. All sequences may also be used to generate STS's. So far, 21 fragments from five different clones have been completely sequenced, with fragments from eight more clones in progress. Constant improvement of methods to increase efficiency and accuracy combined with utilization of the most current databases available make sample sequencing a useful tool for reaching the goals of the Human Genome Project.

INTRODUCTION

DNA, the molecule that controls all functions of life, is itself surprisingly simple. It is composed of four different bases: adenine, cytosine, guanine, and thymidine (A, C, G, T) arranged in series like beads on a necklace. The DNA sequence is made up of control

regions, "junk" DNA with no known purpose, and coding regions, or exons, which are scattered randomly throughout the sequence and make up genes. The goal of the Human Genome Project is to determine the exact sequence of all 3 billion basepairs of human DNA. Lawrence Livermore's genome effort focuses on Chromosome 19 specifically. Although this is one of the smaller chromosomes, it is relatively gene-rich. It is estimated to contain approximately 2,000 genes, only 200 of which have been mapped to specific locations.

Although there are already many methods of finding genes, sample sequencing has the potential for finding not only gene sequences, but their exact locations. Basically, sample sequencing consists of generating short (300 bp) stretches of sequence from specific places on the chromosome and using databases to scan those sequences for genes.

MATERIALS AND METHODS

Cosmid library. The first step in sample sequencing is to isolate the human DNA from the cloning vector where it is stored. The library used in this study was prepared from flow-sorted hamster-human hybrid DNA at Lawrence Livermore Lab as part of the National Gene Library Project. The vector is Lawrist 16. Each clone contains about 40,000 basepairs of human DNA and is thought to contain, on average, one gene.

DNA preparation. Cosmid DNA was isolated using Promega Wizard MiniPreps. About 2 ug were cut with 5 U EcoRI and run out on a 1% agarose gel containing ethidium bromide for UV visualization. After separation, bands of DNA less than 4 kb in length were cut out and the DNA was eluted from the gel in 40 ul of water at 37° C for 30 minutes.

The vector used for subcloning was pBluescriptII SK+ vector (Stratagene) cut with EcoRI and gel-purified. A 2:1 molar ratio of insert to vector was ligated for 45 minutes at 16° C with Ready-To-Go T4 DNA Ligase (Pharmacia). Transformations were done with DH5 competent cells (BRL) and spread on LB amp XGal plates. Incubation was overnight at 37° C. Two white colonies from each plate were

picked and grown up overnight in LB-amp broth, then 3 ul were purified using Promega MiniPreps. 500 ng of DNA was cut with EcoRI to check that the insert was the proper size.

Sequencing. Sequencing reactions were done using the Taq DyeDeoxy Terminator Cycle Sequencing Kit from Applied Biosystems (ABI). 1 ug of DNA was labelled with fluorescent dyes (a different dye for each base that makes up DNA). Primers included commercial forward and reverse primers (T3, T7, M13F and M13R) as well as primers generated at Lawrence Livermore using the PRIMER program. pGEM-3Zf with M13F was the control sequence. The reactions were cycled in a Perkin Elmer 9600 thermal cycler using the conditions specified in the sequencing protocol. Samples were purified with Centri-Sep spin columns in a variable-speed microfuge to remove excess dye terminators. Sequencing was done on an ABI 373A automated sequencer. Finally, the sequence was manually edited to an average length of 300 bp.

Databases. Each sequence was sent to four different databases for analysis. Blastn (Altschul, 1990) compares the nucleotide query sequence with nucleotide sequence databases (GenBank, GenBank updates, EMBL, and EMBL updates); similarly, blastx compares the query sequence translated in all six reading frames to protein sequence databases (SWISS-PROT, PIR, GenPept, and GenPept updates). Both these programs use the algorithm BLAST (Basic Local Alignment Search Tool) and can be accessed through the BLAST e-mail server address: blast@ncbi.nlm.nih.gov. GRAIL (Gene Recognition and Analysis Internet Link) is designed to analyze nucleotide sequence to locate regions most likely to contain exons (grail@ornl.gov). Geneid also analyzes nucleotide sequence to predict exon locations and gene structure (geneid@darwin.bu.edu). A positive gene prediction is indicated by a match in more than one database.

RESULTS AND DISCUSSION

Up to this point, I have obtained and analyzed sequence from 21 fragments (Figure 1). Only one fragment (20760 E1 T7) showed

CLONE ID	FRAGMENT	SIZE bp	PRIMER	SEQ LENGTH	BLASTN	BLASTX	GENEID	GRAIL
19977	A1	4.7	KSGR	270	Alu	*	*	*
19977	B1	3.8	KSGR	172	*	*	*	*
19977	C1	3.6	KSGR	231	*	*	*	*
19977	C1	3.6	T3	185	*	*	*	*
19977	D1	2.4	KSGR	333	*	*	*	*
20760	B2	1.8	T3	328	*	*	exon	*
20760	B2	1.8	T7	364	*	*	*	*
20760	C1	2.1	T3	330	*	*	*	*
20760	C1	2.1	T7	332	*	*	*	*
20760	D2	2.2	T3	304	*	*	*	*
20760	D2	2.2	T7	316	*	*	*	*
20760	E1	2.3	T3	326	*	*	*	*
20760	E1	2.3	T7	293	*	dopamine rec	exons	*
28423	C2	3.1	KSGR	312	*	*	*	*
28861	A1	1.1	KSGR	380	*	*	*	*
28861	A1	1.1	M13F	356	*	*	*	*
28861	A1	1.1	T3	342	*	*	*	*
28861	B2	1.3	T3	247	*	*	*	*
28861	B2	1.3	T7	308	*	*	*	*
28861	C1	1.3	T7	288	*	*	*	*
30381	F1	1.1	KSGR	273	Alu	*	*	*

Figure 1: Fragments analyzed to date. 20760 E1 is the only fragment to show positive matches in more than one database. * indicates an unknown sequence.

hits in more than one database, indicating a match to a dopamine receptor protein sequence.

Irrespective of the exon prediction, sequence can be used to generate a sequence-tagged site (STS), a unique DNA marker that is found nowhere else in the genome. One of the goals of the Human Genome Project is to find STS markers approximately every 100,000 bases. PCR primers will be generated using the PRIMER program to amplify a stretch of DNA around 100 basepairs long that is unique to a single area of chromosome 19. Optimization of PCR conditions for each STS will be accomplished by varying magnesium concentrations in the buffer.

In order to analyze how well sample sequencing is working, I determined how much sequence would actually have to be generated in order to expect to hit one gene. To begin with, the entire genome is 3 billion basepairs in length. Of that, chromosome 19 contains 60 million bp (or 2% of the total genome). Each cosmid contains 40,000 bp of human DNA. This means that a minimum of 1500 cosmids is necessary to span the entire chromosome with no overlap. (This is where the estimate of one gene per cosmid comes from.) Each plasmid is about 4000 bp in length, and an average of 600 bp from each plasmid is actually sequenced. It is estimated that 10% of the genome is coding regions (exons), and the average length of an exon is 123 nucleotides. So the minimum number of bases sequenced to hit a gene is 1230 bp. However, since only part of an exon will be hit in most cases, in reality more than 1230 bp would have to be sequenced to find a gene. A recent study (Smith, 1993) found 19 "genes" (exons or positive matches) in 116 kb of sequence, which is approximately 1 exon every 6000 bp. I sequenced 6290 bp and had one positive match. Although my result is similar to what their study indicated (and what might be realistically expected), this similarity will have to be supported by more data to be statistically reliable.

Another factor I looked at was GC content, or how much of the sequence consists of the bases guanine and cytosine. Coding regions of DNA have approximately 60% GC content, while genomic DNA has only 40% GC content. The sequence I obtained had 48% GC content,

not significantly higher than for genomic DNA. In addition, about 10% of genomic sequence is made up of repeating elements of DNA (such as Alu). My sequences showed around 400 bp of Alu repeats, or about 6% of the total.

SUMMARY

In order for sample sequencing to compete with other methods of finding genes, a faster, more efficient way of obtaining and analyzing sequence must be developed. If throughput could be increased to one sequencing gel per day, over 7,000 basepairs (corresponding to roughly one gene) would be obtained daily. Of course, time would be required for verification and further analysis, including obtaining the complete cDNA sequence and full-length mRNA, Northern blotting, and expression studies. There is also the possibility of sequencing directly from the ends of cosmids and skipping the subcloning process altogether, which would be more time- and cost-effective. With these improvements, sample sequencing has the capacity to become one of the fastest ways to determine specific locations of genes on Chromosome 19.

ACKNOWLEDGEMENTS

We thank the US Department of Energy Office of Energy Research for sponsoring this project, and also members of the cDNA and Sequencing Labs.

REFERENCES

Altschul, S.F., Gish, W., Miller W., Myers, E.W., and Lipman, D.J. (1990). Basic local alignment search tool. *J. Mol. Biol.* **215:** 403-410.

Smith, Michael W., *et al.* (1993). A sequence-tagged site map of human chromosome 11. *Genomics* **17:** 699-725.

Evaluation and Assessment of Education Programs

Mona L. Ramsey

Fort Valley State College

Lawrence Livermore National Laboratory
Livermore, CA 94550

December 13, 1993

Prepared in partial fulfillment of the requirements of the Science and Engineering Research Semester under the direction of Richard Farnsworth, Research Mentor, in the Lawrence Livermore National Laboratory.

*This research was supported in part by an appointment to the U.S. Department of Energy Science and Engineering Research Semester (hereinafter called SERS) program administered by LLNL under Contract W-7405-Eng-48 with Lawrence Livermore National Laboratory.

Evaluation and Assessment of Education Programs

Mona L. Ramsey
Fort Valley State College

Science Education Center
Lawrence Livermore National Laboratory

ABSTRACT

To ensure quality products, the Department of Energy is emphasizing the evaluation and assessment of education programs. In response, Lawrence Livermore National Laboratory is preparing its program managers to conduct formative evaluations of each education program. In preparation for designing evaluation tools the program managers have been exposed to an assessment guide that will broaden their knowledge of writing goals and objectives. Data collected will support the design of evaluation tools created by each of the program managers.

Introduction

The Science Education Center at LLNL consist of Science Education Programs. Education Programs are those that give service to classroom teachers, students and colleges and universities. For example the Lawrence Elementary Science Study of Nature (LESSON) provides elementary and middle school teachers with broader experiences and greater exposure to the sciences hoping that they will return to their classrooms teaching more minutes of science. In addition, the Science and Engineering Research Semester caters to the needs of college students providing them with a semester of research in their area of interest. To ensure quality service of these programs and programs like them, the Department of Energy is emphasizing evaluation and assessment. In response, LLNL is preparing its program managers to conduct formative evaluations of each education program.

Prior to the recent emphasis in evaluation and assessment the satisfaction scale was the extent of evaluation. The satisfaction scale only measures the happiness of the participant and not the effectiveness of the program. With the research that was done this semester future evaluation will be far more thorough.

Explanation of Methods

The gathering of information was completed in two separate parts. The first being the literature review that was necessary to gather information on evaluation and assessment and the second

was the information that was gathered from meeting with the program managers .

The search for information on evaluation and assessment began with Melvyl which provides access to the libraries of the University of California library system. Within Melvyl I could obtain access to ERIC which is an education data base. As titles and abstracts that seemed relevant appeared, they were selected and I journeyed to Berkeley to the Education Psychology Library to gather the materials. In the process of gathering information I found books that proved to be quite useful.

The information that I gathered was organized and put into a guide that was written for the program managers. The purpose of the guide was to better inform program managers of how to go about designing a method of evaluation for their particular program. The Guide to Evaluating Education Programs was the tool that I used to gather the information that I needed on each of the programs.

Discussion

The Department of Energy requires each Laboratory to develop and conduct formative evaluations of all education programs managed at that facility. DOE Headquarters will conduct summative evaluations of these programs after they become established. At the moment DOE's primary concern is with Summative and Formative evaluations. Formative evaluations compare a program's expected outcomes with the actual outcomes. The assessment investigates how the learning opportunities affect

participants and is used by program developers to improve the program. Summative evaluations are used to assess established programs. These programs are ones that have been functioning for years and are consistently achieving program goals and objectives. DOE will conduct summative evaluations for the laboratories, comparing two or more programs with similar goals, to determine which is more effective. Evaluation is a systematic process of collecting, analyzing and interpreting information to determine the extent to which participants are achieving the nine components of evaluation. The nine components are as follows: Describe the programs instructional strategy; Specify the goals; Specify objectives (outcomes) for the program; Specify the methods of assessment to be used; Develop instrumentation to collect the assessment data; Develop data collection protocol; Analyze the data collected; report the results of the assessment, and Use the assessment results to make changes to the program. In completing this research project we were only able to complete the first three steps of the evaluation process. The first deals with the instructional strategy. Every program has one because it is that statement that explains the basic structure of the program content and why it is necessary for a specific group of learners to understand the information at hand. The instructional strategy generally includes a description of the concepts, principles and theories on which the program is designed. It also identifies the assumptions made about the values, skills and needs of the target audience. The second of the nine components deals with writing goals. Goals reflect the philosophy and values of the program developers. The purpose of the goals is to provide direction to the

program. The goals of a program are so important because they make the connection between the instructional strategy and the instructional objectives. Which finally brings us to exactly what it is that the program participants should be doing. Instructional objectives state what it is that a program participant should be able to do as a result of having experienced the program.

After having taken the aforementioned information to the program managers, they found that their programs did not actually have well establish goals and objectives. This being the case the guide included an appendix that is designed to help program managers to state their goals and objective more clearly. Since our project could not be completed the process of evaluation will continue and the guide will continue to grow. I have made the following recommendations to the Science Education Center for the continuation process.

Recommendations

The program managers should along with the rest of the staff should use the first half hour of weekly staff meetings to finish defining each program's goals and objectives. Program managers should begin to establish the methods of evaluation that each program will use to evaluate its program. The entire staff should work together in small sub-teams as well as one big team to complete the evaluation process. The team concept will avail each program manager knowledge and input in the other programs.

Neural Network Analysis of Nuclear Waste Glass Composition vs. Durability*

Cindy K. Seibel

University of California at Davis

Lawrence Livermore National Laboratory
Livermore, California 994550

December 12, 1993

Prepared in partial fulfillment of the Science and Engineering Research Semester under the direction of Farid Dowla, Research Mentor, at the Lawrence Livermore National Laboratory.

*. This research was supported in part by an appointment to the U.S. Department of Energy Science and Engineering Research Semester (hereinafter called SERS) program administered by LLNL under Contract W-7405-Eng-48 with Lawrence Livermore National Laboratory.

Neural Network Analysis of Nuclear Waste Glass Composition vs. Durability

ABSTRACT

The relationship between the chemical composition of oxide glasses and their physical properties is poorly understood, but it is becoming more important as vitrification (transformation into glass) of high-level nuclear waste becomes the favored method for long-term storage. The vitrified waste will be stored deep in geologic repositories where it must remain intact for at least 10,000 years. A strong resistance to groundwater exposure; i.e. a slow rate of glass dissolution, is of great importance.

This project deals specifically with glass samples developed and tested for the nuclear fuel reprocessing facility near West Valley, New York. This facility needs to dispose of approximately 2.2 million liters of high-level radioactive liquid waste currently stored in stainless steel tanks. A self-organizing, artificial neural network was used to analyze the trends in the glass dissolution data for the effects of composition and the resulting durability of borosilicate glasses in an aqueous environment. This durability data can be used to systematically optimize the properties of the complex nuclear glasses and slow the dissolution rate of radionuclides into the environment.

Introduction

The long radioactive half-lives of actinides in high-level nuclear waste require that they be isolated from the biosphere for 10,000 years. The waste disposal system under consideration in the United States is a deep geologic repository for the solidified waste. A multibarrier system used to control the release of radionuclides will have the following release control mechanisms: delay of ingress of water, slow dissolution of radionuclides from vitrified material, slow flow rate of groundwater, and delay due to sorption on the geological medium.

A stainless steel barrier surrounding the glass will delay the ingress of water, a glass material engineered for durability in an aqueous environment will slow the dissolution rate of radionuclides,

and sorption, a naturally occurring mechanism which binds radionuclides to soil particles in certain ground layers of the repository, will delay the dispersion of radionuclides.

This project deals with the second barrier, the glass material engineered for durability in an aqueous environment. The principal objective of the nuclear waste glass development is to optimize the glass composition for the nuclear waste glass to be durable enough to survive long periods of geologic time and aqueous attack.

Durability

When glass is brought into contact with water, the glass components begin to leach out from the glass into the solution and the concentration of these components gradually increase. The term "chemical durability" is used to express the resistance of glass toward environmental agents. There is no definite measure of chemical durability and glasses are usually graded relative to one another after being tested under the same experimental conditions.

The immobilization medium selected for the disposal of West Valley waste is borosilicate glass. The West Valley High-level Nuclear Waste Glass Development Project has selected the composition WV205 as the initial reference glass composition. The composition of WV205 is shown on page 11.

The leach rate of glasses was determined using a modified Materials Characterization Center 3 (MCC3) test in which the sample glass is ground up and placed in distilled water. Samples of the water are analyzed after 7, 28, and 56 days for boron content. For all tests boron is used as indicator of glass durability because it is the most soluble element, thus the least likely to reprecipitate out of the water solution into another form. A low measure of boron for a glass sample demonstrates a low leach rate of the glass components and thus indicates a more durable glass for water.

Dissolution rate dependence on silica concentration (WV205 glass)

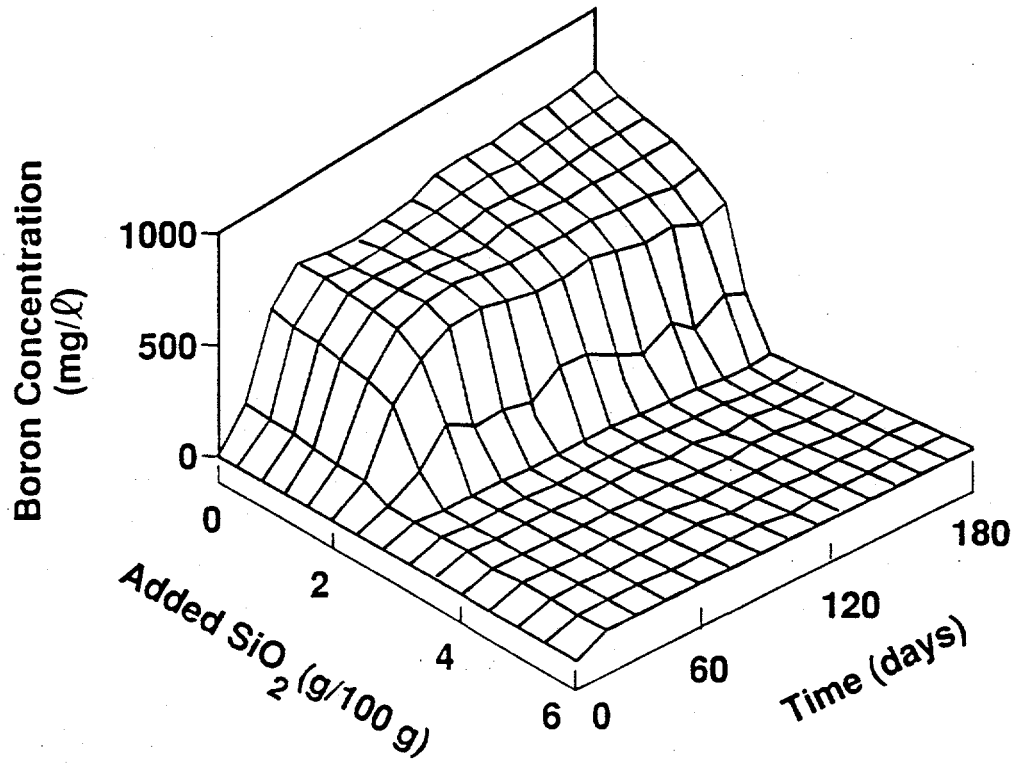

This is a graph of the WV205 glass as silica is added. Note the steep decline of boron concentration (increase of durability) at approximately the 2 weight percent mark of added silica. This is a good example of the nonlinear relationship between glass composition and durability for which standard statistical analysis is not capable of discerning. Neural networks excel at solving this type of relationship.

Method

The structure of even the simplest glasses and its relationship to properties such as leach behavior are far from being completely understood. The nuclear waste glasses are much more complex, usually containing between 15 and 30 oxide components which affect the durability in a non-linear manner. It is due to this non-linear relationship between composition and durability of glass that we decided to apply neural networks to this problem. We employed two types of neural networks to this data and have found some general patterns in durability.

Neural Network Analysis

An artificial neural network (ANN) is a collection of highly interconnected processing elements which can model nonlinear functions from a data set. The ANN learns by adjusting the weights of the connections between the processing elements according to the examples which it encounters. There are two important classes of neural networks: the supervised learning networks, such as the backpropagation network, and the unsupervised learning network such as the Kohonen's self-organizing network. We briefly discuss these networks in the following:

Backpropagation Networks

Backpropagation networks are parallel, non-linear systems capable of complex non-linear mapping of input-output relationships. Given a large number of examples the learning algorithm systematically modifies the interconnecting weights of the non-linear processing units (neurons) until the network is able to solve the input-output relationship accurately. When a large number of examples are available and the network architecture is sufficiently

Backpropagation Network

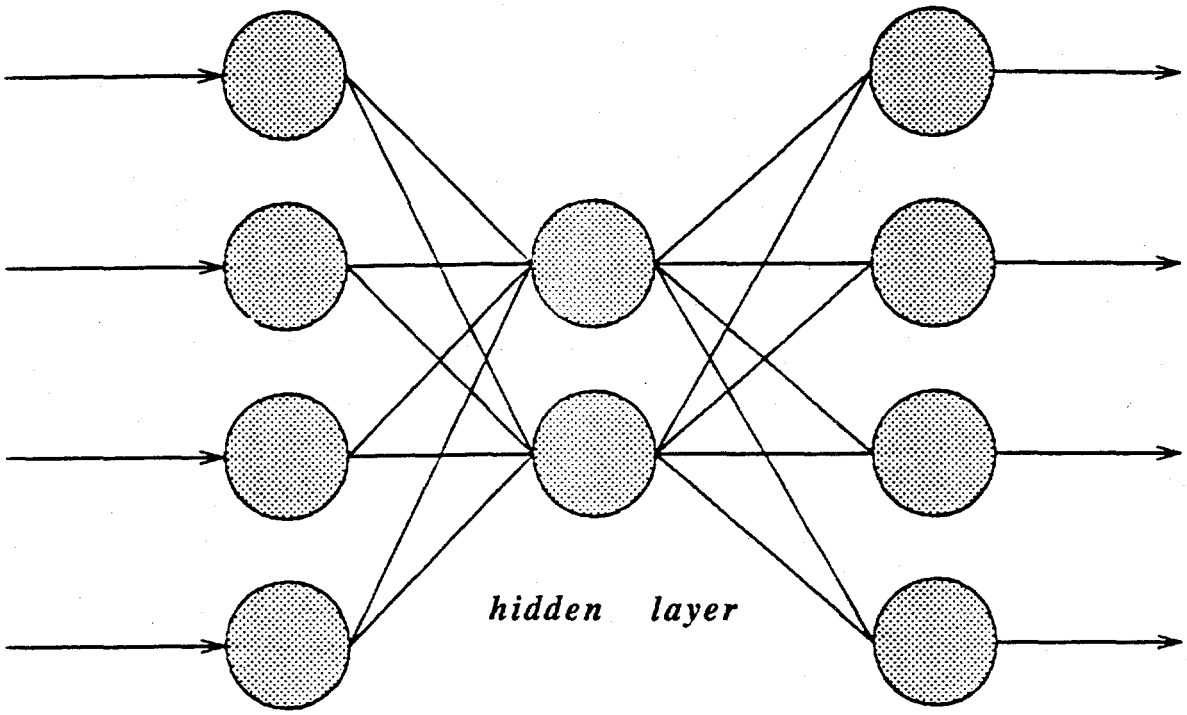

The input layer contains the molar fraction of the elemental oxides in vector form. The output layer contains the boron concentration of the glass sample. The hidden layer is a series of sigmoid functions that describe the input-output relationship of the glass sample. When properly trained, the backpropagation network should be able to predict the output (boron concentration) when given only an input vector.

simple, backpropagation networks can generalize patterns from the training set and apply them to predict the input-output relationship to new, unseen data. However, the network cannot learn, or minimize the error of the output when the example set consists of members of conflicting input-output relation.

Kohonen's Self Organizing Network

Kohonen self-organizing networks are unsupervised learning networks (no training set is needed) which cluster the data into various groups according to the similarity of the pattern vectors. The important property of this network is that it not only clusters the data into different groups, the network actually organizes the cluster groups in a systematic topological order. This unsupervised learning model is a simple model of the brain's ability to represent information in a way that allows only particular groups of neurons in the brain to respond to certain input signals. The internal parameters of the processing units occur in the same topological order as the similarity metric of the input patterns. The self-organizing procedure is an adaptive filter that forms localized responses through the use of feedback and modification among the neighboring units. This lateral feedback is necessary for the formation of meaningful clusters. The following general rules form the basis of self-organizing learning:

1. Locate the best matching group or unit for each pattern.

2. Increase the matching at this unit and its topological neighbors by an appropriate weight modification rule.

3. Repeat this learning process through the entire training set until all patterns have converged to their groups.

A diagram of a self-organizing network is on the next page.

Kohonen Self-Organizing Network

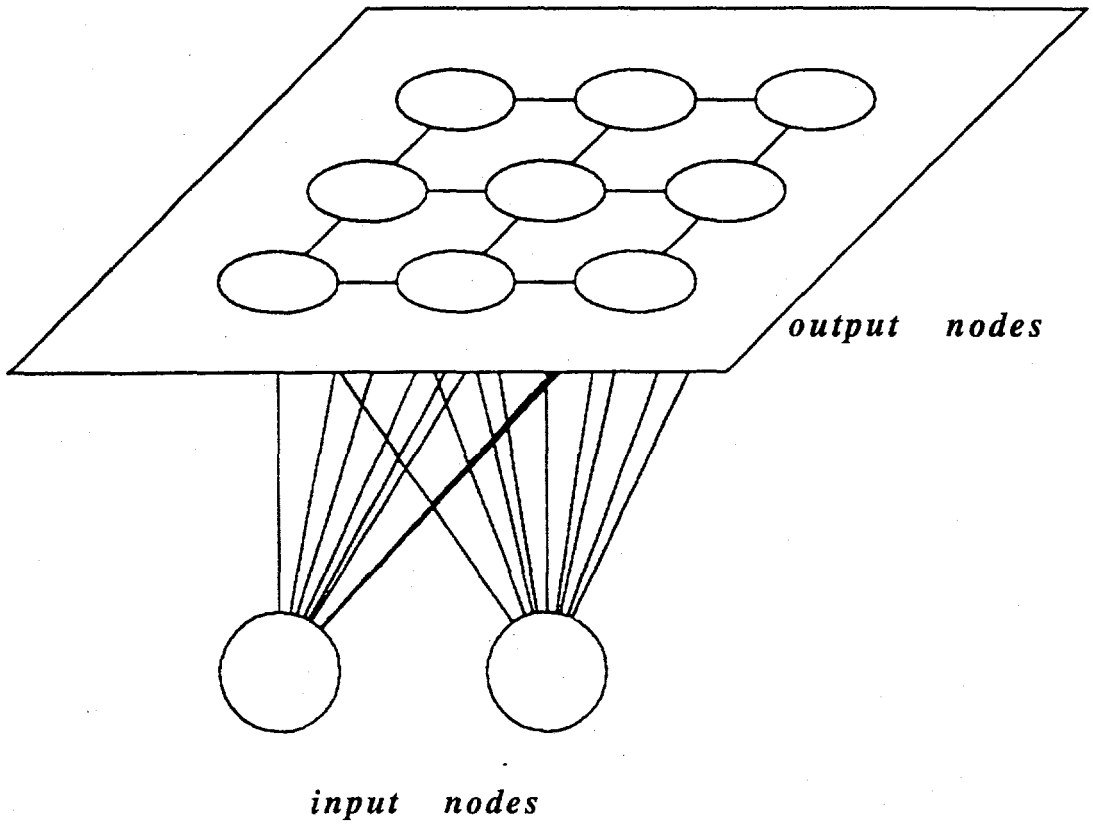

The input nodes contain the molar fractions of elemental oxides, i.e. Al2O3 and SiO in vector form. The output nodes contain the error value, ε, which indicates how well the input vector matched the reference vector of that node. The node with the smallest ε value will have the largest weight value assigned to it.

Data Analysis and Results

The raw data was obtained from Xiangdong Feng's PhD thesis from the Catholic University of America. It contained the weight percent of each oxide present in approximately 100 glasses and the dissolution results of boron for each of the glasses. I converted the data from weight percent to the molar fraction of oxides.

Performance of the Networks

Backpropagation Learning

1st trial - We grouped together the elements that behave in a similar geochemical manner in the glass structure to minimize the number of input variables. Eight input groups and one output (56-day boron) were assigned to the network. Network would not train.

2nd trial - Input 28 individual elements with 56-day boron as the output. Network still would not train.

We observed that the output error could not be reduced to a very small number, thus the neural net could not train on the set of data we had. This is an indication that the data probably consists of groups of data whose input output relations are not only different but are actually conflicting. For such a data set, it is best to use an unsupervised learning network, such as the Kohonen network.

Kohonen Learning

Preliminary trials - insignificant results

1st trial - We entered the 28-input and 1-output (56-day boron) element as a single 29-element vector. When we applied the Kohonen network the data clustered itself into a five

distinct groups and there were 11 examples which did not belong to any group, but were assigned one of their own due to some component differences. Results were still inconclusive.

2nd trial - Upon noticing a large jump between the lower and higher boron concentrations, I separated the lowest leach rate (boron < o.5 mg/L) glasses into a "strong" glass category and the highest leach rate (boron > 5.o mg/L) glasses into a "weak" glass category. I then let each category of glass run separately in the Kohonen network. The weak samples (16 of them) clustered into one group of 12 glasses, one group of two glasses, and two groups of one glass each. The strong samples (64 of them) clustered into one group of 61 glasses and three groups of one glass each. I speculate that the samples that do not fit into the larger groups contained experimental errors. The dominant clusters in each group indicate there is a strong similarity in glasses the are strong or weak. I studied the differences of the oxide fractions between these two groups to determine which may be key elements in the durability of borosilicate glasses.

Conclusions

Overall, aluminum caused the greatest increase in durability. This was a bit of a surprise, as I expected it would be silicon. Silicon had only slight evidence for increasing durability. I did observe that the glasses that were included in the "strong" category which had a low Silicon value (47% to 50%), had higher levels of zirconium, implying that zirconium would greatly increase the durability of glass. This is not an absolute observation though, as the levels of zirconium were so low (0% to 2%).

There was strong evidence that increased levels of potassium decreased durability. There was also slight evidence that increased boron and barium levels increase the durability, and higher copper and zinc levels decrease the durability.

Future Research

The definite evidence for the effects of aluminum was due to relatively large percentages (up to 8%) and the wide variations present (2% to 8%) in the samples. It would, therefore, be worth while to expand the quantity of data in the data set and expand the variation of oxide concentrations present in the samples. I would have a particular interest in several samples with exceptionally low silicon(40%) and high zirconium (5% to 10%) levels to prove or disprove the theory that zirconium has a strong effect on glass durability.

The Kohonen network should be used to eliminate the experimental errors in the data set; i.e. abnormal data that would not converge into a dominate group should be eliminated, then retrain the backpropagation network on the data set which should have no conflicting data.

Element	Oxide	CUOC	DWRG	WVCM47	WVUTH52	SRL131	CU39	WV205	WVUTH9
Al	Al2O3	0.02143037	0.04367508	0.05653543	0.0710451	0.02458647	0.02186682	0.02228886	0.02032798
B	B2O3	0.09476321	0.06338814	0.12896618	0.12859372	0.09634218	0.09677624	0.09851902	0.09751247
Ba	BaO	0.00258259	0	0.00061243	0	0	0.00265206	0.00269477	0.0010115
Ca	CaO	0.00718729	0.02338259	0.00772837	0.00311247	0.00966503	0.00737614	0.0074907	0.01194234
Ce	CeO2	0.00061625	0.00038672	0.00029377	0.00295779	0.0039363	0.000611	0.00060015	0.00028671
Cr	Cr2O3	0.00097701	8.7588E-05	0.00147328	0.0006699	0	0.01877411	0.00099679	0.00139147
Cs	Cs2O	0.00038593	0.00121093	0.00035043	0.00030872	0.00287597	0.00042516	0.0004176	0.000342
Cu	CuO	0	0	0.00027242	0	0	0	0	0.00044312
Fe	Fe2O3	0.04887687	0.04330228	0.05476339	0.05427316	0.05763724	0.04990805	0.05083066	0.05304964
K	K2O	0.02462265	0.00310921	0.00981561	0.00710317	0	0.02515735	0.02558772	0.02581997
La	La2O3	0	0	6.6512E-05	8.9288E-05	0	0	0	6.4912E-05
Li	Li2O	0.06862628	0.1100413	0.04883041	0.04989418	0.08389138	0.07015374	0.07144252	0.06888918
Mg	MgO	0.02140429	0.01453316	0.0236571	0.02544273	0.0235338	0.02174394	0.02221196	0.02203876
Mn	MnO2	0.01057385	0.01355187	0.01088448	0.00819822	0.03506916	0.01080642	0.01077287	0.01143364
Na	Na2O	0.11751304	0.09708532	0.10733838	0.12438221	0.13226878	0.12001939	0.12222052	0.11977135
Nd	Nd2O3	0	0.00019782	0.00040788	0.00038906	0	0	0	0.00037712
Ni	NiO	0.0062477	0.01693036	0.00328777	0.002434	0.02086062	0.00638223	0.00645323	0.00330309
P	P2O5	0.0116571	0.00093787	0.01272217	0.01306527	0	0.01190362	0.01212879	0.01201893
Pd	Pd	0	0	0	0	0	0	0	0
Rh	Rh	0	0	0	0	0	0	0	0
S	SO3	0.00105991	0	0.00198498	0.00199854	0.00084627	0.00113846	0.00111824	0.00184919
Si	SiO2	0.49840892	0.5574544	0.50853323	0.48537829	0.49501693	0.50886864	0.51828133	0.50885909
Sr	SrO	0	0.0030834	0.00020913	0	0.00588461	0	0	0
Th	ThO2	0	0	0.00979396	0.00969561	0	0	0	0.00934485
Ti	TiO2	0.00831919	0.00083309	0.00885984	0.00910242	0.00593573	0.00842387	0.00861898	0.0262933
U	U3O8	0	0.00237926	0.00051468	0.00050092	0	0	0	0.00048556
Zn	ZnO	0	0	0.00017752	0	0	0	0	0.00025988
Zr	ZrO2	0.05474756	0.00442962	0.00170005	0.00112143	0.00164953	0.01701276	0.0173253	0.00257457
56 day boron		0.21336	0.21961	0.30177	0.89405	1.56313	3.84368	7.3765	13.18666

References

1. Beale, R., Jackson, T., Neural Computing, Adam Hilger, New York, New York,1991.

2. Ewing, R. C., Lutze, W., editors, Radioactive Waste Forms for the Future, Elsevier Science Publishing Company, Inc., New York, New York, 1988.

3. Feng, X., Composition Effects on Chemical Durability and Viscosity of Nuclear Waste Glass - Systematic Studies and Structural Thermodynamic Models, PhD Thesis, The Catholic University of America, Washington, DC, 1988.

4. Hinton, G. E., "How Neural Networks Learn from Experience," *Scientific American*, September, 1992.

Cathode Development for a Rechargeable Lithium Ion Battery

Dyuti Sengupta

University of Washington, Seattle

Lawrence Livermore National Laboratory
Livermore, CA 94550

December 15, 1993

Prepared in partial fulfillment of the requirements of the Science and Engineering Research Semester under the direction of John Feikert and Steve Mayer, Research Mentors, in the Lawrence Livermore National Laboratory.

*This research was supported in part by an appointment to the U.S. Department of Energy Science and Engineering Research Semester (hereinafter called SERS) program administered by LLNL under Contract W-7405-Eng-48 with Lawrence Livermore National Laboratory.

ABSTRACT

Lithium ion rechargeable batteries have been the subject of much research since 1990, when Sony announced their intention to market such a battery. The cathode of this battery continues to pose many processing questions, in terms of additive content and fabrication procedure. Some of these questions have been examined in this report. Experiments involving several additives in varying amounts with lithium cobalite powder, the primary material in the battery cathode have been performed. A brief analysis of the Sony battery was also completed.

INTRODUCTION

Lithium ion rechargeable batteries offer many advantages over standard rechargeable batteries. These advantages include a metal-free system, high theoretical energy densities (400 Wh/kg) [1], long cycling-life (up to 1200 cycles)[2], high voltage output (3.6 V), and wide temperature range for operation.

The battery system is lithium metal-free because it operates by means of intercalation of a lithium ion from a non-metal anode to a non-metal cathode. Anodes are usually comprised of carbon materials which intercalate at up to 90% or better. Previous studies indicate that the best cathode material is lithium cobalite ($LiCoO_2$)[3], based on cost and performance compared to the other transition metal oxides ($LiCoNi_2$, $LiCoMn_2$). This is the only group of compounds which can maintain its crystallographic structure with repeated intercalation and deintercalation of the lithium ion[4]. Only the Sony corporation has been able to process this oxide such that it adheres to the aluminum current collector, and conducts ions through a usually non-conductive oxide material ($LiCoO_2$). The focus of this research project was to analyze the Sony cathode, experiment and examine additives for lithium cobalite mixtures and

their electrochemical behavior, and search for additional literature on the topic.

ANALYSIS OF SONY'S CATHODE

The main goal of this analysis was to determine the nature of the particles on the cathode with the SEM and the amount of organic matter and oxides (by weight percent) present in a given portion of the cathode.

SEM analysis (see figures 1-3) showed that oxide particles were very uniformly distributed on the substrate. The particle size distribution in also thought to play an important role in the commercial manufacture of this cathode. In addition, the very thin layer of oxide (0.003") provides the best path for maximum intercalation and deintercalation. There is little opportunity for internal resistance in the material since the ions do not have much distance to travel to intercalate most of the material. Maximum possible intercalation for the lithium cobalite is around 50% at the operating voltages in this battery; this is an intrinsic property of the material.[5] Finally, SEM analysis showed that no extremely high temperatures (above 800 C) were used to process this material since no evidence of sintering was seen.

Another important issue in the fabrication of this cathode involves the amount of binder and additives present. Since processing additives are organic, it was possible to heat a known weight of the Sony cathode oxide, removed from the current collector, and heat it at temperatures known to burn out hydrocarbon compounds (600 C) without affecting the oxide material. Approximately 17% of the material on the current collector was found to be organic. From this

discovery, experimentation of oxide and additive content began with mixtures of 81%-83% oxide.

EXPERIMENTATION

Since the lab was not an oxide processing lab, but a chemistry lab, resources were limited. For this reason, only the following combinations of materials were used in experimentation:

by w/o name	Oxide	Carbon Black	Graphite	Resin	Al powder	Alumina
A1	81	7		3.5	8	
A2	83	6		8	3	
B1	81	7	8	3.5		
B2	83	6	3	8		
C1	81	7		3.5		3.5
C2	83	6		8		8
Sony	----	----	----	----	----	----

Each powder combination was pressed in a hot die into pellet form at 10000 lbs pressure. Once this process was complete, the pellets were weighed (to determine the current to be run through the sample in the battery tester) and wrapped in aluminum exmet material. The exmet served as a current collector for the sample. The pellet was then placed in electrolyte with a counter electrode (Lithium metal which provided lithium source) and a lithium metal reference electrode. All experiments were performed in an argon atmosphere to avoid water contamination, which often leads to small side reactions or even violent reactions of lithium and water. These battery cathodes were tested for a varying number of cycles with the Maccor^{tm} battery tester.

RESULTS

Figures 4 - 10 illustrate voltage vs. time relationships for the tested samples. The six samples made in the lab were to be compared to the Sony cathode (fig 4). Figures 5 and 6 (batch A) show a highly polarized sample which gave little useful discharge in repeated cycling, if any. Batch B (fig 8, 9) shows a significantly better discharge curve (approximately 2 hours discharge) than A. B2 (fig 8), with only 1 hour of discharge, did not perform as well as B1 since more phenolic resin in this mix probably inhibited the conductivity of lithium ions. Finally, batch C gave very little energy in the discharge portion of the curve, and both C1 and C2 had high polarization.

CONCLUSIONS

From the resulting voltage vs. time plots, low amount (3.5% weight) of binder (phenolic resin) with conductive carbon material gives the best discharge curve. The materials aluminum and alumina are not useful as either binders or conductive materials, as they induced extremely high polarity in the samples.

A thorough literature search yielded information regarding a "multicoating" machine[6], which is believed to be used in the application of oxides to metallic substrates. Such a machine is used with oxide slurries that are applied to the metallic substrate, and then is run through a series of rollers. A rapid drying process is also employed in this process. This is most likely the key to Sony's large scale (or even prototype R & D) cathode fabrication. Many additional oxide processing issues arise from this technology, however, including particle size distribution, particle sizes, viscosities, and additives within the slurry.

Bibliography

1. Progress in Batteries and Battery Materials, Vol. 10 (1991) 218.

2. ibid.

3. J. Electrochem. Soc., Vol. 139, No. 8, Aug. (1992) 2091.

4. ibid.

5. Mat. Res. Bull., Vol. 19, No. 10, (1984) 1383.

6. Progress in Batteries and Battery Materials, Vol. 10 (1991) 261, 262.

FIGURE 1
SEM showing side profile of the Sony battery cathode

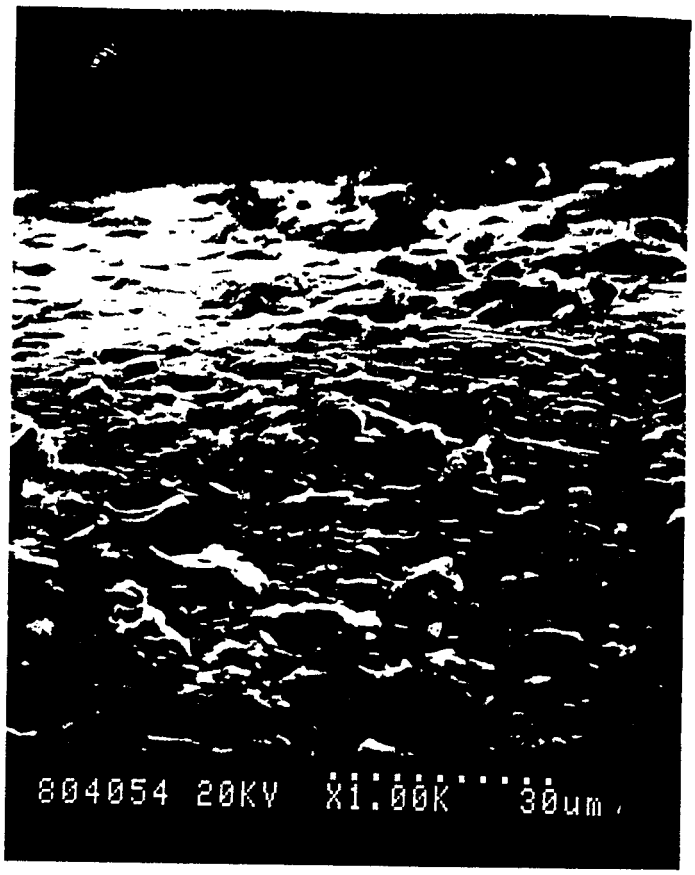

FIGURE 2
SEM illustrating the cathode surface with oxide removed

FIGURE 3
SEM illustrating the nature of particles in the cathode

FIGURE 4

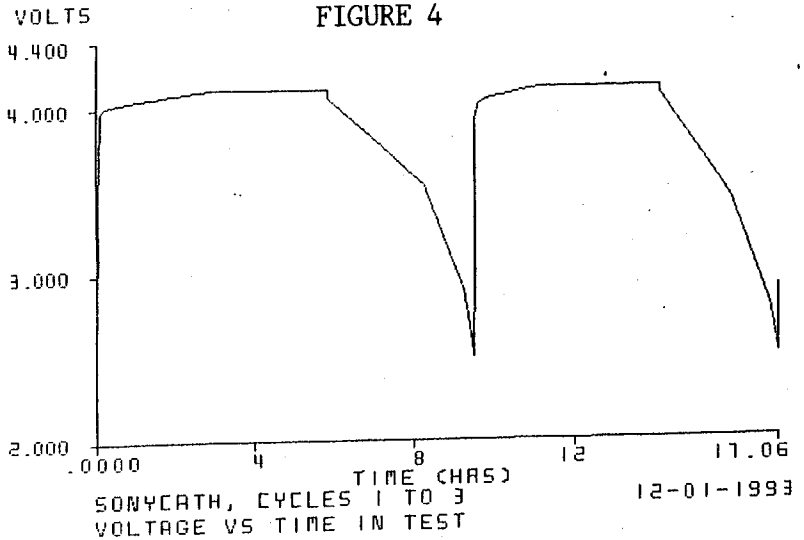

FIGURE 5

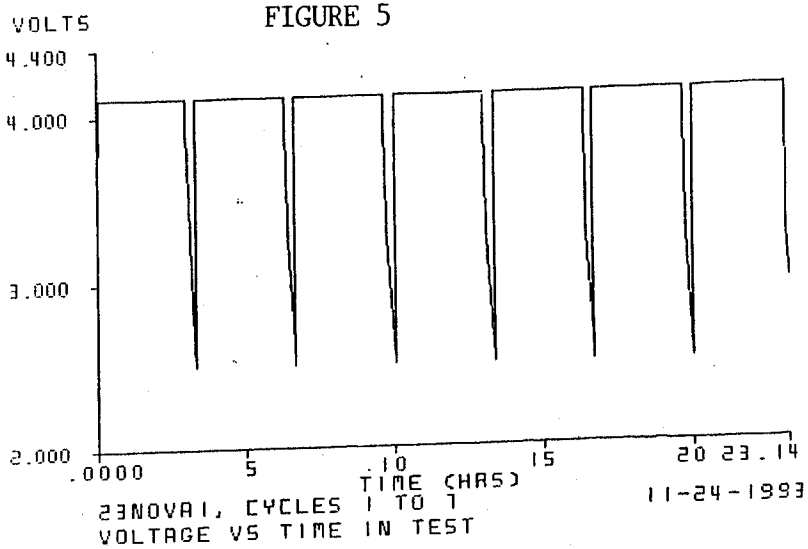

FIGURE 6

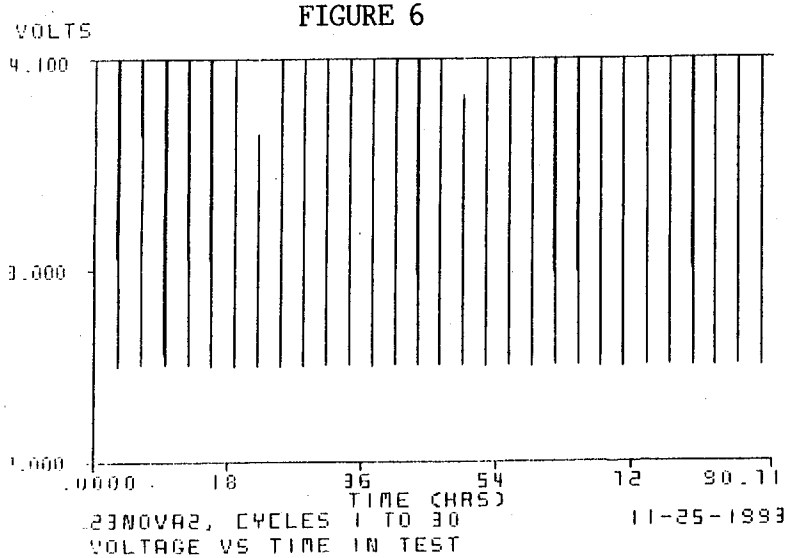

FIGURE 7

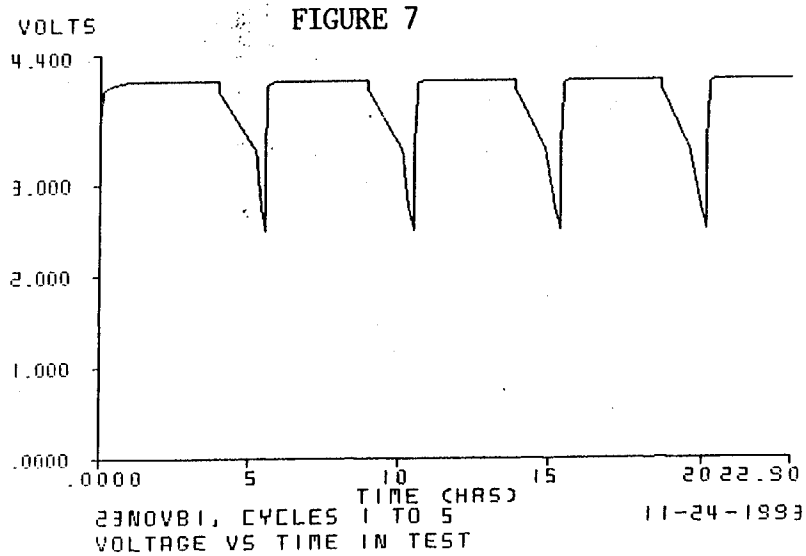

FIGURE 8

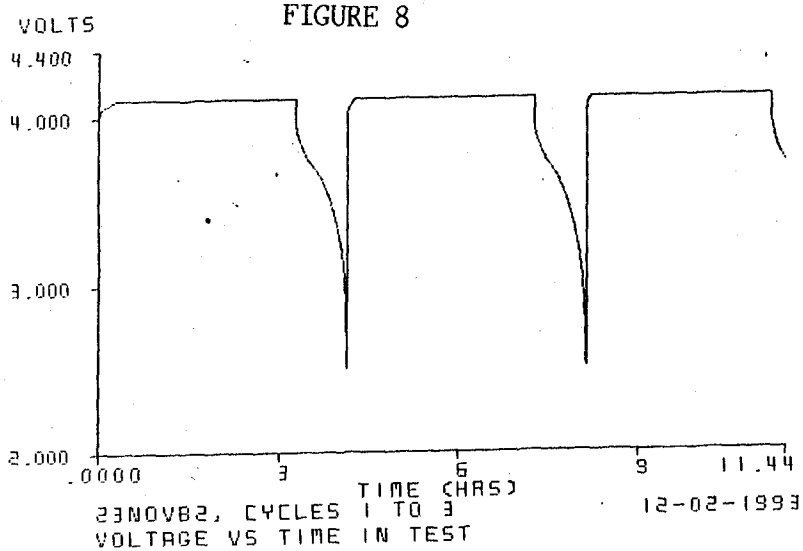

FIGURE 9

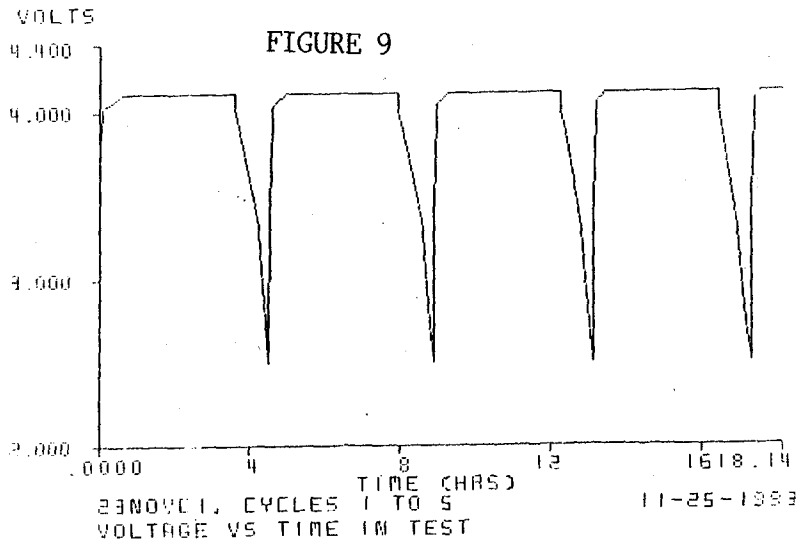

FIGURE 10

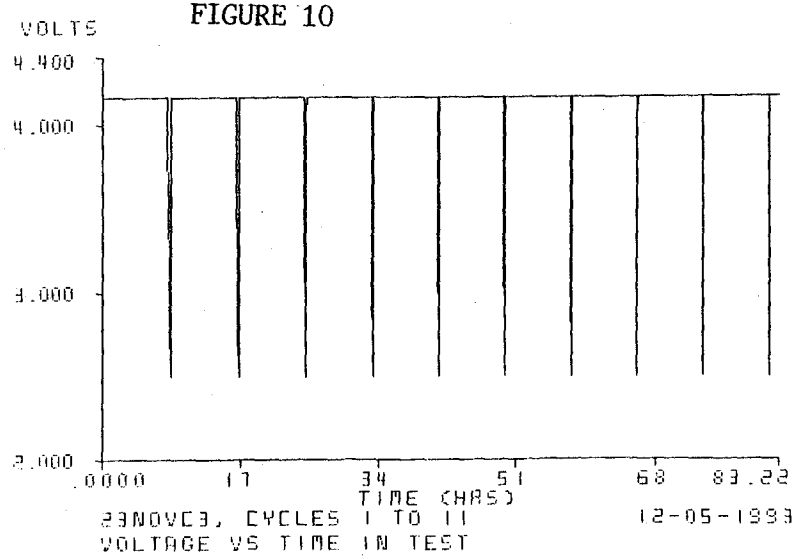

Indonesian Snails: *Key to Ocean Circulation* *

Timothy W. Sullivan

Michigan State University

Lawrence Livermore National Laboratory
Livermore, California 94550

12/15/93

Prepare in partial fulfillment of the requirements of the Science and Engineering Research Semester under ther direction of Dr. Michaele Kashgarian, Research Mentor, in the Lawrence Livermore National Laboratory.

* This research was supported in part by an appointment to the U.S. Department of Energy Science and Engineering Research Semester (hereinafter called SERS) program administered by LLNL under Contract W-7405-Eng-48 with Lawrence Livermore National Laboratory.

Indonesian Snails: Key to Ocean Circulation

Timothy W. Sullivan
Michigan State University
Center for Accelerator Mass Spectrometry

Abstract: Previous radiocarbon measurements using mollusks indicate that reservoir ages vary considerably throughout the Indonesian Seaway. By studying ^{14}C concentrations in mollusk shells, we investigate the source of this variation. Mollusks of a known age were sampled along their growth axis and analyzed at the Center for Accelerator Mass Spectrometry. Results indicate that radiocarbon concentrations along growth axes fluctuate seasonally. We attribute this fluctuation to the upwelling of deep, "old" water during seasonal monsoon weather patterns. Furthermore, we believe the source of variation in the reservoir ages may be caused, in part, by sampling mollusks at only one location and not averaging over their growth axes.

Introduction

Certain species of mollusks that create calcite ($CaCO_3$) shells in isotopic equilibrium with surrounding waters are particularly useful when studying marine radiocarbon (^{14}C) activities. Recent studies have employed these sea shells to regionally calibrate marine ^{14}C ages.[1]

The use of particle accelerators as mass spectrometers began in the mid-1970s.[2] Conventional radioactive decay-counting methods were inefficient and required gram-sized samples. Accelerator Mass Spectrometry (AMS) made ^{14}C dating far more efficient and only requires milligram-sized samples.

We have applied techniques of AMS to the study of ^{14}C profiles in marine snail shells. In particular, we have looked for variablility in ^{14}C concentrations of shell samples taken along growth spirals of marine dwelling mollusks. The purpose of the measurements was to investigate the local variablility observed ^{14}C dates obtained from shells in the Indonesian conduit. We have discovered that ^{14}C concentrations fluctuate seasonally in shells collected off the coasts of Java, Thailand, and the Phillipines. We have also observed regional variability in reservoir ages throughout the seaway. Further work needs to be done to explain these results.

Past levels of marine ^{14}C can be studied by sampling certain types of mollusk shells. Snails and clams produce hard calcite shells by incorporating dissolved inorganic carbon from the water in which they live. Because new shell is created in isotopic equilibrium with surrounding waters, these sea shells keep a record of local ^{14}C concentrations. We have used the *Thais distinguenda* species for our measurements. These snails create shells that spiral around a central growth axis.

Recent work has employed these shells to regionally calibrate ^{14}C dates. Shells of a known age are ^{14}C dated at their mouth or death edge. The difference between the measured ^{14}C age and the known calendar age is a location's reservoir age. The marine ^{14}C age calibration curve relates a sample's calendar age to its ^{14}C age. Reservoir ages derived from the marine ^{14}C age calibration curve do not account for inter-regional variation among reservoirs, but instead are averaged over the entire globe.[3]

Recent studies indicate that reservoir ages deviate from those predicted by the calibration curve depending on the geographical location of the reservoir. A map with values of ^{14}C ages throughout the Indonesian conduit is shown in Figure 1[4]. These ages were obtained from mollusk shells between 80 to 110 years old. Radiocarbon ages measured on these shells range from 360 years to 640 years. It is unclear to what degree regional variability in reservoir ages or temporal fluctuations in ^{14}C concentrations influence these results.

Methods

Snails collected in surface waters throughout the Indonesian conduit were sampled around their exterior growth spiral. Specimens were obtained from the Smithsonian Institution shell collection. Shells were collected between 1910 and 1928 in surface water off the coast of Java, Thailand, and the Phillipines. Samples are prepared for analysis by first drilling out 10 mg of calcium carbonate powder from a mollusk shell. This powder is then dissolved in phosphoric acid to create CO_2 gas. Solid carbon is obtained by reacting this gas with hydrogen gas and a cobalt catalyst at 575° C. Radiocarbon

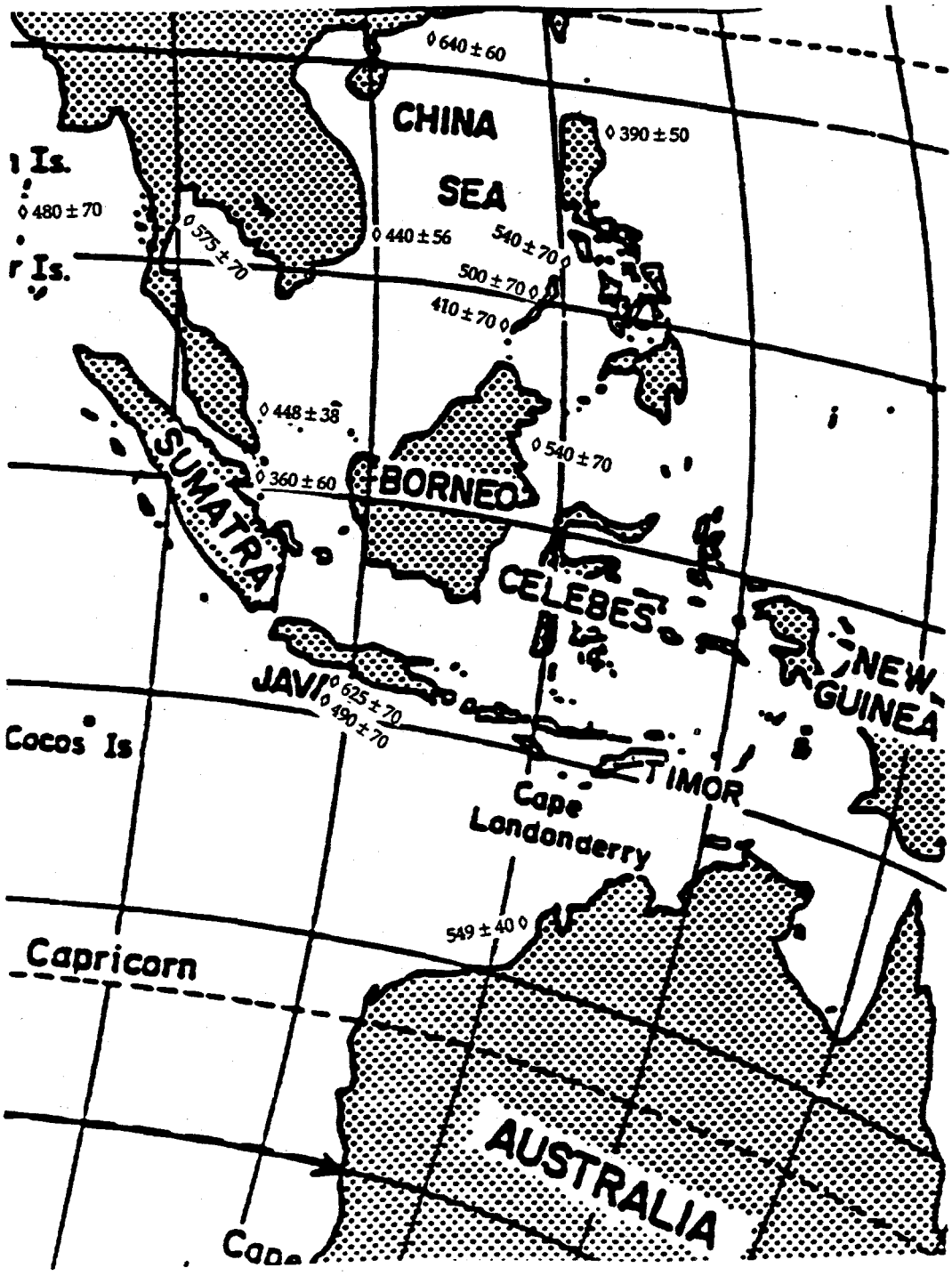

Fig. 1. Radiocarbon ages (In Years BP) obtained from mollusks in the Indonesian conduit.

ages were obtained from AMS measurements of the ratio of ^{14}C to stable carbon. These ages are typically measured to a precision of ± 70 years.

Results

Plots of ^{14}C ages (years BP) versus distance from death edges (mm) are shown in Figures 2-4. The results indicate that ^{14}C levels are not constant throughout the shell. The degree to which ^{14}C activities fluctuate in individual shells is not constant. Radiocarbon ages vary from 250 years in the shell from Thailand to as much as 400 years in the shell from the Phillipines. This implies that the ^{14}C concentrations vary with time in the surface waters of the areas where the samples were collected. These species are believed to have lifespans from 1 to 5 years, but the exact lifespans of our samples are unknown. Therefore, it is diffucult to say with any certainty the timescale of these fluctuations.

The difference between the average ^{14}C age and the reservoir age, the ΔR value, gives a measure of the regional correction that needs to be made to marine calibration curvebased reservoir ages. A comparison of the ΔR values for the three shells reveals that values range from 29 years in the Phillipines to 153 years in Java. This indicates that there is considerable regional variation in the ^{14}C concentrations of this area.

Conclusions

The variability in ^{14}C activity within each shell suggests that the way in which snails are sampled is important when interpreting results obtained from these species. Mollusks used for the regional calibration of the

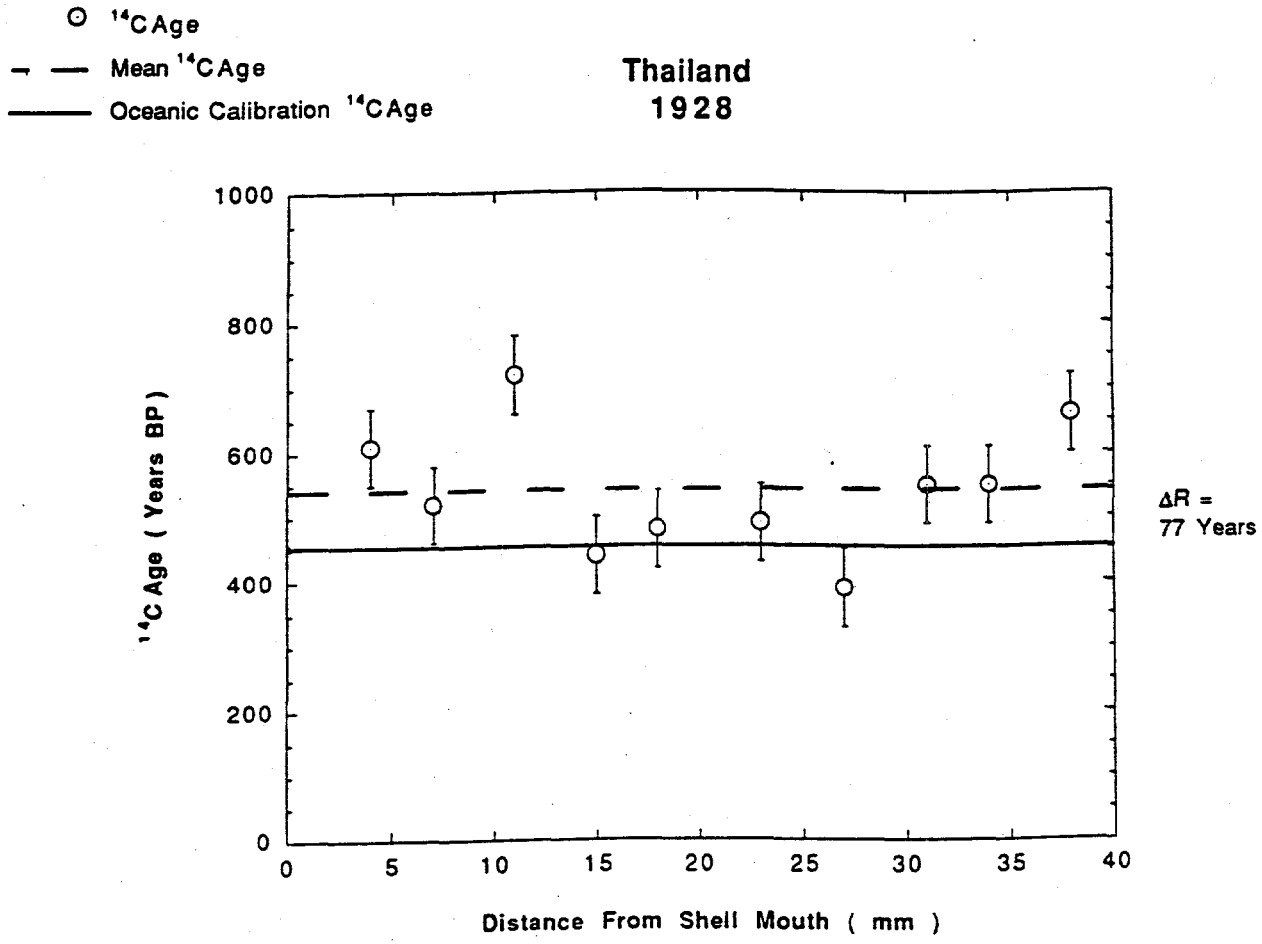

Fig. 2. Radiocarbon activity of USNM# 361252. Mollusk was collected off the coast of Thailand in 1928.

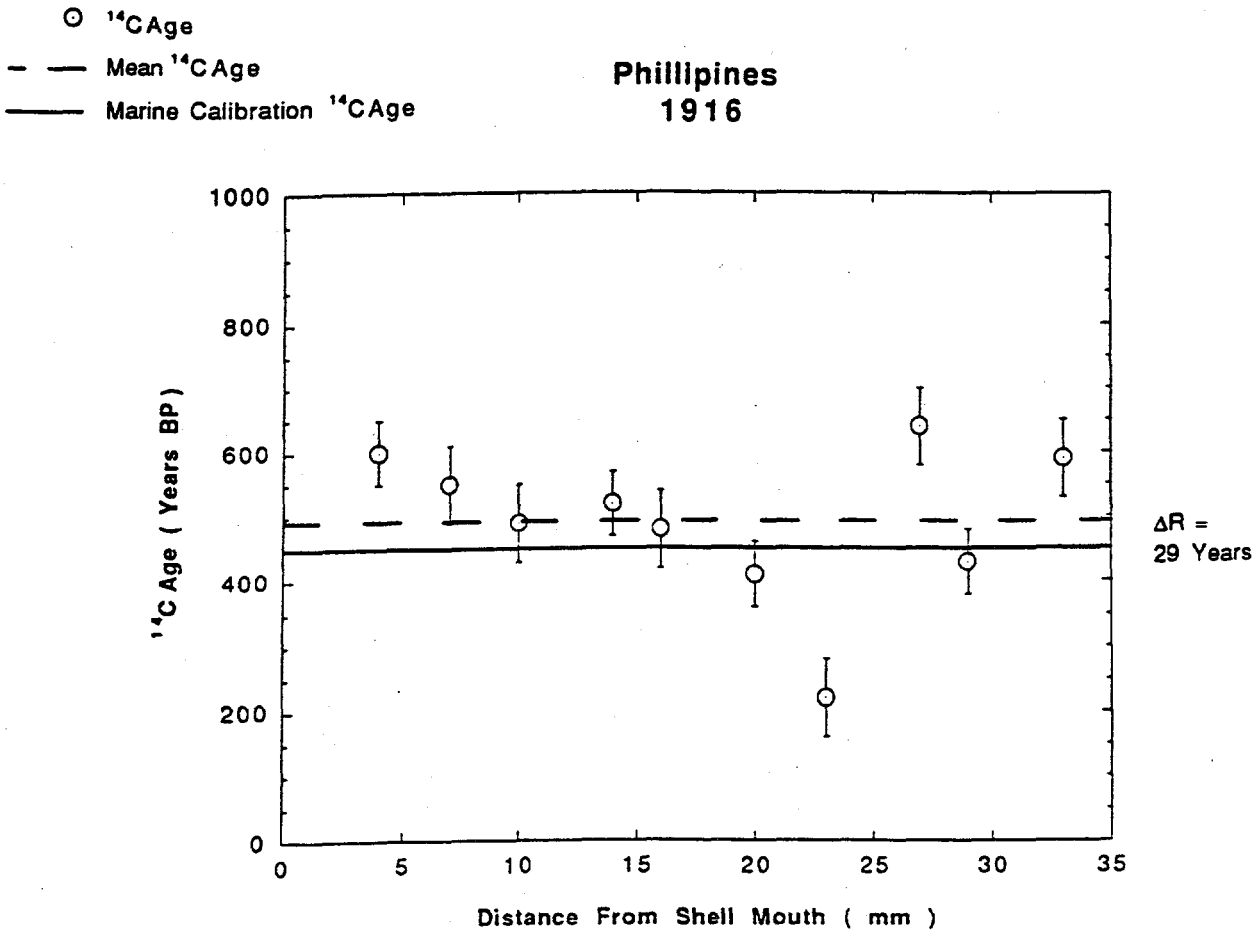

Fig. 3. Radiocarbon activity of USNM# 309579. Mollusk was collected off the coast of the Phillipines in 1916.

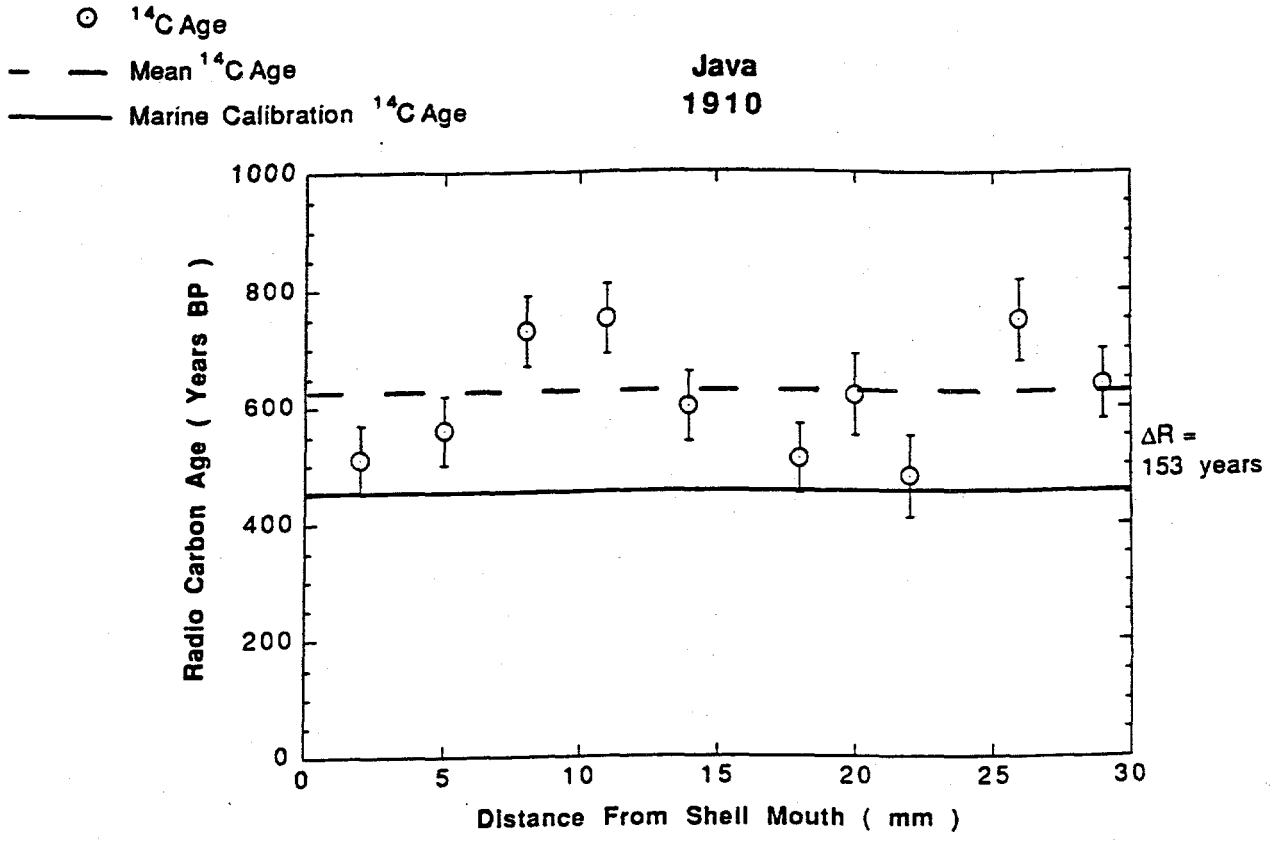

Fig. 4. Radiocarbon activity of USNM# 260602. Mollusk was collected off the coast of Java in 1910.

Indonesian conduit were sampled only at the shell's death edge. This may account for some of the variability observed in this area. Part of this variability may also be caused by the regional differences in reservoir ages observed in the three areas.

Although the cause of the seasonal fluctuation in ^{14}C concentrations of surface waters observed in the conduit is unclear, it may be the result of coastal upwelling initiated during the monsoon seasons. Parts of the Pacific and Indian Oceans are characterized by seasonal weather patterns that initiate strong winds and influence current patterns in the surface water. The circulation of surface water during the winter monsoon in February and during the summer monsoon in August is depicted in figure 5[5]. These seasonal patterns may result in varying degrees of coastal upwelling which would influence the ^{14}C activity of surface waters by bringing ^{14}C- depleted deep waters to the surface.

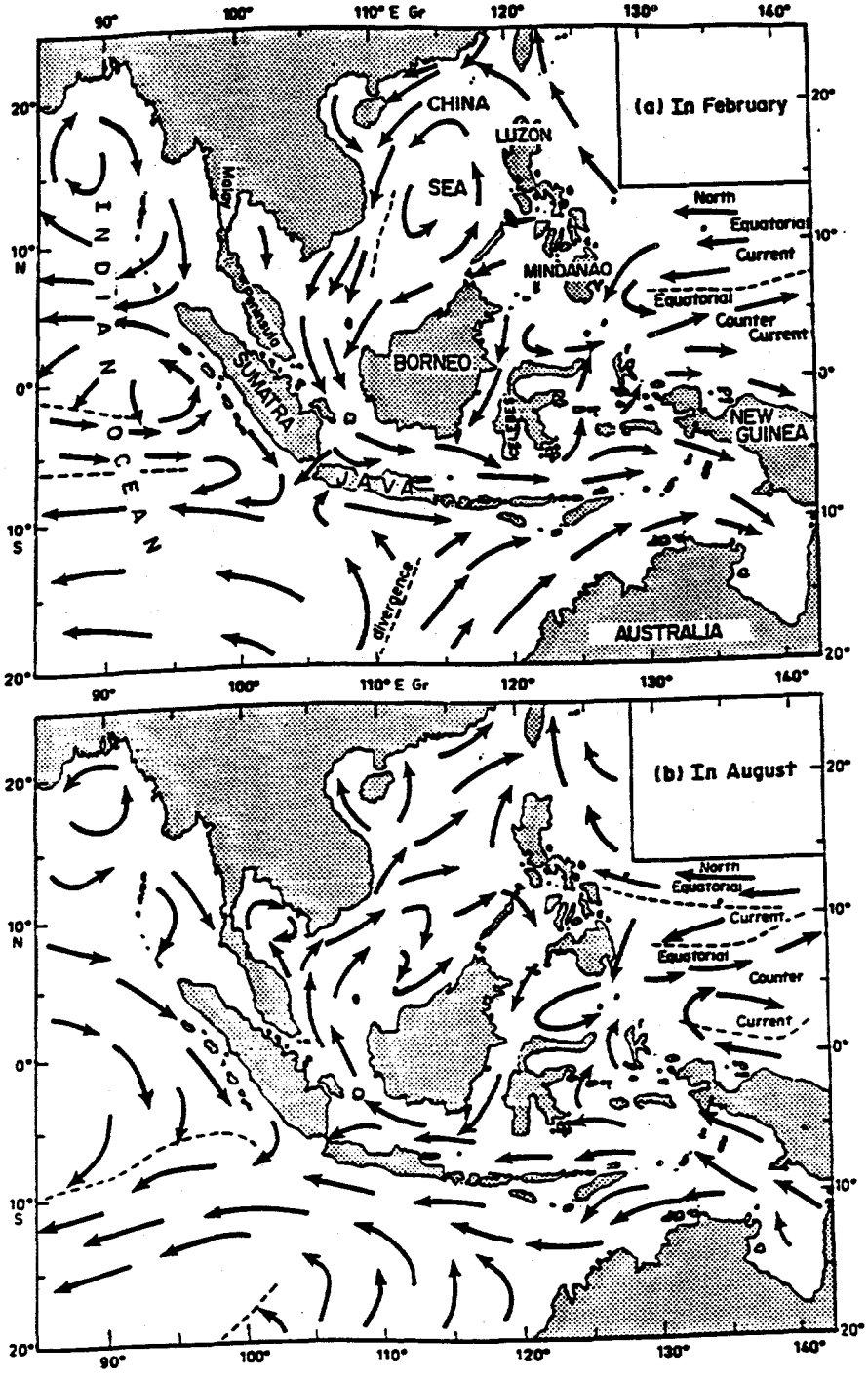

Fig. 5. Map of surface water currents in the Indonesian conduit a) during the winter monsoon b) during the summer monsoon.

References

[1,4] M. Kashgarian, Personal communication.

[2] R.A. Muller, *Science* **196,** 489 (1977).

[3] M. Stuiver, T.F. Braziunas, *Radiocarbon* **35,** 137 (1993).

[5] Tchernia, Descriptive Regional Oceanography, 229 (1980)

Optimization and Characterization of a Fibre Channel Switching System

Marcus Weber

Santa Clara University, Santa Clara

Lawrence Livermore National Laboratory
Livermore, CA 94550

December 15, 1993

Prepared in partial fulfillment of the requirements of the Science and Engineering Research Semester under the direction of Bob Bryant, research mentor, at the Lawrence Livermore National Laboratory.

*This research was supported in part by an appointment to the U.S. Department of Energy Science and Engineering Research Semester (hereinafter called SERS) program administered by LLNL under Contract W-7405-Eng-48 with Lawrence Livermore National Laboratory.

Optimization and Characterization of a Fibre Channel Switching System

ABSTRACT

Fibre Channel, as defined in the ANSI standard X3T9.3, is an emerging technology in high speed data communications and has become the choice of many organizations for their future data networking needs. The system tested is a distributed three stage switching system based on the Fibre Channel Standard. Testing and Optimization of the three stage switching system is necessary to characterize the performance of the prototype system before a production system is implemented. This paper presents a discussion of optimization techniques and achieved performance numbers under different conditions as well as a comparison to a single stage switching system.

Introduction

Recently, there has been a great need for faster computer communications networks. Applications for high-speed networks include high-speed, high resolution video images, high speed file transfer and a network for distributed processing. To keep abreast with high performance computing requirements, a prototype High Performance Switching System is being developed that will conform to the Fibre Channel Standard (FCS) developed by the American National Standards Institute (ANSI).

The FCS defines a high-speed communication channel to interconnect computers and to connect computers to peripherals such as RAID disk systems. Fibre Channel utilizes fiber optic links with data rates up to 1.0625 Gbit/sec. It is being embraced by a wide variety of companies as a possible future communication network solution.

We analyzed the three stage switching system prototype developed to serve as the fabric in the network. The switching system is based on an early version of the FCS and operates at 266 Mbps. The three stage switch is a scaleable system able to support up to 4096 hosts. Its primary goal is to perform simultaneous fast data movements between many attached systems. Performance of the switch largely defines the performance of the network and therefore characterization of the switch is important in predicting network performance.

This paper presents a brief overview of the Fibre Channel Standard, a description of the three stage switching system, the testing procedures and results. Finally, some conclusions are drawn and recommendations for future work are made. For more details on the Fibre Channel Standard see [1]. For more details on the switch design and its operation see [2].

Fibre Channel Standard Overview

The FCS defines a high performance serial link operating at speeds up to 1.0625 Gbit/sec. Fibre Channel supports fiber optic links with data rates up to 100 MBytes/sec over distances of up to ten kilometers. The Lawrence Livermore National Laboratory is installing a prototype Fibre Channel network as the basis of a high-speed local area network.

The interconnection system between host machines in the FCS is referred to as the fabric. The fabric is composed of a fabric controller and a specified number of fabric ports (F_Ports). Each F_Port can be linked to a N_Port, or node port, which interfaces the host machine. See figure 1.

The fabric, in this case the three stage switching system, has addresses assigned to each of the F_Ports. A dedicated connection can be made between a pair of F_Ports, linking the two N_Ports attached by fiber optic cables to the F_Ports. This provides a communication path for the two N_Ports.

The FCS defines three classes of service, Class 1, 2 and 3. Class 1 service provides a dedicated connection where a physical circuit is locked down between two F_Ports providing a path for communication between the to N_Ports. This connection is guaranteed by the fabric until one of the N_Ports breaks it. Class 2 and 3 provide a connectionless service, where frames are passed from buffer to buffer through the switch. In Class 2 acknowledgments are provided while in Class 3 they are not. In this evaluation, Class 1 service is studied.

Three Stage Switching System

The three stage switching system architecture is scaleable up to 4096 ports, built from racks made of 64 port crossbar switches. The three

sections of the switch are referred to as the I/O section, the Transfer section and the Cross-Connect section. See figure 2.

In order to set up a connection between two ports in the switch, the sending N_Port makes a connection request. This is sent into the F_Port and routed from section to section through the switch to the correct output F_Port and to the receiving N_Port. The receiving N_Port then sends back an acknowledgment to the connection request which is routed back through the switch. During this process a connection path is established between the N_Ports. Now that a dedicated connection has been locked down by the switch, data can be sent between the two N_ports. When the receiving N_Port has received all of the data, it sends a disconnect frame that propagates through the switch, disconnects the circuit between the N_Ports, and notifies the sender that the data was received.

Control of the switch is distributed throughout the three sections. When a connection request frame enters the F_Port, it is processed by the I/O section and then passed on and processed by the Transfer section. Even though the Transfer section may be busy building a connection, the I/O section may lie idle, ready to process another frame. Each 16 port module in the switch, which makes up one fourth of a 64 port stage, has its own microprocessor and so there can be multiple requests processed simultaneously. The switch configuration we used for testing consisted of a single 16 port I/O module, 16 port Transfer module and 16 port Cross-Connect module. See figure 4.

Testing Configuration

The testing configuration used four of the F_Ports in a single 16 port I/O module. A VME adapter was then linked to each of these ports with

fiber optic cabling. IBM PCs were linked through the RS 232 ports of the PCs to the serial diagnostic ports on the VME adapters. See figure 3.

In order to initiate traffic through the switch we used the FASTCXT code. FASTCXT was developed in order to test the operability and performance of the switch. It is downloaded into the VME adapters from the PCs. FASTCXT allowed us to direct the VME adapter to send Class 1, Class 2 or Class 3 packets singly or continuously. A packet refers to the frames needed to set up the connection, pass the data through the switch and then tear down the connection. Sending a packet continuously using Class 1 service involves the following process. A connection is requested and established, the data frame is sent, and then the connection is broken. Then this process is repeated continuously. For every 256 packets that were sent a character was displayed on the screen. In this way we could send a large number of packets and have a fairly accurate count of the number sent. Since the amount of data in this frame was small, only 64 bytes, and the frame was sent once the dedicated connection was made, sending the data frame added little time to the overall packet send time. Thus, we were primarily measuring switch connection setup and tear down time.

In order to time the average packet send time we would send thousands of packets in a continuous sequence and time the sequence with a hand timer. We then would divide out the time for a single packet. To assure accuracy in the hand timings we did this several times and averaged the hand timings.

Test Results

The first goal was to find out how fast the switch could operate with the FASTCXT code sending Class 1 packets continuously. In the original configuration of the switch only 51.2 packets per second could be sent between the N_Ports with no other switch traffic. This corresponds to an average packet time of 19.53 ms. By adjusting some parameters in the PROM code, that time was reduced to 6.42 ms (155.7 packets per second).

There were three parts of the PROM code that were changed to achieve this speed increase. One was the trace function. The trace function in the switch stored the actions taken by the microprocessors in the switch. For instance, each time a frame was sent or received, the type of frame and its source and destination were recorded in the trace buffer. Turning off this function required that a single bit be changed in the PROM code. Making this change led to a 6.8% decrease in average packet time.

The other two parts of the PROM that were changed dictated the number of wait states that were associated with the PROM and with other circuitry on the switch module including the Very High Speed Communications Interface (VHSCI) chip. The VHSCI provides the Fibre Channel protocols and does the 8b/10b code conversion. The microprocessor in the switch is a 16 MHz microprocessor, with a 62.5 nanosecond clock cycle. When running from the original PROM code, before fetching the instructions, the processor was instructed to wait seven clock cycles. This error in the code caused an unnecessary 437.5 nanosecond delay on each instruction fetch cycle. Correcting this error led to an additional decrease in packet time of 58.6%. The other circuitry also originally had seven wait states. We found it ran reliably with only two

wait states. This saved 312.5 nanoseconds every time devices in this circuitry were accessed leading to another 4.1% increase.

The next set of tests utilized more than two adapters at a time and investigated how the switch would perform with varying traffic patterns. We started with a base time derived from having one adapter send to another with the trace function on and the minimum number of wait states. With only adapter A sending to adapter B, under these conditions, the average time for a packet to be sent and received was 8.08 ms. This is referred to as the base time.

In test 1, we sent packets from two adapters to one. Adapters A and B sent packets to the third adapter C. C received the packets at an average of one every 5.63 ms, faster than the 8.08 ms it took to receive a packet in the situation with only A sending to B. As expected, the two sending adapters, A and B, each sent a packet once every 11.25 ms, or twice the time taken for C to receive the packet. The reason the receiving adapter is faster in receiving than the base time is because of the connection setup process. When adapter A has made a connection to adapter C, B can not get through to the receiving adapter C. However, when B sends a request, the construction of the connection is started and the request is queued in the switch at the output F_Port. When A breaks the connection, B's request is almost immediately given to C to be processed. At the same time, A's next request is being queued while A waits for B to finish the connection. This saves time and leads to a receive rate faster than the base rate. We saw similar results using the 16 port single stage switch. The sending times for A and B increased while the receive time decreased in comparison to the base time. The percentage that the receive time dropped in the single stage switch was smaller than that of the three stage

switch because the connection time is so much shorter in a single stage switch.

For the second test, we had adapter B send packets and receive packets at the same time. B sent packets to C and received them from A. Since A and C alternated connections with B, the average time for the connection was the same for both of them at 13.94 ms. B sent and simultaneously received packets in that same average time. The reason this time is more than the 8.08 ms base time is that B would take the 8.08 ms to send to C, but would have to wait for A to finish its connection before it could send again. A is queued while B is sending to C so when the transfer from A to B takes place, it takes less than the base time of 8.08 ms. By subtracting the base time from the total time to send and receive a packet we get the time to receive a queued packet from A, 5.86 ms. This number corresponds closely with the 5.63 ms it takes for a queued packet to be received in the test above.

The third test involved four active adapters, two sending and two receiving. A was sending to B while a parallel channel was setup with C sending to D. Ideally, both sets of adapters would have been able to send or receive packets at the base time. What happened, however, was that they each slowed down by 22% from the base time to a average time of 9.88 ms per connection. The probable reason for this is that the microprocessors are not fast enough to handle multiple connection requests without degrading performance. Because the adapter processing times do not change, the switch has added 1.8 ms to the average connection time. Again, while running the same test with the single stage switch, we got similar results. The single stage switch slowed down 36% when a parallel channel was added.

The fourth test yielded an unexpected result. Three adapters, A, B and C, were all attempting to send packets to adapter D, competing for access to D. Unlike test one, when two adapters split time accessing a single receiver, two of the three adapters in this case were completely shut out while the other adapter sent packets at the same speed as the base speed. When one of the sending adapters was disconnected while the test was running, degrading the test to the case where two adapters send to one, the two remaining adapters split the time as in the first test. Using the single stage for this test gave better results. The three sending adapters shared access to the receiver port. Each took turns sending packets to the receiver.

Conclusions

We found that the performance of the switch was largely dependent on the amount of traffic that it was required to handle. Of particular interest is the 22% slowdown when adding a parallel channel in test three. Processing multiple connection requests within a single sixteen port module simultaneously will be required of the switch and therefore the slowdown seen when adding traffic is important to understand. A faster microprocessor in the switch would reduce the slowdown. Concerns also arise from test four where two adapters were not able to make any connections at all. This appears to be a bug in the prototype switch.

Future work should include differentiating the time the adapter spends processing commands from switch connection setup and break-down times. More adapters should be added so more parallel channels can be setup on the switch and the performance can be characterized. Tests should be conducted where more than one I/O and Transfer module are

used to see if the same results occur when the connections are distributed further throughout the switch.

References

1. ANSI Accredited Standards Committee X3T9.3. Fibre Channel Physical and Signaling Interface (FC-PH), Rev. 4.2, 1993.

2. V.Sahai, "Performance Evaluation of a High-Speed Switching System." Masters Dissertation, Computer Engineering, University of California, Santa Cruz, 1992.

Topology of Fibre Channel

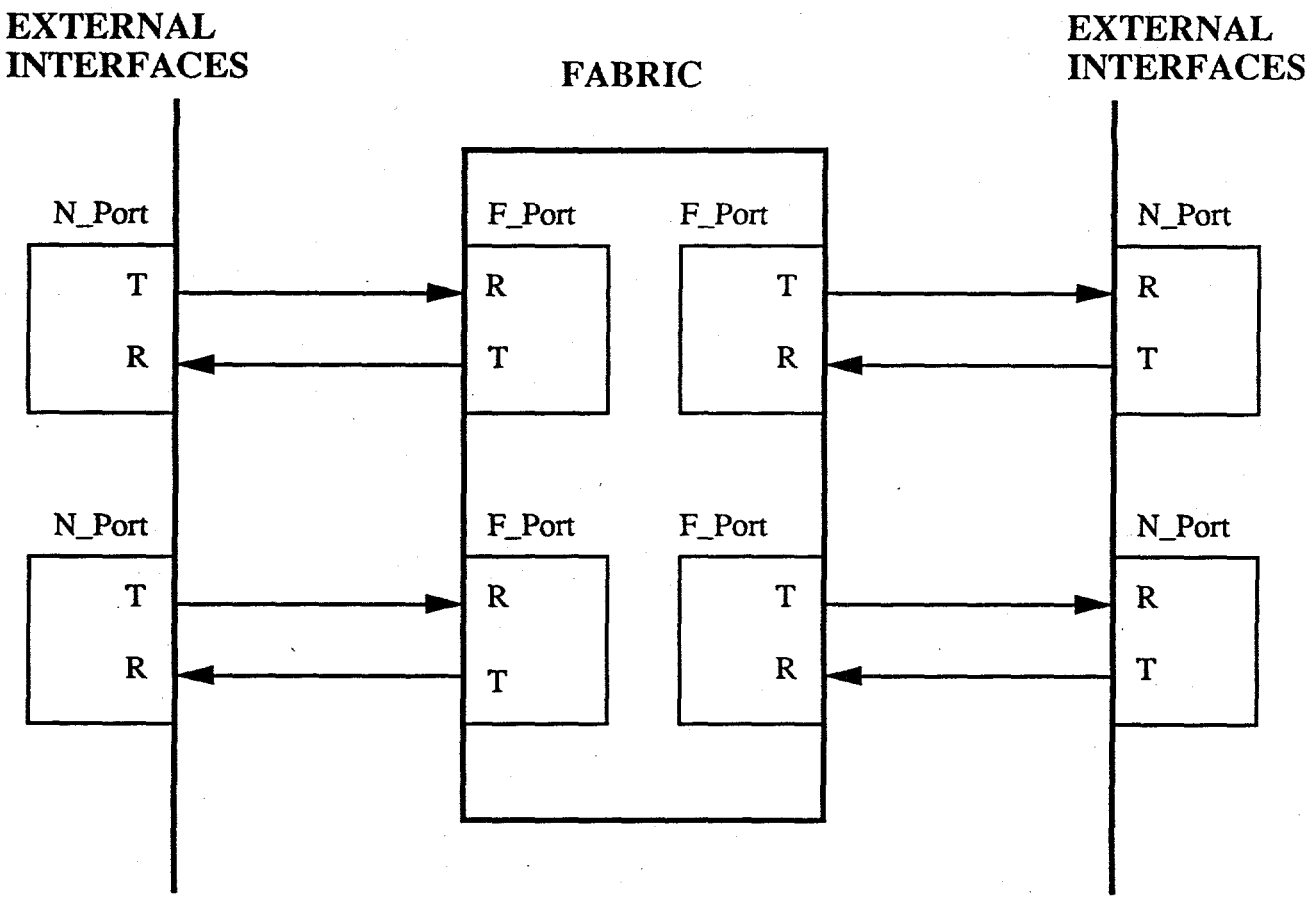

Figure 1

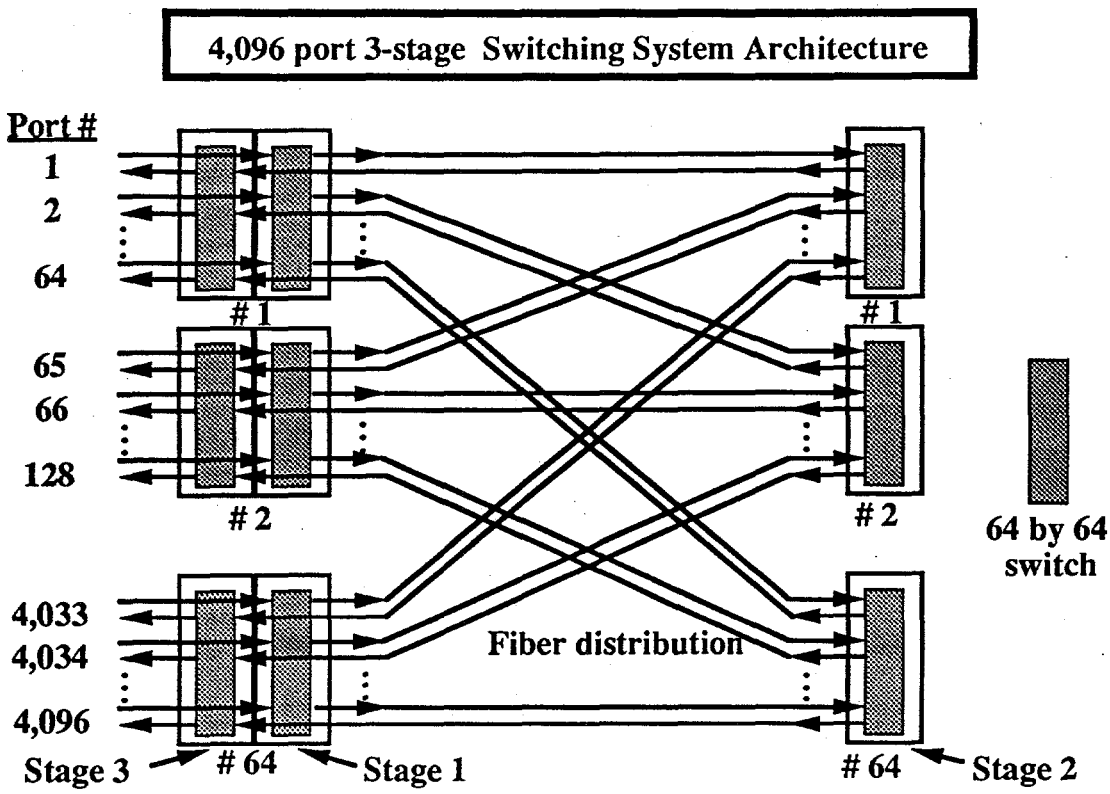
4,096 port 3-stage Switching System Architecture
Port #
1
2
64
65
66
128
4,033
4,034
4,096
1
2
64
1
2
64
64 by 64 switch
Fiber distribution
Stage 3
Stage 1
Stage 2

Figure 2

Hardware setup for Switch Performance Timings

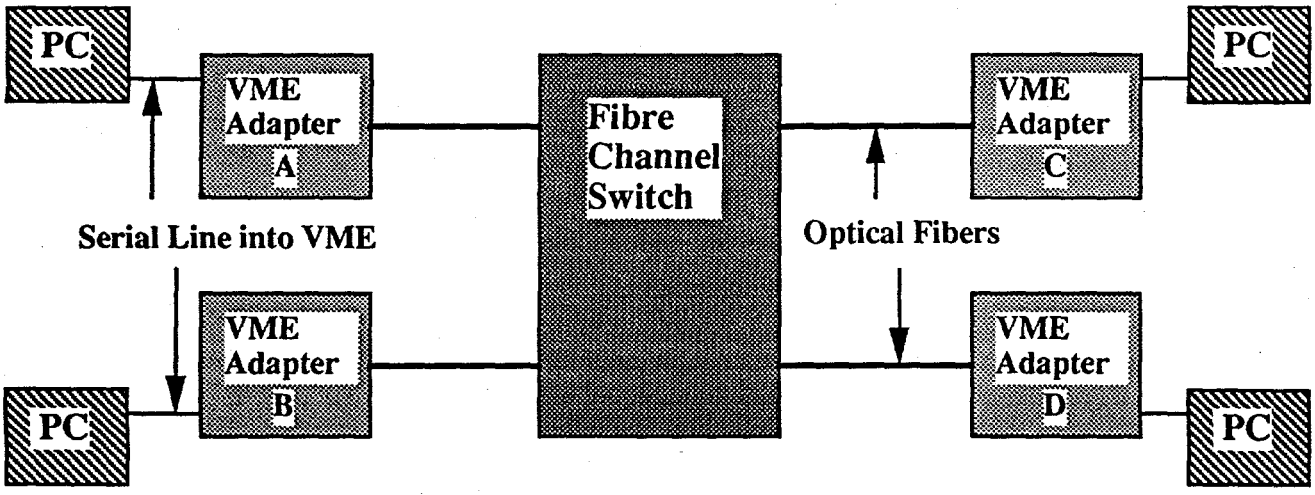

IBM PCs load FASTCXT code into VME adapter cards.

figure 3

Three Stage Switch Configuration for Tests

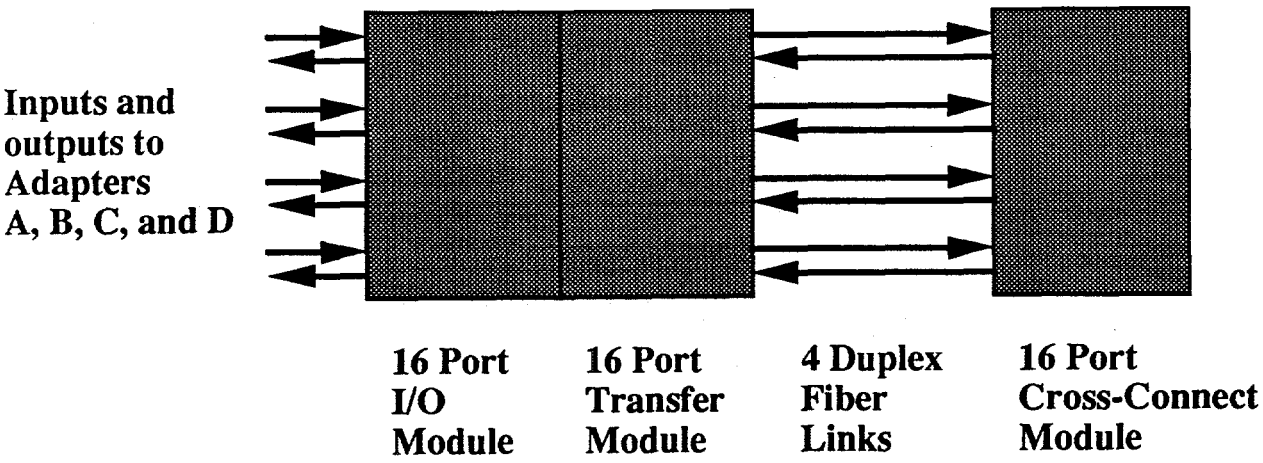

Figure 4

Three Stage Switch			
	Send or		
A send to B (base time)	Receive time		
A (send time ms)	8.08		
B (send time ms)	8.08		
A send to C, B send to C			% difference
			from base time
A (send time ms)	11.25		28
B (send time ms)	11.25		
C (receive time ms)	5.63		44
A send to B, B send to C			
			% difference
A (send time ms)	13.94		42
B (send time ms)	13.94		
B (receive time ms)	13.94		
C (receive time ms)	13.94		42
A send to B, C send to D			% difference
A and B time (ms)	9.88		22
C and D time (ms)	9.88		22
A, B, and C send to D			
A (send time ms)	8.08		0
B (send time ms)	none		
C (send time ms)	none		
D (reveive time ms)	8.08		0
Single Stage			
A send to B (base time)			
A (send time ms)	1.35		
B (send time ms)	1.35		
			% difference
A send to B, C send to D			From base time
A and B time (ms)	1.84		36
C and D time (ms)	1.84		36
A and B send to C			
A (send time ms)	2.56		90
B (send time ms)	2.56		90
C (receive time ms)	1.28		5.5
A and B and C send to D			
A, B and C (send time ms)	3.82		183
D (receive time ms)	1.28		5.5

Computer Optimization of Photoreceiver Designs†

Mark Wistey
Electrical Engineering Department
Montana State University
Bozeman, Montana 59715

Lawrence Livermore National Laboratory
Livermore, California 94550

December 16, 1993

Prepared in partial fulfillment of the requirements of the Science and Engineering Research Semester under the direction of Jeff Kallman, Research Mentor, in the Lawrence Livermore National Laboratory (LLNL).

† This research was supported in part by an appointment to the U.S. Department of Energy's Science and Engineering Research Semester (hereinafter called SERS) program administered by LLNL under Contract W-7405-Eng-48 with Lawrence Livermore National Laboratory.

Computer Optimization of Photoreceiver Designs

Mark A. Wistey
Montana State University
LLNL Engineering Research Division

ABSTRACT

We customized an existing simulator which uses the beam propagation method to analyze optoelectronic devices, in order to test the wavelength filtering characteristics of a number of photoreceiver designs. We tested the simulator against traditional analytical techniques and verified its accuracy for small step sizes. Finally, we applied a simulated annealing algorithm to the BPM simulator in order to produce photoreceiver designs with improved wavelength filtering characteristics.

1 Introduction

In nearly all types of communication over optical fibers, the speed bottleneck is not in the fiber itself, but in the transmitters and receivers at each end of the fiber. We hope to increase the amount of data which can be carried over existing optical fiber networks. New photoreceiver designs should meet these criteria:

- Narrow bandwidth: sensitive to only one wavelength of light.
- Fast switching time: quickly recognizes a change in the incoming signal.
- Tunable wavelength: activated by a selectable wavelength.
- Easy to manufacture: no unusual equipment needed.
- Small physical size: comparable to small small microelectronics devices.

Existing photoreceivers can be tuned by changing the refractive indices of the photoreceiver using a steady electric field[1]. However, most photoreceivers operate over a broad bandwidth: they are sensitive over most of the range of wavelengths of light which optical fibers can efficiently carry, from 1.3 μm to 1.55 μm. If photoreceivers could be developed with narrower bandwidths, numerous channels could be carried over the same optical fiber, each on a separate wavelength. Additionally, existing photoreceivers are handicapped by large sizes compared to ordinary microelectronics. The larger size is necessary to make the photoreceiver sensitive enough to detect weak signals, but slows the photoreceiver's response.

The remainder of this paper is organized as follows: The next section (Section 2) describes the Beam Propagation Method (BPM) which we used to simulate various photoreceivers on a computer. Section 3 describes our modifications

to a particular BPM software package while working on this project. Next, in Section 4, I describe the special techniques used to analyze a particular photoreceiver design. Section 5 discusses the process of simulated annealing as it was applied to design optimization. Finally, Section 6 presents a summary of the conclusions of the project.

2 Beam Propagation Method

The beam propagation method (BPM)[2] numerically simulates the passage of a beam of light through a material. This method relies on the assumption that the electric field of light in a medium can be described by the scalar Helmholtz equation

$$\frac{\partial^2 E}{\partial x^2} + \frac{\partial^2 E}{\partial y^2} + \frac{\partial^2 E}{\partial z^2} + \frac{\omega^2}{c^2} n^3(\omega,\ x,\ y,\ z)E = 0. \tag{1}$$

where ω is the frequency of the light, n is the refraction index of the material, and c is the speed of light. Note that n will be a complex number if the material is a photoabsorber, such as a photodiode. It can be shown[2, 3] that an operator solution to Equation 1 is

$$E(x,\ y,\ z+\Delta z) = O\left[(\Delta z)^3\right] + \tag{2}$$
$$\exp\left(-\frac{i\Delta z}{4k}\nabla_\perp^2\right) \times \exp\left[-i\Delta z\chi(x,y)\right] \times \exp\left(-\frac{i\Delta z}{4k}\nabla_\perp^2\right) \times E(x,\ y,\ z)$$

where $k = (n_0\omega)/c$, n_0 is the refractive index of the substrate or of air, and χ defined by the paraxial approximation

$$\chi(x,y) = \frac{k}{2}\left\{\left[\frac{n(x,\ y)}{n_0}\right]^2 - 1\right\}. \tag{3}$$

The beam propagation method iteratively applies Eq. 2 to the electric field of the incoming wave, simulating the material as a series of thin lenses.

I compared simulations of a coupled waveguide with analytical solutions provided by R. J. Deri, and found that the value of χ originally given in [2],

$$\chi_o(x,y) = k[(\frac{n}{n_0}) - 1], \tag{4}$$

led to nearly 50% error in the coupling length produced by the simulation. Similar tests using the paraxial approximation in Eq. 3 showed less than 5% error in coupling length. This disagreed with an assertion in Ref. [4] that the paraxial approximation would contribute more phase error than the approximation in Eq. 4.

3 Modifications to BPM Software

The large size of the devices being simulated forced us to find ways to improve the speed of our BPM software. In its original form, BEEMER, the BPM program we used at LLNL, required up to 8 hours on a Sun IPC workstation to simulate a wave passing through a 500 μm device. I eliminated redundant calculations in BEEMER, which improved its speed by 30% and actually reduced roundoff errors. Porting BEEMER to the National Education Supercomputer, a Cray X-MP, gave only a 10-fold increase in speed over the Sun workstation. However, replacing BEEMER's Complex Fast Fourier Transform routine with a native Cray subroutine produced another 3-fold speed improvement. These changes shrank BEEMER's simulation time to just 6 minutes on the NES and 5 hours on Sun IPC workstations. This improvement made it feasible to simulate larger photoreceivers and to perform computerized optimization, as described in Section 5.

In order to simulate a photoreceiver's ability to filter out different wavelengths of light, we had to simulate the passage of more than 20 different wave-

lengths of light through the device. Because this process could be handled by multiple computers operating simultaneously, I adapted BEEMER to take its commands from files, a batch mode. This allowed the user to make a new design with the interactive version of BEEMER and have the photoreceiver's wavelength filtering analyzed by up to 21 computers at the same time, drastically reducing the amount of time the user had to wait for the results.

4 Problems in Photoreceiver Analysis

We applied BEEMER to simplified version of a vertical, integrated, coupled-waveguide photoreceiver described, for example, in [5]. This photoreceiver, shown in Figure 1, is composed of a source waveguide on a substrate with another waveguide above it, near enough that a beam in either waveguide would slightly overlap the other. Photodiode segments are added above the upper waveguide, which draw out and absorb most of the light from the upper waveguide under those regions.

Our first dilemma was to accurately simulate the photodiode segments in the photoreceiver. We accomplished this by including a complex refractive index for the diode material. The imaginary (i.e. absorption) component of the refractive index was taken to be 0.043, following data supplied to us by R. J. Deri.

More difficult was the choice of the propagation step size; larger step sizes would mean faster simulations but possibly inaccurate results. I repeated the same simulation with step sizes from 0.5λ down to 0.001λ and found consistent results for a step size less than 0.02λ; this agrees well with the restriction in Ref. [3]'s equation 12:

$$\Delta z_{max} \ll \frac{\lambda}{2} \frac{n_0}{n_1^2 - 1} \sim \frac{\lambda}{18} \tag{5}$$

for our simulation, where n_0 is the smallest index of refraction encountered by the wave (usually equal to unity) and n_1 is the largest index of refraction. Decreasing the step size Δz (i.e. increasing the resolution) far beyond the restriction in Eq. 5 only negligibly improved the accuracy of the simulation. In fact, for values of

$$\Delta z < 0.002 \Delta z_{max}$$

roundoff errors in the intensity of the output beam became noticeable.

Another concern was the inability of BPM to handle backward-reflected light. Because the incoming beam of light in the photoreceiver would be crossing large steps in refractive index as it moved from one material to another, some of the beam should have been reflected back toward the source, which the ordinary BPM could not handle. This would cause the most change near the photodiode segments, as they are separated by air. We reasoned that most of the light which was backreflected would be absorbed in the diode segments, so we added a thin, stronly photoabsorbant surface to the back of each diode in the simulation, opposite the incoming beam. The real part of the refractive index of these superabsorbers was the same as that of the diode segment to which it was attached, so the beam did not scatter or reflect as it passed into the superabsorber from the diode.

5 Optimization of Photoreceiver Designs

Once the BPM simulation tools were complete, I sought to have the computer perform the tedious task of optimizing each design: I wanted the computer to test numerous small variations on a given design in order to find the best variation, a role filled by a variation of simulated annealing[6].

Figure 1: An Integrated, Coupled Waveguide Photoreceiver

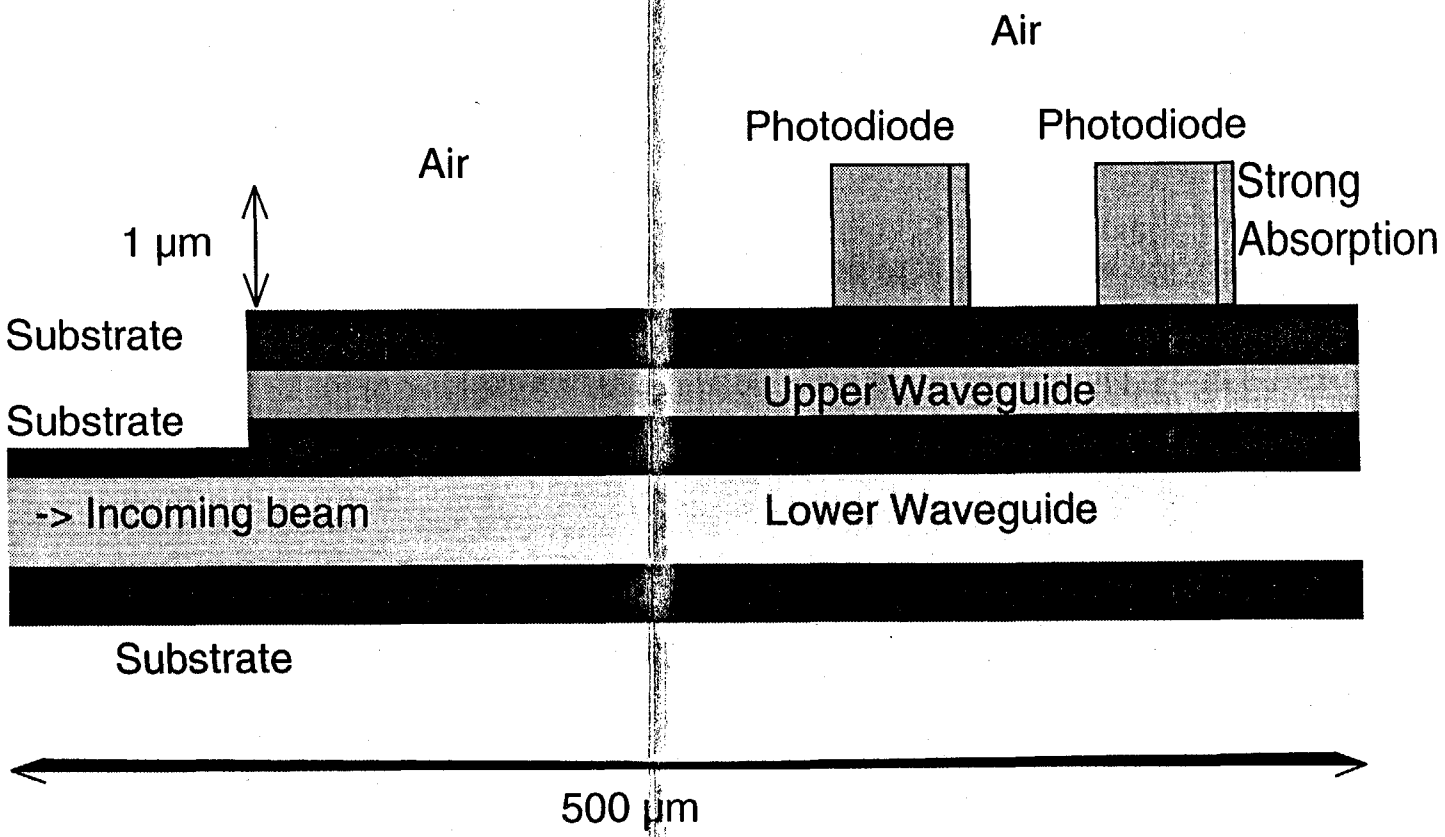

In the natural annealing process, a liquid such as molten glass is slowly cooled. While the glass is cooling, thermal agitation drives individual atoms to unstable (higher-energy) positions within the slowly-forming solid. The atoms may then drop into positions of lower energy than their original position. If enough time is allowed to pass as the solid is cooled, most atoms will reach highly stable positions in the solid and thus make the whole solid highly stable. There is no way to guarantee that the solid has reached a perfectly stable configuration, but such thermal agitation with slow cooling almost always yields a highly stable product.

We tested both true simulated annealing and threshold annealing: when a proposed design change produces a slightly less stable design, true simulated annealing would randomly accept or reject the degradation based on a Boltzman distribution of thermal energies, just as the atoms in a cooling glass have a range of energies, allowing some of them to jump to much higher energy states. In threshold annealing, we would compare the degradation to a threshold value, which, in the analogy of cooling glass, treats all of the atoms in the glass as if they had the same energy for jumping into other positions. I found that threshold annealing produced better results 2–4 times as often as the original form of simulated annealing, for reasons which are not yet understood.

We use the same principles of slow cooling and random agitation in simulated annealing. Our algorithm is presented in Figure 2. The criterion for testing improvements or degradations was to measure the photoreceiver's effectiveness at narrowing the bandwidth of light which it absorbed.

The optimizing program acts as a master controller, controlling up to 25 slave computers running the beam propagation software at the same time, each with a different wavelength of light. This parallelism allows the optimizer to work at

Figure 2: Threshold Annealing

Threshold annealing is a global optimization algorithm which mimics the natural process of annealing, or slow and orderly cooling. At first, wild changes may be made to the system which is being optimized, but they are gradually restricted until only beneficial changes are accepted.

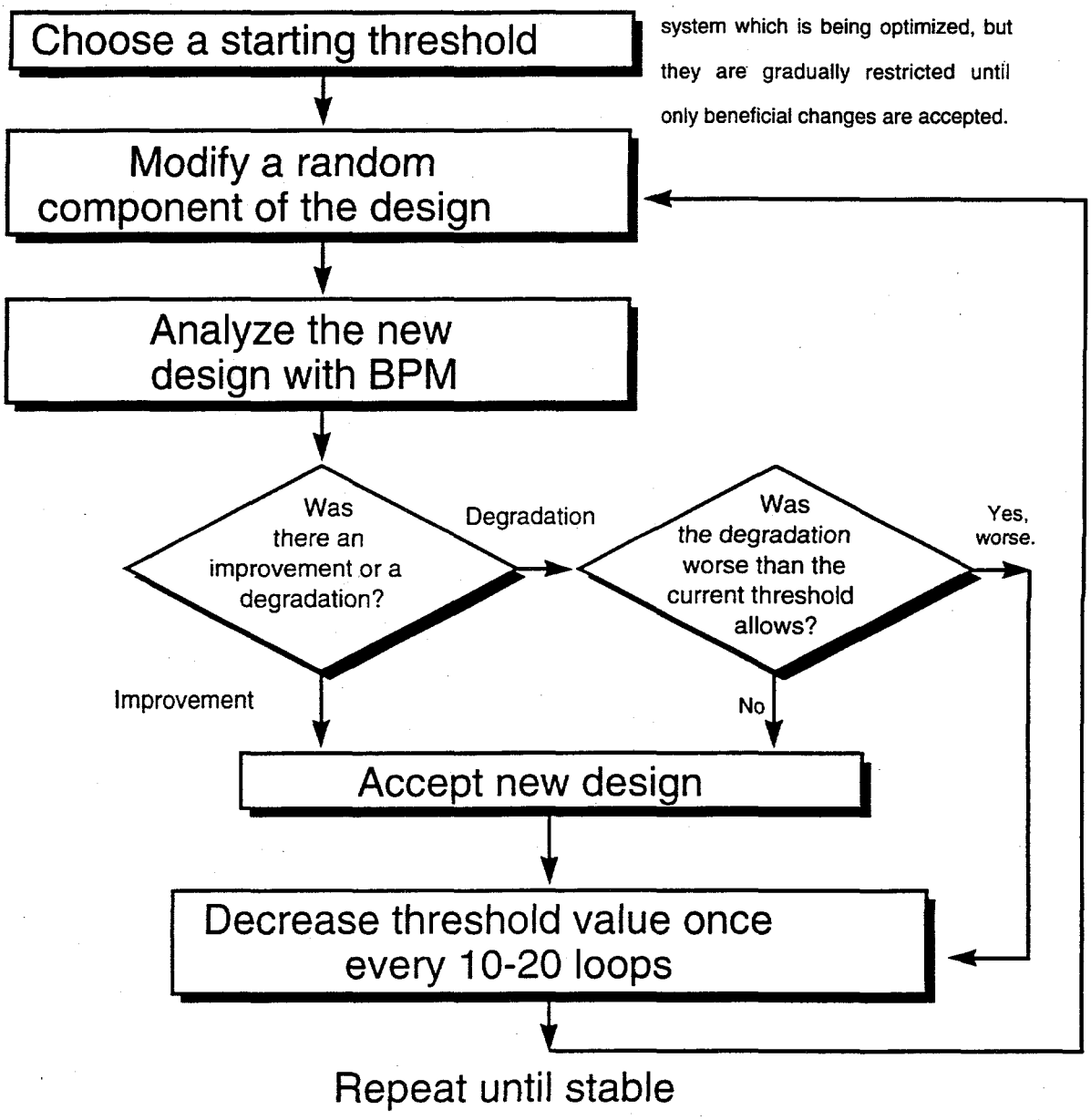

nearly the same speed on a mainframe, on a fast multiprocessor minicomputer, or on a group of workstations.

6 Conclusions

We have improved a beam propagation method simulator to quickly analyze large (1000 μm) photoreceiver designs. We found good agreement between the results of an analytic study of a coupled waveguide and those from a BPM simulation of the waveguide, using the propagation step size recommended by Feit and Fleck [3]. Finally, we applied a simulated annealing optimization algorithm to improve the wavelength-filtering characteristics of photoreceivers, and adapted a BPM simulator to serve as a slave to the optimizer.

I would like to thank Jeff Kallman for his encouragement and helpful discussions.

This research was supported in part by an appointment to the U.S. Department of Energy's Science and Engineering Research Semester program administered by LLNL under Contract W-7405-Eng-48 with Lawrence Livermore National Laboratory.

References

[1] R. C. Alferness and R. V. Schmidt, "Tunable optical waveguide directional coupler filter," Applied Physics Letters **33**, 2 (1978).

[2] M. D. Feit and J. A. Fleck, Jr., "Light propagation in graded-index optical fibers," Applied Optics **17**, 24, (1978).

[3] M. D. Feit and J. A. Fleck, Jr., "Analysis of rib waveguides and couplers by the propagating beam method", Journal of the Optical Society of America-A **7**, 1 (1990)

[4] M. D. Feit and J. A. Fleck, Jr., "Beam nonparaxiality, filament formation, and beam breakup in the self-focusing of optical beams", Journal of the Optical Society of America-B **5**, (1988)

[5] R. J. Deri, N. Yasuoka, M. Makiuchi, O. Wada, A. Kuramata, H. Hamaguchi, and R. J. Hawkins, "Integrated waveguide/photodiodes using vertical impedance matching," Applied Physics Letters **56**, 18 (1990).

[6] S. Kirkpatrick, C. D. Gelatt, Jr., M. P. Vecchi, "Optimization by Simulated Annealing", Science **220**, 4598 (1983)